BEYOND CLASSICAL NUCLEATION THEORY: A 2-D LATTICE-GAS AUTOMATA MODEL

by

Joseph Hickey

Thesis submitted to the

Faculty of Graduate and Postdoctoral Studies

in fulfillment of the requirements of the

Master's of Science, Physics program.

Department of Physics

Faculty of Science

University of Ottawa

August 8, 2012

Table of Contents

List of Figures and Tables

List of Symbols

a	Molecular area of a crystal particle
C_{in}	Initial concentration of solute
C_{eq}	Equilibrium concentration of solute
$\hat{C}$	Bulk concentration of solute
$\vec{c}_i$	Lattice directions in a D2Q4 cellular automata
D	Diffusion coefficient
d	Density of particles at a cellular automata lattice node
E_{ss}	Bonding energy of solid particle-to-solid particle in crystal phase
E_{sw}	Bonding energy of solid particle-to-water particle in dissolved phase
ΔE	Change in direct interaction energy upon attachment or detachment of solid particle to crystal
$f(\rho)$	Tolman expression
G	Free energy of supersaturated system
ΔG^*	Free energy barrier to nucleation
J	Nucleation rate

k_B	Boltzmann constant
l_s	Lattice spacing of diffusion lattice
N	Number of particles forming a crystal
N^*	Number of particles forming a crystal of critical size
n_i	Occupation number of particles at a cellular automata lattice node
$\overline{n}_i$	Average occupation number of particles at a cellular automata lattice node
R	(Effective) radius of crystal
R^*	(Effective) critical radius of crystal
S	Supersaturation
T	Temperature
t_s	Time step
Z	Zeldovitch factor
β	Kinetic coefficient of particle attachment to cluster surface
δ	Tolman parameter
η	Next-to-nearest neighbour bonding interaction coefficient in solid phase
μ_s	Chemical potential of crystal phase
μ_d	Chemical potential of dissolved phase
ν	Volume of a (new-phase) cluster particle (three-dimensional case)
ρ	Scaled (effective) crystal radius
ρ^*	Scaled (effective) critical crystal radius

Σ Scaled surface tension (non-classical, two-dimensional case)

Σ_0 Scaled surface tension (classical, two-dimensional case)

σ Surface tension (non-classical, two-dimensional case)

σ_0 Surface tension (classical, two-dimensional case)

$\overline{\sigma}_0$ Surface tension (classical, three-dimensional case)

$\tau(N)$ Mean first-passage time for crystal growth

ω_N^+ Rate constant for single-particle attachment to cluster

ω_N^- Rate constant for single-particle detachment from the cluster

Abstract

Nucleation is the first step in the formation of a new phase in a thermodynamic system. The Classical Nucleation Theory (CNT) is the traditional theory used to describe this phenomenon. The object of this thesis is to investigate nucleation beyond one of the most significant limitations of the CNT: the assumption that the surface tension of a nucleating cluster of the new phase is independent of the cluster's size and has the same value that it would have in the bulk of the new phase. In order to accomplish this, we consider a microscopic, two-dimensional Lattice Gas Automata (LGA) model of precipitate nucleation in a supersaturated system, with model input parameters E_{ss} (solid particle-to-solid particle bonding energy), E_{sw} (solid particle-to-water particle bonding energy), η (next-to-nearest neighbour bonding coeffiicent in solid phase), and C_{in} (initial solute concentration). The LGA method was chosen for its advantages of easy implementation, low memory requirements, and fast computation speed. Analytical results for the system's concentration and the crystal radius as functions of time are derived and the former is fit to the simulation data in order to determine the system's equilibrium concentration. A mean first-passage time (MFPT) technique is used to obtain the nucleation rate and critical nucleus size from the simulation data. The nucleation rate and supersaturation are evaluated using a

modification to the CNT that incorporates a two-dimensional, radius-dependent surface tension term. The Tolman parameter, δ, which controls the radius-dependence of the surface tension, decreases (increases) as a function of the magnitude of E_{ss} (E_{sw}), at fixed values of η and E_{sw} (E_{ss}). On the other hand, δ increases as η increases while E_{ss} and E_{sw} are held constant. The constant surface tension term of the CNT, Σ_0, increases (decreases) with increasing magnitudes of E_{ss} (E_{sw}) fixed values of E_{sw} (E_{ss}), and increases as η is increased. Together, these results indicate an increase in the radius-dependent surface tension, Σ, with respect to increasing magnitude of E_{ss} relative to the magnitude of E_{sw}. Σ_0 increases linearly as a function of the change in energy during an attachment or detachment reaction, $|\Delta E|$, however with a slope less than that predicted for a crystal that is uniformly packed at maximum density.

Acknowledgements

I would like to thank my supervisor on this project, Professor Ivan L'Heureux, for his guidance, aid, and mentorship over the past years. I also thank the past and present members of Dr. L'Heureux's research group for their help, including creative discussions with Dave McNamee, sample Lattice-Boltzmann code provided by Steve Zhang that was helpful at the beginning of this work, and help with preparation for presentations from Rimma Bektursunova, Severin Stojanovic, Marc-André Théberge, Jean-François Meunier, Julie Bourdeau, and Dr. Tony Fowler. I initially registered in the M.Sc. program under the supervision of Dr. Denis Rancourt. I thank him and his former graduate student, Philippe Marchand, for guidance and inspiration at the outset of this work.

I acknowledge financial support for this research from the National Sciences and Research Council of Canada in the form of a Canada Graduate Scholarship.

Chapter 1

Introduction

Nucleation is the formation of the first small clusters (nuclei) of a new phase of matter in a thermodynamic system. It is therefore a fundamental process in materials science and geochemistry, from self-assembly of nano-scale technological components to formation of igneous rocks, nanoparticle precipitation in aquatic and atmospheric environments, cloud formation, and dynamics of volatiles in magmatic systems [Laaksonen 1995, Gránásy 1999a, Frenkel 2006, Shevchenko 2006, Zhang 2008].

In geochemical systems, most reaction processes of interest are heterogeneous and complex, yet part of the difficulty in advancing the understanding of such processes is the lack of a well-functioning theory of the relatively simpler homogeneous nucleation. Although the Classical Nucleation Theory (CNT) has long been established as the dominant theoretical framework used to describe this phenomenon, the CNT is known to be seriously flawed when compared to experimental studies of nucleation rates. Without a reliable theory

of nucleation, scientists are limited in their ability to further develop theories of more complicated processes – for example, a key stage in a volcanic eruption is the exsolution of dissolved gas from magma at shallow depths in the magma chamber where the pressure is low enough for this to occur. Quantification of the rate of gas bubble nucleation in the magma is required in order to predict the mass fraction of gas in the eruption's explosive gas flow and the flow's exit velocity [L'Heureux 2007]. A theory of nucleation that would be of use to a volcanologist would permit the researcher to accurately predict bubble nucleation rates in magma given the initial conditions [Zhang 2008].

Another example in geochemistry where deeper insight into the physics of new phase formation is needed is the coprecipitation of environmentally active nanoparticles in aquatic environments. A case that has been studied at the University of Ottawa is the coprecipitation of the iron-based nanomineral ferrihydrite with phosphate or toxic metals such as arsenic [Marchand 2009a, Thibault 2009]. When coprecipitation of two or more chemical species occurs in the environment, the resulting cluster of the new solid phase often has an anisotropic bond structure, and consequently a surface and bulk structure that is complex at a microscopic scale. The CNT does not account for these features, which are thought, however, to have a significant influence on nucleation rates. In order to further research into the formation of nanoparticles, nucleation theories and computational simulations that go beyond the limiting assumptions of the CNT are required.

In his textbook *Geochemical Kinetics*, Youxue Zhang wrote that "the best characterization of the present status of our understanding on nucleation is that we do not have a quantitative understanding of nucleation" [Zhang 2008]. Accordingly, and due to its

prevalence across many disciplines of scientific research, there is an acknowledged need for the scientific community to improve the theory of nucleation. It is with this challenge in mind that we have undertaken the investigation of "non-classical" (i.e. non-CNT) nucleation phenomena presented in this thesis.

This introduction continues with a brief overview of the key elements of the Classical Nucleation Theory (CNT) and the central problem of the theory, the capillarity approximation, which leads to the assumption of a size-independent (constant) surface tension term. The research objective of this thesis and the simulation and analysis methodology are described next, followed by an outline of the chapters making up the thesis.

1.1 CNT and the Capillarity Approximation

Since the work of Gibbs [Gibbs 1928], Becker and Doring [Becker 1935], Frenkel [Frenkel 1955], and others up to the present day, the theory of nucleation has been handled predominantly by the CNT and its modified versions. The CNT is a theory of homogeneous nucleation, which occurs when the particles of the new phase come together to form a nucleus without the aid of a foreign substance such as the surface of a container or a dust particle. Therefore, the following discussion and the rest of the thesis will deal with homogeneous nucleation.

The key feature of the CNT is the competition between i) a thermodynamic driving force that decreases the free energy of the system, G, thus making the appearance of a small "cluster" (nucleus) of the new phase statistically favourable and ii) an energy cost due to the

creation of a new surface separating the two phases, parameterized by a constant surface tension. Under the CNT, the competition between these two factors establishes a free-energy barrier, ΔG^*, to the nucleation of the new phase, which has as its reaction coordinate the number of particles in a nucleus, N. The stochastic formation and dissolution of small clusters of the new phase occurs until, eventually, some clusters contain a critical number of particles, N^*, at which point they are more likely to grow to larger sizes than to dissolve. A cluster containing N^* particles is termed a "critical nucleus." Nucleation occurs upon formation of a critical nucleus and is followed by growth of the cluster as additional particles of the new phase bond to it. The nucleation rate, J, is the number of nuclei formed per unit volume (or area, in two-dimensions) per unit time. J is a quantity of interest in nucleation research, because it provides a means of comparing experimental results to nucleation theory.

Experimental studies of nucleation are based on methods that enable one to count the number of nuclei that form per unit time per unit volume under favourable thermodynamic conditions, thus permitting data to be obtained for the nucleation rate J, as a function of the undercooling, ΔT, for liquid droplet formation from a vapour or crystal formation from a melt, or as a function of the supersaturation, S, in the case of precipitation from solution. The greatest source of doubt about the correctness of the CNT is that the experiments consistently show nucleation rates orders of magnitude different than those given by the CNT (larger, in the case of crystal nucleation) [Turnbull 1952, Wood 1970, Miyazawa 1974, Flageollet 1980, Wyslouzil 1991, Djikaev 2004, Gonzalez-Oliver 1980, Gránásy 1999a, Ruckenstein 2005, Zhang 2008].

1.1.1 The capillarity approximation

A central assumption of the CNT is the **capillarity approximation**. Under this assumption, the nucleating phase has the same properties that it would have in its bulk form, such as the molecular density, chemical potential, and surface tension. The interface separating the nucleating and parent phases is approximated as a sharp, infinitely thin barrier, and the nucleus is assumed to take its equilibrium crystal or droplet shape, (spherical in the three dimensional case, circular in the two dimensional case).

Although the capillarity approximation allows for simplifications essential to the development of the CNT, it leads to the presence of the macroscopic surface tension as a key parameter. This is considered to be one of the major shortcomings of the theory, since nucleation occurs at a microscopic scale at which bulk thermodynamic properties are not necessarily relevant. [Kaschiev 2000, Markov 2003, Ruckenstein 2005, Zhang 2008]. In section 2.2 of Chapter 2, some of the main attempts to move beyond the capillarity approximation toward non-classical theories of nucleation are outlined, and in section 4.1 of Chapter 4, a non-classical theory of two-dimensional nucleation that incorporates a size-dependent surface tension term is derived.

1.2 Research Objective and Methodology

In this thesis, a simulation approach was used to study **two-dimensional** nucleation using a microscopic description of the interactions between solute particles and precipitating clusters. The simulated nuclei form with complex geometries, in contrast to the equilibrium

shape that follows from the capillarity approximation in the CNT picture. The concept of an energy cost due to formation of a new surface under tension is a fundamental feature of the CNT. Because this concept is essentially a means of modeling the microscopic physical process of chemical attachment (bonding) and detachment (bond-breaking) of individual molecules of the new phase to and from the surface of a nucleating cluster, the primary goal of this research was to use a microscopic model to investigate the surface tension in a way that goes beyond the limitation of the constant bulk value inherent to the CNT. In view of this, an approach similar to Dillmann and Meier's [Dillmann 1989, Dillmann 1991] was followed to modify the CNT's "energy cost" term to include a radius-dependent surface tension, as derived from thermodynamic considerations by Tolman [Tolman 1949]. Some authors, such as Ruckenstein and Nowakowski [Ruckenstein 1990, Nowakowski 1991, Ruckenstein 2005], have questioned the use of the surface tension-as-energy cost concept in nucleation theory, and have created alternative kinetic theories based on probabilistic calculations of attachment and detachment of particles from the surface of the nucleating cluster. However, we will see that the non-classical extension to the CNT presented in this thesis improves the analysis of the simulation data over the classical case.

Rather than comparing it to experimental data for crystal nucleation, which has been acknowledged to be difficult to obtain [MacFarlane 1983, Laaksonen 1995], the present non-classical approach is evaluated using a two-dimensional lattice gas automaton (LGA) microscopic model of crystal nucleation to simulate data for the nucleation rate, J. This model simulates precipitation nucleation and growth in a two-dimensional diffusion field on a fixed-directional grid. In this thesis, we will refer to the solvent as "water" for the sake of argument. Simulation input parameters include water particle-to-solid particle bonding

energy, E_{sw}, solid particle-to-solid particle bonding energy, E_{ss}, a coefficient controlling the next-to-nearest neighbour solid particle-to-solid particle bonding strength, η, and the initial concentration of particles in the system, C_{in}. J is obtained from mean first-passage time techniques, described in Chapter 5. The nucleation rate calculated from the non-classical theory is fitted to the simulation data for J to determine the parameters δ, the Tolman length, which controls the size-dependence of the non-classical surface tension, and Σ_0, the constant surface tension of the classical case. These parameters and how they fit into the non-classical nucleation theory are described in more detail in Chapter 4.

The choice of an LGA model and the decision to limit the study to two dimensions was inspired by ease of implementation, ease of testing, and low computational memory requirements allowing for faster simulation runs. All the essential features and parameters of the three-dimensional case of the CNT also exist in the two-dimensional case, as outlined in section 2.1, and the same is true for the non-classical features that are presented in Chapter 4. Furthermore, two-dimensional precipitate nucleation has practical applications – for example, it is one of the mechanisms by which crystal growth occurs on a smooth surface, as described in section 2.3.2.

As it applies to nucleation phenomena, this combination of LGA molecular dynamics, first-passage time statistics, and the use of the Tolman length concept is novel and allows one to make a straightforward investigation of the effect of radius-dependent surface tension in two-dimensional oversaturated systems. Additionally, the use of an exact analytical solution to the Tolman expression in two-dimensions appears not to have been

done before in research on nucleation. This study provides a necessary first-step before investigating nucleation in more realistic three-dimensional systems using this method.

A multitude of other approaches has been used with the goal of developing a better understanding of the nucleation process beyond CNT. Some of the major approaches are described in section 2.2 and include molecular dynamics computational simulations, models based on density functional theory calculations, and phenomenological and semi-empirical models [Laaksonen 1995, Gránásy 1999a, Ruckenstein 2005]. Molecular dynamics simulation offers the advantage of allowing the researcher to work within a microscopic viewpoint of nucleation, but it is often limited by vast computational memory requirements. Molecular models based on the density functional theory are reported to provide impressive results regarding the nucleation of simple systems, and the phenomenological diffuse interface theory, as well as the semi-empirical modeling approaches, correspond well with experiments[Gránásy 1999a, Ruckenstein 2005]. However, the relative simplicity of the LGA approach presented here makes it a practical tool to probe nucleation phenomena beyond the classical case. An additional advantage of this method is that it offers a straightforward and pedagogical presentation of nucleation and growth phenomena.

1.3 Thesis Outline

The thesis begins with a review of nucleation and growth theory in Chapter 2. The central elements of the CNT are derived and important non-classical theories of nucleation are discussed, followed by a brief overview of the steps involved in the crystal growth phase, which follows nucleation.

Chapter 3 presents a description of the microscopic LGA model of nucleation and growth used to obtain the simulation data for this study.

Chapter 4 provides derivations of the analytical results pertaining to the simulation, including the incorporation of surface tension dependence on crystal size into the nucleation theory, the behaviour of the concentration in a supersaturated system as a function of space and time, and the growth of a cluster's radius as a function of time under different boundary conditions of the system.

Chapter 5 presents the mean-first passage time (MFPT) technique of Wedekind et al. [Wedekind 2007], and explains how it is used in this research to extract the values of the nucleation rate and critical nucleus size from the simulation data.

Chapter 6 contains the research results and a discussion. From the analysis of the simulation data generated by the two-dimensional LGA model, we will see that the inclusion of a radius-dependent surface tension allows for an improved agreement between the simulation data and theory when compared to the CNT. Plots of the parameters δ and Σ_0 as functions of molecular bonding energies are analyzed and interpreted.

The thesis ends with a conclusion, acknowledgements, six appendices containing additional mathematical derivations, an appendix containing the simulation code, and a list of references.

Chapter 2

Review of Nucleation and Growth Theory

In this chapter, we begin with a derivation of the CNT for precipitation in a two-dimensional supersaturated system, leading up to the classical expressions for the radius of a critical nucleus, R^*, the energy barrier to nucleation, ΔG^*, and the nucleation rate, J. The R^*, ΔG^*, and J equations for the CNT in the three-dimensional case are included, for reference. The CNT for other phase transitions such as liquid droplet formation in vapour, or solid formation in a melt can be derived following the same fundamental steps.

In section 2.2, we review some of the major attempts to advance nucleation theory with new theoretical approaches. These include the phenomenological, kinetic, and microscopic non-classical nucleation theories. In particular, section 2.2.1 describes the phenomenological theory of Dillmann and Meier [Dillmann 1991], which includes an expression for the radius-dependence of the surface tension of a liquid droplet [Tolman

1949] as an extension to the CNT. We will examine a similar modification to the CNT via incorporation of the two-dimensional (exact) form of Tolman's surface tension expression in Chapter 4. That equation is then used to examine the simulation data produced by the nucleation simulations in Chapter 6.

The present chapter concludes (section 2.3) with an overview of the principal mechanisms and theory explaining crystal growth in a supersaturated system, including a brief description of the growth stages of Ostwald ripening and aggregation, which occur at times well beyond the completion of the nucleation stage.

2.1 Derivation of the CNT

The following derivation of the equations for R^*, ΔG^*, and J follows from I. Markov's *Crystal Growth for Beginners* [Markov 2003], which in turn is based on the historical formulation of the CNT. The procedure is followed for nucleation in two dimensions, to correspond with the two-dimensional nucleation simulation that is the focus of this work.

2.1.1 Critical radius, R, and energy barrier to nucleation, ΔG^**

We begin by considering a two-dimensional area of solution at a constant temperature T that contains N_d dissolved solute particles with chemical potential μ_d. In this dissolved state, the free energy of the system is:

$$G_1 = N_d \mu_d .$$

If a small cluster of the solid phase spontaneously forms, its free energy, $G(N)$, will be the sum of the chemical potential of the small cluster's particles plus a free energy "cost" due to the formation of the cluster's perimeter:

$$G(N) = N\mu_s + 2\pi R\sigma_0 , \qquad (2.1)$$

where N is the number of particles in the solid cluster, μ_s is the chemical potential of the solid phase, R is the cluster's (effective) radius, and σ_0 is the (constant) two-dimensional surface tension in the solid phase. As discussed in Chapter 1, the equilibrium shape (circular, in two dimensions) and constant surface tension assumption in Eq (2.1) are a part of the capillarity approximation, which is considered to be a key problem with the CNT.

Let us take a moment to define the effective radius. In the lattice gas automata model presented in Chapter 3, the crystal phase grows on a square lattice, as a cluster of square molecules. Because the clusters that form in the simulations may have complex, non-circular shapes, we describe a crystal by its effective radius, which is the radius the crystal would have if its N crystal particles were arranged to fit into a circle having the same total area, Na, as the crystal, where a is the molecular area of a crystal particle. The effective radius is then $R = \sqrt{Na/\pi}$, and this can be re-expressed in terms of N, as:

$$N = \pi R^2 / a . \qquad (2.2)$$

Now, the change in free energy of the system upon the formation of a single solid cluster, $\Delta G(N)$, is equal to $G(N)$ minus the product $N\mu_d$ (the chemical potential of the particles having been removed from the dissolved phase):

$$\begin{aligned}\Delta G(N) &= N\mu_s + 2\pi R\sigma_0 - N\mu_d \\ &= -N(\mu_d - \mu_s) + 2\pi R\sigma_0.\end{aligned} \tag{2.3}$$

Substituting N with R as per Eq. (2.2) into Eq. (2.3) gives us:

$$\Delta G(R) = -\frac{\pi R^2}{a}\Delta\mu + 2\pi R\sigma_0\,, \tag{2.4}$$

where $\Delta\mu = \mu_d - \mu_s$. $\Delta G(R)$ has a parabolic form (Fig. 2.1) with the maximum located at the critical radius size:

$$R^* = \sigma_0 a/\Delta\mu\,, \tag{2.5}$$

in the case when the solid phase is more stable than the dissolved phase ($\mu_s < \mu_d$). The value of the energy barrier to nucleation is then:

$$\Delta G^* = \Delta G(R^*) = \frac{\pi a {\sigma_0}^2}{\Delta\mu}\,. \tag{2.6}$$

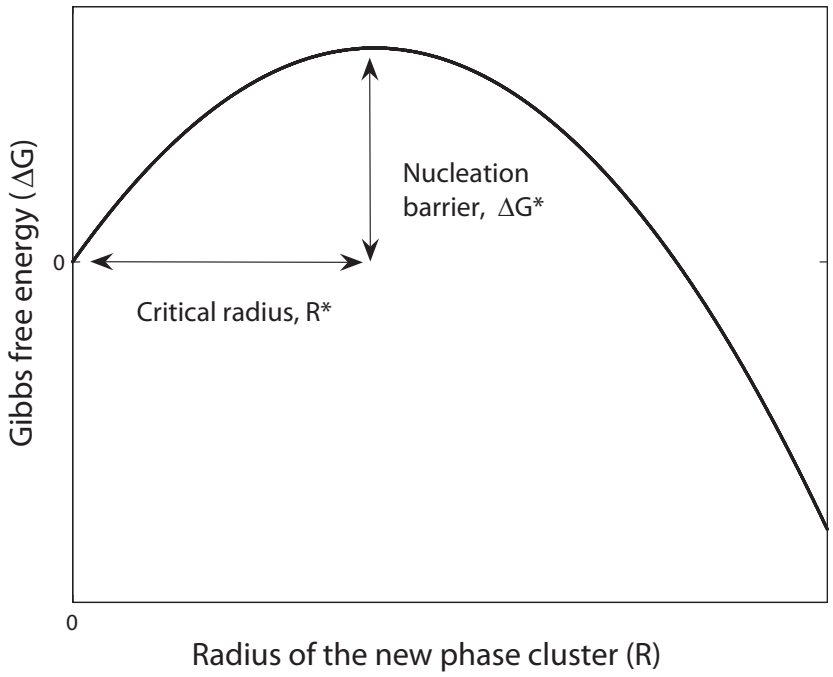

FIG. 2.1. Free energy barrier to nucleation in the two-dimensional CNT.

2.1.2 Nucleation rate, J

In addition to the capillarity approximation, and the assumption that new-phase clusters have the equilibrium (circular) shape, the derivation of the nucleation rate is made possible with the aid of the simplifying assumptions that i) clusters of a size $M >> N^*$ are removed from the system and replaced by an equivalent number of dissolved particles, in order to maintain a constant system concentration, and ii) the growth and decay of precipitate clusters only happens one molecule at a time.

We begin by looking at the rate of change of concentration C_N of all clusters of size N in the system, $dC_N(t)/dt$, which is determined by the rates of attachment of particles to

clusters of size N and N-1, and of detachment of particles from clusters of size N and N+1 as follows:

$$\frac{dC_N(t)}{dt} = \omega_{N-1}{}^{+}C_{N-1}(t) - \omega_N{}^{-}C_N(t) - \omega_N{}^{+}C_N(t) + \omega_{N+1}{}^{-}C_{N+1}(t), \qquad (2.7)$$

where $\omega_N{}^{+}$ and $\omega_N{}^{-}$ indicate the rate constants for single-particle attachment (forward reaction) and detachment (reverse reaction) from the cluster.

The net flux of clusters increasing from size N-1 to N particles is equal to

$$J_N = \omega_{N-1}{}^{+}C_{N-1}(t) - \omega_N{}^{-}C_N(t),$$

which means that Eq. (2.7) can be re-written as follows:

$$\frac{dC_N(t)}{dt} = J_N(t) - J_{N+1}(t). \qquad (2.8)$$

After a certain time, the system reaches a steady state in which the concentrations C_N do not change with respect to time. Substituting $dC_N(t)/dt = 0$ into Eq. (2.8), allows us to define the steady state nucleation rate, J_{ss}:

$$J_N(t) = J_{N+1}(t) = J_{ss}$$

where J_{ss} is also equal to J_{N^*}, the steady state nucleation rate at the critical nucleus size. In fact, we can write out the following list of equalities to J_{ss}:

$$
\begin{aligned}
J_{ss} &= \omega_1^{+} C_1 - \omega_2^{-} C_2, \\
J_{ss} &= \omega_2^{+} C_2 - \omega_3^{-} C_3, \\
&\cdots \\
J_{ss} &= \omega_N^{+} C_N - \omega_{N+1}^{-} C_{N+1}, \\
&\cdots \\
J_{ss} &= \omega_{M-1}^{+} C_{M-1}.
\end{aligned}
\tag{2.9}
$$

Recall that $C_M = 0$ as in the first assumption, above. Now multiply the first equation in Eq. (2.9) by $1/\omega_1^{+}$, the second equation by $\omega_2^{-}/\omega_1^{+}\omega_2^{+}$, up to the *N*th equation, which is multiplied by $\omega_2^{-}\omega_3^{-}\ldots\omega_N^{-}/\omega_1^{+}\omega_2^{+}\ldots\omega_N^{+}$. After summing up the resulting equations and reorganizing, we obtain the general expression for the steady state nucleation rate first presented by Becker and Doring [Markov 2003]:

$$
J_{ss} = C_1 \left[\sum_{N=1}^{M-1} \left(\frac{1}{\omega_N^{+}} \frac{\omega_2^{-}\omega_3^{-}\ldots\omega_N^{-}}{\omega_1^{+}\omega_2^{+}\ldots\omega_{N-1}^{+}} \right) \right]^{-1} \tag{2.10}
$$

Here ω_0^{+} and ω_1^{-} have been defined to be equal to unity.

The next step relates the sum of ratios of rate constants in Eq. (2.10) to the free energy of a precipitate cluster. Following Markov, in the case of condensation of a liquid droplet from a vapour, the ratio of reverse and forward rate constants, $\omega_N^{-}/\omega_{N-1}^{+}$, can be related to the cluster's radius by way of the Thompson-Gibbs equation, as shown in Appendix A. Markov states that the result is the same for precipitate formation from solution, and that it takes the form:

$$\frac{\omega_2^- \omega_3^- \ldots \omega_N^-}{\omega_1^+ \omega_2^+ \ldots \omega_{N-1}^+} = \exp\left\{\frac{\Delta G(N)}{k_B T}\right\}. \tag{2.11}$$

Combining Eq. (2.11) with Eq. (A.7), from Appendix A, and noticing that $\Delta G^* = \Delta G(N^*) = \sigma_0 \sqrt{\pi a N^*}$, we re-write Eq. (2.10), replacing the product of rate constants that appears in the sum:

$$J_{ss} = C_1 \left(\sum_{N=1}^{M-1} \left(\frac{1}{\omega_N^+} \exp\left\{ \frac{\Delta G^*}{k_B T} \left[2\left(\frac{N}{N^*} \right)^{1/2} - \frac{N}{N^*} \right] \right\} \right) \right)^{-1}. \tag{2.12}$$

Next, we replace the sum in Eq. (2.12) with an integral:

$$J_{ss} = C_1 \left(\int_1^{M-1} \frac{1}{\omega_N^+} \exp\left\{ \frac{\Delta G^*}{k_B T} \left[2\left(\frac{N}{N^*} \right)^{1/2} - \frac{N}{N^*} \right] \right\} dN \right)^{-1}, \tag{2.13}$$

then Taylor-expand the argument in the exponential on the right-hand side of Eq. (2.13) to facilitate integration:

$$\frac{\Delta G^*}{k_B T} \left[2\left(\frac{N}{N^*} \right)^{1/2} - \frac{N}{N^*} \right] \cong \frac{\Delta G^*}{k_B T} \left[1 - \frac{1}{4} \left(\frac{1}{N^{*2}} \right) (N - N^*)^2 \right], \tag{2.14}$$

and re-insert into Eq. (2.14) to obtain the equation:

$$J_{ss} = C_1 \left(\exp\left(\frac{\Delta G^*}{k_B T} \right) \int_1^{M-1} \frac{1}{\omega_N^+} \exp\left\{ -\frac{\Delta G^*}{k_B T} \frac{1}{4N^{*2}} (N - N^*)^2 \right\} dN \right)^{-1}. \tag{2.15}$$

Two approximations are needed to complete the integration of Eq. (2.15). First, we extend the limits of integration from -∞ to +∞, on the basis that the exponential term within the

integral is sharply peaked in the area near N^*. Second, we assume that the forward rate constant for attachment to a cluster of any size is the same, and therefore $\omega_N^+ \approx \omega^*$, where ω^* is the rate constant for attachment of particles to the critical nucleus. This allows us to integrate as follows, making the substitution $\phi = N - N^*$ on the second line, and using the Gaussian integral solution $\int_{-\infty}^{+\infty} \exp(-cx^2)dx = \sqrt{\pi/c}$, where c is a constant:

$$
\begin{aligned}
J_{ss} &= C_1\left(\frac{1}{\omega^*}\exp\left(\frac{\Delta G^*}{k_B T}\right)\int_{-\infty}^{\infty}\exp\left\{-\frac{\Delta G^*}{k_B T}\frac{1}{4N^{*2}}(N-N^*)^2\right\}dN\right)^{-1} \\
&= C_1\omega^*\exp\left(-\frac{\Delta G^*}{k_B T}\right)\left(\int_{-\infty}^{\infty}\exp\left\{-\frac{\Delta G^*}{k_B T}\frac{1}{4N^{*2}}(\phi)^2\right\}d\phi\right)^{-1} \\
&= C_1\omega^*\exp\left(-\frac{\Delta G^*}{k_B T}\right)\left(\sqrt{\frac{\Delta G^*}{4\pi k_B T N^{*2}}}\right) \\
&= C_1\omega^* Z\exp\left(-\frac{\Delta G^*}{k_B T}\right),
\end{aligned}
$$

where $Z = \sqrt{\Delta G^*/4\pi k_B T N^{*2}}$ is called the Zeldovich factor. This factor indicates the degree to which the distribution of cluster sizes in the supersatured system under steady-state conditions differs from the distribution of cluster sizes under equilibrium conditions [Markov 2003].

C_1 represents the concentration of single molecules in the parent phase. Since nucleation occurs at early time, we assume that the concentration of solute at the cluster surface, is approximately equal to the initial concentration, C_{in}: $C_1(R,t) = C(R,t) \approx C_{in}$ We therefore write the nucleation rate as follows:

$$J_{ss} \approx C_{in}\omega^* Z \exp\left(\frac{-\Delta G^*}{k_B T}\right) \equiv J \,. \tag{2.16}$$

The equation for $J_{ss} \equiv J$ shown in Eq. (2.16) is the CNT result, containing the constant surface tension σ_0. In Chapter 4 we will introduce an extension to the CNT which includes a radius-dependent surface tension, σ, that modifies ΔG^* in Eq. (2.16).

Let us also define the system's supersaturation, $S = C(r,t)/C_{eq}$, where $C(r,t)$ is the system concentration as a function of the radial distance, r, from the system centre, and time, t, and C_{eq} is the equilibrium concentration of the system (the concentration at which cluster growth or dissolution do not occur, on average). One of the objects of this study is to examine the nucleation rate as a function of supersaturation, as we will see in Chapters 4 and 6.

2.1.3 CNT in three dimensions

The three-dimensional form of the CNT equations for R^*, ΔG^*, and J are as follows:

$$R^* = \frac{2\bar{\sigma}_0 v}{\Delta\mu}$$

$$\Delta G^* = \frac{16\pi}{3}\frac{\bar{\sigma}_0^{\,3} v^2}{\Delta\mu^2}$$

$$J = C_{in}\omega^* Z \exp\left(-\frac{\Delta G^*}{k_B T}\right) \tag{2.17}$$

where $\overline{\sigma}_0$ represents the standard surface tension in three dimensions, with units of energy divided by surface area, v is the volume of a new phase molecule, and $Z = \sqrt{\Delta G^* / 3\pi kTN^{*2}}$ in the three-dimensional case.

2.2 Non-Classical Theories of Nucleation

Many efforts have been made to improve nucleation theory, either by making modifications to the CNT or by introducing alternative approaches. Theories that aim to explain nucleation phenomena beyond the limitations of the CNT are termed "non-classical" in the literature.

Non-classical nucleation theories that may be categorized as **phenomenological** make use of macroscopic thermodynamic parameters, and consist of attempts to modify and extend the standard CNT. These include the Dillmann-Meier theory, the self-consistent classical theory, and the diffuse interface theory [Laaksonen 1995, Gránásy 1999a].

Kinetic theories begin with Eq. (2.7) in order to determine how $C_N(t)$ changes with time during nucleation. A non-classical kinetic theory of nucleation was proposed by Nowakowski and Ruckenstein [Ruckenstein 1990, Nowakowski 1991, Ruckenstein 2005] that allows calculation of the nucleation rate without requiring calculation of ΔG^* and without explicitly requiring the capillarity approximation or the macroscopic surface tension term of the CNT. However, this model depends on the intermolecular potentials between particles, for which the relevant parameters must be determined by fitting to experimental data for the surface tension and density [Laaksonen 1995].

Non-classical nucleation theories that begin from the interactions of molecules are categorized as **microscopic** and consist primarily of density functional theories. These model the nuclei as fluctuations in the (continuous) density of the system, and the thermodynamic quantities, such as the system's free energy, as functionals of the density profile. In this method, maxima and minima in the free energy landscape determine the equilibrium density profile of the system under study, which is then used to determine the microscopic nucleation parameters.

Phenomenological, kinetic, and microscopic non-classical nucleation theories can be evaluated in comparison to experimental or simulated nucleation data. However, experimental data for nucleation is often difficult to obtain, especially in the case of crystal precipitation [MacFarlane 1983, Laaksonen 1995], meaning that simulation data is often required in order to evaluate a non-classical nucleation theory. Microscopic **simulations** have the advantage of providing data on the level of molecular interactions, allowing one to examine nucleation behaviour in the immediate vicinity of the nucleation barrier, for example [Gránásy 1999a]. Molecular dynamics and Monte Carlo simulations are two commonly used simulation methods, and are discussed below. The Lattice Gas Automata method that is the focus of this work is described in detail in Chapter 3.

2.2.1 Phenomenological non-classical theories of nucleation

The **Dillmann-Meier Theory (DMT)** is a modification of the (three-dimensional) CNT that incorporates a surface tension dependence on nucleus size, as well as translational, rotational, vibrational, and configurational degrees of freedom [Dillmann 1991]. The size-

dependence term is known as the "Tolman expression" for surface tension, and was derived by R. Tolman in 1949 [Tolman 1949]. In the DMT, the free energy in the nucleating system takes the form:

$$\Delta G(N) = f_{DMT}(N)\overline{\sigma}_0 A_s(N) + d_0 \ln(N) - \ln(q_0 V(N)) - N\Delta\mu,$$

where $A_s(N)$ and $V(N)$ are the surface area and volume of the nucleus as functions of N, d_0 and q_0 are variables that account for the supplementary degrees of freedom, and $f_{DMT}(N)$ is an approximation of the Tolman expression in three dimensions:

$$f_{DMT}(N) = 1 + \alpha' N^{-1/3} + \alpha'' N^{-2/3}.$$

In the DMT, α' and α'' are parameters that are chosen based on the fluid's saturated vapour pressure and the second coefficient of its virial equation of state. For the formation of liquid droplets from the gas phase of nonane and water, the DMT predicts nucleation rates that are much closer to experimentally measured rates than the predictions of the CNT [Dillmann 1991, Laaksonen 1995]. In Appendix B (referred to in Chapter 4), we derive the exact form of the Tolman expression in two dimensions – in that case, a single parameter, δ, controls radius-dependence of the (two-dimensional) surface tension.

Self-consistent classical theories of nucleation (SCCT) address two issues where self-consistency is lacking in the CNT. The first is that the CNT does not predict $\Delta G = 0$ for the formation of a one-particle cluster (monomer). The energy barrier to nucleation is corrected by simply subtracting the free energy of the system containing one monomer of the new phase, $\Delta G(1)$, from the energy barrier in the CNT case [Goodrich 1963, Wilemski 1995, Gránásy 1999a]:

$$\Delta G^*_{SCCT} = \Delta G^* - \Delta G(1)$$

The second self-consistency problem regards the failure of the CNT to obey the law of mass action for the equilibrium concentration of a nucleating cluster [Wilemski 1995]. This was first corrected by G. Courtney [Courtney 1961], by specifying the partial pressure of a (liquid drop) cluster in the change of chemical potential ($\Delta\mu$) for molecules leaving the parent phase and joining the nucleus. Taking the two self-consistency corrections into account, the SCCT's propose an extra multiplicative factor of $e^{\theta/S}$ in the nucleation rate (Eq. (2.16)) [Girschick 1990, Wilemski 1995], where $\theta = A_s\overline{\sigma}_0/k_BT$, A_s is the surface area of the cluster, and S is the supersaturation. This result was incorporated into a kinetic nucleation theory by Kalikmanov and van Dongen who obtained positive results for vapour-liquid nucleation for nonpolar chemicals [Kalikmanov 1993].

The **diffuse interface theory (DIT)** put forward by Gránásy [1993, 1994, 1996] pictures a nucleating cluster that has the properties of the bulk solid phase at its centre, surrounded by an interface region of a set thickness that does not depend on the radius of the cluster. By writing the Gibbs energy as a function of distance from the centre of the cluster, $\Delta G(r)$, in terms of the system's enthalpy and entropy times temperature profiles, and by assuming a constant length scale δ_{DIT} that characterizes the difference between these profiles at the cluster surface, a radius-dependence of surface tension appears and depends on the single parameter δ_{DIT}. This contrasts with the DMT and SCCT approaches, which both use at least two additional parameters to achieve a radius-dependent surface tension. The DIT is reported to produce positive results in comparison with experimental results for the nucleation of nonane and toluene, but not for polar substances [Laaksonen 1995].

2.2.2 Kinetic non-classical theory of nucleation

In the classical kinetic theory of nucleation, Eq. (2.7) is reduced to continuous form by making the assumption that $N >> 1$ (capillarity approximation), and by Taylor expanding the right-hand side and truncating after the lowest order terms. This produces the following partial differential equation [Ruckenstein 2005]:

$$\frac{\partial C_N(t)}{\partial t} = \frac{\partial}{\partial N}\left(A(N)C_N(t)\right) + \frac{\partial^2}{\partial N^2}\left(B(N)C_N(t)\right), \qquad (2.18)$$

where the coefficients $A(N)$ and $B(N)$ are related to the rates of particle detachment from and attachment to the cluster. When Eq. (2.18) is solved under the appropriate boundary conditions, the steady state nucleation rate can be obtained. However, in the classical case, the calculation of ω_N^- requires the use of the capillarity approximation.

Nowakowski and Ruckenstein's non-classical kinetic theory avoids this problem by modeling particle detachment as the escape of molecules from a potential well surrounding the cluster, and by using the mean passage time of this process to calculate ω_N^-. The result is that ω_N^- depends on the intermolecular potential of the parent phase as well as the crystal structure of the nucleating solid. Nucleation rates predicted by this theory were greater than those predicted by CNT. Extensions of the model to include aspects of the density functional theory have been proposed, e.g., by allowing the density profile of the nucleating cluster to be non-uniform.

2.2.3 Microscopic non-classical theories of nucleation

The density functional theory (DFT) has been applied as a means of examining the thermodynamics of nucleation, beginning from the interactions of the molecules in a nucleating system [Oxtoby 1988, Zeng 1991, Talanquer 1994], This is done by considering the entire system, including the nucleating cluster, as an inhomogeneous fluid with density $\rho(r)$, composed of molecules that interact through a predefined potential, $\varphi(r)$, where r is the position from the centre of the system. Within the crystal, $\rho(r)$ is usually represented by Gaussian functions centred around the crystal's lattice points [Gránásy 1999a].

The thermodynamic equilibrium points of the system are found by solving the equation

$$d\Omega[\rho(r)] / d\rho(r) = 0\,, \tag{2.19}$$

where $\Omega[\rho(r)] = F[\rho(r)] - \mu\int \rho(r)dr$ is the grand potential functional of the system and $F[\rho(r)]$ is the system's Helmholtz free energy, which depends uniquely on the density [Zeng 1991, Oxtoby 2003]. Since N^* is located at an unstable equilibrium point, an iterative method must be used to determine its location following Eq. (2.19) and, correspondingly, the value of ΔG^* can be found.

In the DFT method, the molecular interaction potential, $\varphi(r)$, is split into a repulsive part, $\varphi_{rep}(r)$, and an attractive part, $\varphi_{att}(r)$, such that $\varphi(r) = \varphi_{rep}(r) + \varphi_{att}(r)$. The $\varphi_{rep}(r)$ and $\varphi_{att}(r)$ potentials can be further divided into long and short-range components. Likewise, the free energy functional, F, can be split into two parts, F_{ref} and F_{ex}, where F_{ref} is the free

energy of a reference system for which the particles are subject only to the repulsive part of the potential, $\varphi_{rep}(r)$, and F_{ex}, called the "excess" contribution to the free energy, corresponds to the attractive portion of the potential, $\varphi_{att}(r)$ [Gránásy 1999a, Ruckenstein 2005]. The F_{ref} can be calculated directly in the case of vapour-liquid nucleation, by using the ideal gas as a reference system. However, in the case of crystal nucleation, both the calculations of F_{ref} and F_{ex} require approximations, and it is through the application of different approximation methods that the various DFT approaches originate [Oxtoby 1991, Gránásy 1999a, Ruckenstein 2005].

As an example, the first DFT model of the crystal-liquid interface, proposed by Haymet and Oxtoby [Haymet 1981], employed a "perturbative" approach which handled the $F_{ex}[\rho(r)]$ term by making a Taylor expansion with respect to the local difference between the densities of the nucleating solid and the liquid, $\Delta\rho(r)$. Truncation of the expansion of $F_{ex}[\rho(r)]$ after the second order term was problematic due to the size of $\Delta\rho(r)$ in comparison to the density of the liquid. This issue was later resolved using an approach known as the "weighted density approximation", in which the real density is smoothed out using a weighting function to reduce the high density variability throughout the nucleating structure. More recent methods to evaluate the free energy functional have been developed, including an adaptation of fundamental-measure theory for hard spheres, in which the density weighting function is tailored to the geometry of the molecules forming the nucleating cluster [Oxtoby 2003, Lutsko 2008].

What makes the DFT attractive is its continuous density profile, which allows nucleation to be investigated without needing to make use of the capillarity approximation,

and consequently without needing to include a macroscopic surface tension term. Rather, the surface tension can be determined (for large enough crystals) from the microscopic parameters, such as the chemical potential. DFT has been used to plot surface tension variation with temperature [Zeng 1991, Gránásy 1999a, Gránásy 1999b] and compared to simulation results favourably. The DFT method is not used to calculate nucleation rates directly, but rather provides predictions of the critical nucleus size and the energy barrier to nucleation. In order to calculate nucleation rates, an estimate of the prefactor $C_{in}\omega^{*}Z$ in Eq. (2.17) is needed, and can be obtained from other non-classical nucleation models. A limitation to the calculation of nucleation rates remains the accuracy of the interaction potentials used in the DFT method [Oxtoby 2003].

The DFT approach to nucleation continues to be developed in concert with advancing simulation methods [Lotsku 2008, Ghosh 2011]. In 2005, Ruckenstein proposed that DFT techniques could be added to his non-classical, kinetic theory of nucleation in order to provide needed detail on the density profile of the nucleating cluster. In 2008, Lutsko demonstrated how a technique for exploring free energy surfaces called the "nudged elastic band" method could be used to expedite the iterative process required in solving Eq. (2.19) in the case of nucleation.

Although the application of the DFT to crystal nucleation from liquid is more difficult than in the case of vapour condensation, due to the need to represent $\rho(r)$ using multiple order parameters, and because of the requirement of weighting approximations in the calculation of F_{ref}, methods exist to reduce the complexity of the problem [Gránásy

1999a, Oxtoby 2003], and there is hope that the DFT approach will further advance the theory of nucleation [Zhang 2008, Ghosh 2011].

2.2.4 Molecular dynamics and Monte Carlo simulations of nucleation

Molecular dynamics (MD) and Monte Carlo (MC) are the two predominant methods used to simulate nucleation. In the MD approach, all simulated particles begin with an initial velocity and position. The dynamics of every particle in the simulation is calculated using Newton's laws, determining the new positions and velocities of every particle at the subsequent time step. The MC approach uses random numbers and the equations of statistical thermodynamics to model how a system of particles evolves in time. In both methods, one must wait a sufficiently long time for nucleation to occur, depending on simulation parameters such as the system size, temperature, initial concentration, the intermolecular potential, etc. Furthermore, simulated nucleation events may be missed due to their rare occurrence, depending on how the system is sampled for results.

"Umbrella sampling" is one example of a technique that has been applied to MD and MC nucleation simulations to improve efficiency by allowing the researcher to stabilize clusters of any size, including the critical size [Torrie 1974, van Duijneveldt 1992, ten Wolde 1994]. This is accomplished by adding a fictitious potential to the real potential energy function of the system in order to bias system states with a certain (e.g. high) free energy. In this way, the critical nucleus can be examined and N^* and ΔG^* can be obtained.

Computational techniques for simulating nucleation continue to develop, and a large variety of approaches are used to determine nucleation rates and critical nucleus sizes

[Chkonia 2009, Fillion 2011, Saika-Voivod 2011]. However, as noted by L. Fillion et al. in the title of a recent publication, "the discrepancy between experiment and simulation persists" [Fillion 2011]. The LGA model presented in Chapter 3 is a cellular automata MC simulation, where the movement of particles and growth of crystals are constrained to lattices in order to enhance the simplicity and efficiency of the simulations.

2.3 Crystal Growth

Following the formation of a stable nucleus of a new phase in a supersaturated system, the growth process begins. Crystal growth occurs as a result of the diffusion of solute particles to the crystal surface, followed by attachment of these particles to the surface by chemical reaction. Attached surface particles may diffuse along the crystal surface, and as a result are most likely to spend the longest time at surface sites where the chemical bonds with other crystal particles are greatest – these positions are called "high-energy" bonding sites, and take the shape of kinks and molecular edges that lie upon the crystal surface [Katsev 2002, Markov 2003, Zhang 2008, Marchand 2009b].

Reviews of crystal growth draw a distinction between growth on *rough* crystal surfaces and growth on *smooth* crystal surfaces [Katsev 2002, Markov 2003, Zhang 2008, Marchand 2009b]. A rough surface is one for which there are many available attachment sites (kinks and edges) for incoming particles to bond to. Growth on a rough surface occurs by the "normal" growth mechanism [Markov 2003], so-called because the new solid matter is added in a direction normal to the crystal surface, on the average. Precipitation from solution under high supersaturation conditions occurs as normal growth [Katsev 2002].

There are few edges or kinks on a smooth crystal surface. As a result, any edge that happens to form serves as the most energetically favourable site for more growth to occur, and the crystal tends to grow in an orderly fashion, creating a series of smooth layers. Alternatively, in the presence of a screw dislocation, a spiral growth pattern can emerge. Crystals in contact with their vapour phase and growing by sublimation often experience one of the smooth surface growth mechanisms [Markov 2003].

A smooth crystal surface can undergo a roughening transition, changing it into a rough surface. In the case of precipitation, this occurs if the supersaturation increases, and for a melt, the transition takes place if there is an increase in the undercooling [Pavlovska 1971].

2.3.1 Crystal growth on a rough surface

A rough surface has many available "high-energy" bonding sites. We can therefore assume that diffusion of attached particles along the crystal surface will be negligible in the rough surface case, since attached particles are likely to remain for a long time in the position in which they first make contact with the crystal surface, or after only a small number of surface diffusion steps. Under this assumption, the crystal growth rate is determined by two main factors: the rate at which solute particles are transported to the crystal surface – which depends upon diffusion and advection – and the rate at which the surface attachment reaction is executed.

The growth rate, dR/dt, can be written in the following form, where the supersaturation, *S*, appears as the "driver" of crystal growth:

$$\frac{dR}{dt} = \beta(S-1) \tag{2.20}$$

and where β is called the kinetic coefficient. This simple form was first proposed by McCabe in 1929 [McCabe 1929]. According to Markov, the kinetic coefficient can be expressed as follows in the case of precipitation from solution:

$$\beta = f_0 d_p \left(\frac{d_p}{\lambda_k}\right)^2 \exp\left(-\frac{\Delta U}{k_B T}\right),$$

where f_0 represents the thermal vibration frequency of the atoms at the solute-crystal interface, d_p is the diameter of a solute molecule, λ_k is the average distance between attachment (kink) sites, and ΔU is the energy barrier that must be overcome by the solute particle in the attachment reaction. A similar procedure is followed to derive the growth rate and kinetic coefficient in the case of crystallization from a melt, where the undercooling, ΔT provides the "driving force" for crystallization, rather than the supersaturation [Markov 2003].

Eq. (2.20) applies in the case of "interface reaction" where attachment to the surface is the rate-limiting step in crystal growth [Zhang 2008]. In a supersaturated system where diffusion is the slowest step, the crystal growth rate can be written as:

$$\frac{dR}{dt} = \frac{DvC_{eq}(S-1)}{\delta_L}$$

where D is the diffusion coefficient of the solute and δ_L is the width of a layer of stationary fluid surrounding the crystal [Nielsen 1980]. In Chapter 4, we assume crystal growth by

interface reaction and use Eq. (2.20) in order to calculate the radius vs. time behavior of simulated crystals in the (large time) growth phase.

2.3.2 Crystal growth on a smooth surface

A smooth surface with no kink or edge sites may grow by the layer spreading mechanism, which begins with the nucleation of one or many new two-dimensional surface layers. These two-dimensional nuclei provide bonding sites for solute particles to attach to, allowing the surface layer to grow laterally across the face of the crystal. The size of the crystal increases via the accumulation of layers as this process is repeated.

In the limit for which lateral growth of the surface layer occurs much more quickly than nucleation of the new surface layer, a process called layer-by-layer growth occurs, with growth rate equal to the two-dimensional nucleation rate, J, from Eq. (2.16) multiplied by the area of the crystal face, A_s, and the height of a surface layer, h:

$$\frac{dR}{dt} = JA_s h .$$

However, if surface nucleation occurs before a layer is able to spread completely across the face of the crystal, then multilayer growth occurs. In this case, layers stack up while simultaneously spreading out laterally, in multiple locations on the crystal surface. The overall growth rate can be expressed as follows [Markov 2003]:

$$\frac{dR}{dt} = h(Jv_s^{\,2})^{1/3},$$

where v_s is the lateral growth rate of a surface layer.

Two-dimensional surface nucleation only occurs on small crystals [Nielsen 1971], and does not occur at very low concentrations – however, crystal growth can take place under low concentration conditions via the spiral growth mechanism [Nielsen 1969]. In this case, solute molecules attach to bonding sites along the edge of a screw dislocation at the crystal surface, thereby preserving the height difference between the two sides of the screw dislocation. New bonding sites are continuously provided by attached molecules, and a spiral or pyramid shape grows on the surface of the crystal until the structure encounters other crystal surface defects or the edge of the crystal face [Nielsen, 1969]. The rate of crystal growth due to the spiral growth mechanism was described by Burton, Cabrera, and Frank as follows:

$$\frac{dR}{dt} = k_S\left(\frac{S^2}{S'}\right)\tanh\left(\frac{S'}{S}\right),$$

where k_s is a constant, and S' is a supersaturation threshold which separates the growth rate into parabolic (low S) and linear (high S) regimes [Burton 1951].

2.3.3 Ripening and aggregation

During the ripening stage of crystal growth, small crystals dissolve and provide material for large crystals to grow further. If we consider the differential variation in free energy, dG, for a cluster of any size, R, we can obtain the equilibrium concentration, $C_{eq}(R)$, for the cluster at that size. In three dimensions, dG is as follows:

$$dG = \mu_s dN_s + \mu_d dN_d + \bar{\sigma}_0 dA_s,$$

where μ_s and dN_s are the chemical potential and change in number of particles in the solid phase, and μ_d and $dN_d = -dN_s$ are the same quantities in the dissolved phase. Setting $dG = 0$ (the condition at equilibrium for constant temperature and pressure), and bringing in the relationship between the supersaturation and the chemical potential of an ideal solution, $\Delta\mu = k_B T \ln\left(C/C_{eq}\right)$, gives the Gibbs-Thomson relationship for the concentration at the surface of a crystal in equilibrium with its surrounding solution:

$$C_{eq}(R) = C_{eq,\infty} \exp\left(\frac{2\overline{\sigma}_0 v}{R k_B T}\right), \tag{2.21}$$

where $C_{eq,\infty}$ represents the equilibrium concentration for a macroscopic crystal ($R \rightarrow \infty$). As can be seen from Eq. (2.21), the $C_{eq}(R)$ of a small crystal is greater than that of a large crystal. Therefore, as the concentration in the system decreases due to the consumption of solute by the growing crystals, it will eventually reach a level equal to the C_{eq} of small crystals before that of larger crystals. Once the system concentration drops below its $C_{eq}(R)$ value, a crystal will begin to dissolve. In this way, small crystals dissolve and produce solute that may be added to larger crystals in their vicinities [Katsev 2002, Zhang 2008, Marchand 2009b]. As Eq. (2.21) depends on the macroscopic surface tension, it may be subjected to the same criticisms as the CNT if applied to small crystals.

Aggregation is a process whereby two or more crystals combine to make a larger structure. This can happen because of collisions between growing crystals, or through "biotic" mechanisms in which bacteria are said to bring nanocrystals into contact with each other [Rancourt 2005, Zhang 2008]. An aggregated crystal typically contains a large amount of surface and bulk defects [Zhang 2008]. As this thesis focuses on nucleation and growth at

times shortly after nucleation, we will not consider the longer-time processes of aggregation and ripening any further.

Chapter 3

Microscopic Lattice Gas Automata Model

This chapter introduces a Lattice Gas Automata (LGA) model that reproduces the essential aspects of solute diffusion and crystal precipitate nucleation and growth in a generic supersaturated thermodynamic system. Restriction of the model to two dimensions renders its design, implementation, and verification simple and efficient, permitting us to take a direct focus on non-classical nucleation phenomena in the context of a novel microscopic simulation and analysis approach.

We begin with a brief explanation of the modeling philosophy and theoretical basis of LGA modeling of diffusion, including a derivation of the microdynamics of diffusion in a two-dimensional, four-directional (D2Q4) LGA. This is followed by a description of the nucleation and growth model in section 3.2.

3.1 LGA Modeling of Reaction-Diffusion Phenomena

In this age of increasingly powerful and inexpensive computer technology, cellular automata modeling has become a popular method for investigating physical systems. This approach is based on simple interactions between the cells of a lattice, for which all the physical variables (e.g. space, time, and the fields) are discrete. The lattice cells may represent features ranging from the states of a physical system at specific spatial positions to the behaviours of person-like agents [Bonabeau 2002], depending on the nature of the system being simulated. The system evolves as the result of the iterative implementation of these interactions, which obey cellular automata "rules." One goal of physics applications of cellular automata modeling is to see if desired macroscopic physical processes emerge from simple microscopic interaction rules – or, seen from another perspective, cellular automata allow us to model the macroscopic outcome of the repetition of a specific microscopic interaction rule [Chopard 1998].

The LGA is a form of cellular automata modeling that arose with the goal of simulating hydrodynamics and reaction-diffusion processes [Hardy 1976, Frisch 1986, Chopard 1998]. As the LGA model that is presented here makes extensive use of random number generation, this model requires the generation of many realisations in order to produce the data from which the nucleation rate, J, the critical nucleus size, N^*, the cluster radius, $R(t)$, and the concentration of solute in the system $C(r,t)$ are obtained.

3.1.1 Cellular automata rule in the LGA model of diffusion

The application of LGA models to diffusion processes is simpler than for hydrodynamics problems, which require more complex lattice geometries and cellular automata rules in order to conserve energy and momentum in the system [Frisch 1986, Wolfram 1986]. In modeling the diffusion of particles in a "background" fluid, however, the details of the fluid's dynamics are not the focus of study. In this case, the diffusing particles are modeled as random-walkers subject to thermal agitation from the background fluid, and with their movement is restricted to the available directions on a lattice. The background fluid absorbs excess momentum and energy, and in this way the model avoids the need to conserve these quantities. A cellular automata rule can be implemented that models diffusion in this context.

We will consider diffusion of particles on a two dimensional diffusion lattice with the four cardinal directions (north, east, south, and west) available for particle movement. This is known as a "D2Q4" lattice, where "D2" indicates that the lattice is two-dimensional, and "Q4" indicates that there are four directions available for the particles to move in. The first part of the cellular automata rule transfers each particle from its original lattice node to an adjacent lattice node according to the direction in which the particle is pointing. Boundary conditions, such as reflective (non-flux) or constant concentration conditions may be implemented, as described in section 3.2.1.

The second part of the rule simulates collisions between particles arriving at a new lattice node and the resulting changes in the directions of the particles' velocities. At the same time, the rule avoids the accumulation of large numbers of particles at any given lattice

node – this feature is included in the rule following the "exclusion principle" of cellular automata modeling, which is imposed in order to avoid having to use an arbitrarily large number of computational bits to describe the state of a lattice node. The exclusion principle is therefore a means of restricting the computational memory required to run a simulation.

In order to avoid having a large accumulation of particles at a given node, we must not allow a large number of particles to leave any one node. This means that the second part of the rule must imitate the collision of particles while also maintaining an occupancy of at most one particle per lattice direction at each node. This is accomplished by randomly rotating every particle at a lattice node by the same angle (either 0, $\pi/2$, π or $3\pi/2$ rad). A different, random rotation angle is chosen for each lattice node. To achieve an isotropic diffusion field, we choose an equal probability for each of the four rotation options, as we will see below.

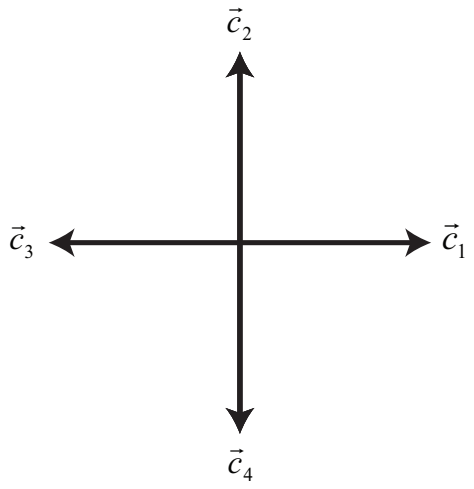

FIG. 3.1. Representation of the velocity directions in a D2Q4 LGA model of diffusion (adapted from [Chopard 1998]).

3.1.2 Microdynamics of the LGA model of diffusion

We follow from the procedure laid out in [Chopard 1998] to demonstrate that Fick's law of diffusion results from the microscopic dynamics of the D2Q4 LGA, in the limit where the lattice spacing goes to infinity and the time step goes to zero.

With the index i = 1…4, the four available lattice directions are labeled $\vec{c}_i$. The number of particles entering a lattice node located at position $\vec{r}$ at time t and pointing in the direction of $\vec{c}_i$ is called the "occupancy number" for that direction, and is represented as $n_i = n_i(\vec{r},t)$. The lattice directions are represented visually in Fig. 3.1. Let l_s be the lattice spacing and t_s the simulation time step. The cellular automata rule that is enacted once per time step and for every lattice node is:

$$n_i(\vec{r} + l_s\vec{c}_i, t + t_s) = \xi_0 n_i + \xi_1 n_{i+1} + \xi_2 n_{i+2} + \xi_3 n_{i+3}, \qquad (3.1)$$

where the i index is cyclic such that $n_{1+3} = n_4$, $n_{2+3} = n_1$, and so on. This rule captures both the transfer and rotation processes described above in section 3.1.1. The angle through which the particle directions are rotated is represented by the Boolean variables, ξ_l ,where l = 0…3. For each lattice node (located at position $\vec{r}$), one of the ξ_l is randomly chosen to equal 1, and the others are set equal to 0, thus selecting one of the rotation angles to implement for that node. Therefore, if $\xi_0 = 1$, then the rotation angle is 0, and particles move to the next cell in the grid without rotation, but if $\xi_1 = 1$, then particles at site $\vec{r}$ undergo a clockwise rotation by an angle of $\pi/2$ before moving on to a neighbouring cell, and so on.

The probability of selecting $\xi_l = 1$ is p_l. We choose $p_1 = p_2 = p_3 = p_4 = p_r = 1/4$ in order to model isotropic diffusion. Seeing that $\overline{\xi}_l = p_r$, where the bar over a variable represents the average over many realizations, and seeing that $p_r \overline{n}_{i+l}$ is the average of $\xi_l n_{i+l}$ we can take the average of Eq. (3.1) and obtain a "lattice Boltzmann" kinetic equation in terms of the rotation angle probability p_r:

$$\overline{n}_i(\vec{r} + l_s\vec{c}_i, t + t_s) - \overline{n}_i(\vec{r}, t) = (p_r - 1)\overline{n}_i(\vec{r}, t) + p_r\left[\overline{n}_{i+1}(\vec{r}, t) + \overline{n}_{i+2}(\vec{r}, t) + \overline{n}_{i+3}(\vec{r}, t)\right]. \quad (3.2)$$

In order to see how the microscopic dynamics compares to the Fick's law view of diffusion, we first do a Taylor expansion of the left hand side of Eq. (3.2) to second order about the coordinate $(\vec{r}, t)$:

$$\overline{n}_i(\vec{r} + l_s\vec{c}_i, t + t_s) - \overline{n}_i(\vec{r}, t) = \left[t_s\partial_t + \frac{t_s^2}{2}\partial_t^2 + l_s(\vec{c}_i \cdot \partial_{\vec{r}}) + \frac{l_s^2}{2}(\vec{c}_i \cdot \partial_{\vec{r}})^2 + t_s l_s(\vec{c}_i \cdot \partial_{\vec{r}}) \right] \overline{n}_i(\vec{r}, t) \quad (3.3)$$

where $\partial_{\vec{r}}$ and ∂_t are the partial derivatives in space and time, respectively. The next step is to apply the Chapman-Enskog expansion [Chopard 1998] to the $\overline{n}_i(\vec{r}, t)$ in the lattice Boltzmann equation Eq. (3.2). In this approach, the average of the occupancy numbers, $\overline{n}_i(\vec{r}, t)$, are expanded in terms of a small parameter, ε:

$$\overline{n}_i = \overline{n}_i^{(0)} + \varepsilon\overline{n}_i^{(1)} + \varepsilon^2\overline{n}^{(2)}{}_i + \ldots$$

where the $\bar{n}_i^{(l)}$ terms are functions of $\vec{r}$ and t. The purpose of this expansion is to represent $\bar{n}_i$ as $\bar{n}_i^{(0)}$ to first order, where $\bar{n}_i^{(0)}$ is the total number of particles divided evenly among the number of directions, and the higher order terms are small perturbations to this value. As explained in [Chopard 1998], in order to compare the microdynamics of this cellular automata rule to diffusion in a macroscopic system, we need to look at the limit where $l_s \to 0$ and $t_s \to 0$. However, in order to obtain a nontrivial solution for the $\bar{n}(r,t)$, it turns out that t_s must approach 0 more quickly than l_s, and that the relationship $l_s^2 / t_s = \text{constant} \neq 0$ must be maintained as $l_s \to 0$ and $t_s \to 0$. We therefore set $t_s \sim \varepsilon^2$ and $l_s \sim \varepsilon$ to account for the difference in the sizes of the time step and lattice spacing.

Under the Chapman-Enskog expansion, the density of particles at position r and time t, $d = \sum_{i=1}^{4} \bar{n}_i^{(0)}$, is equal to the sum of the occupancy numbers over the four directions at that node, and these occupancy numbers are spread evenly among the directions such that $\bar{n}_i^{(0)} = d/4$. Now, looking at the order $O(\varepsilon^1)$ of Eq. (3.2) and Eq. (3.3), we have the following equation:

$$l_s(\vec{c}_i \cdot \partial_{\vec{r}})\bar{n}_i^{(0)} = (p_r - 1)\bar{n}_i^{(1)} + p_r(\bar{n}_{i+1}^{(1)} + \bar{n}_{i+2}^{(1)} + \bar{n}_{i+3}^{(1)}) \qquad (3.4)$$

$\bar{n}_i^{(1)}$ has a solution of the form $\bar{n}_i^{(1)} = \varphi c_{i\alpha} \partial_\alpha d$, where φ is an unknown constant, and $\alpha = 1,2$ represents the two spatial dimensions, summed over using the Einstein summation convention. Then, realizing that $\vec{c}_i = -\vec{c}_{i+2}$, we can write Eq. (3.4) as follows:

$$l_s(\vec{c}_i \cdot \partial_{\vec{r}})\bar{n}_i^{(0)} = (p_r - 1)\varphi c_{i\alpha}\partial_\alpha d + p_r(\varphi c_{i+1\alpha}\partial_\alpha d + \varphi c_{i+2\alpha}\partial_\alpha d + \varphi c_{i+3\alpha}\partial_\alpha d) = -\varphi c_{i\alpha}\partial_\alpha d,$$

which can be simplified by writing $\overline{n}_i^{(0)}$ in terms of d:

$$\frac{l_s}{4}(\vec{c}_i \cdot \partial_{\vec{r}})d = -\varphi c_{i\alpha}\partial_\alpha d \,,$$

such that

$$\varphi = -\frac{l_s}{4},$$

and

$$\overline{n}_i^{(1)} = -\frac{l_s}{4}c_{i\alpha}\partial_\alpha d \,.$$

As a final step, we obtain the diffusion coefficient by considering Eq. (3.2) to 2nd order in ε and sum over the four directions:

$$\sum_{i=1}^{4}\left[t_s\partial_t\overline{n}_i^{(0)} + l_s(\vec{c}_i \cdot \partial_{\vec{r}})\overline{n}_i^{(1)} + \frac{l_s^{\,2}}{2}(\vec{c}_i \cdot \partial_{\vec{r}})^2\overline{n}_i^{(0)}\right] = 0 \,. \qquad (3.5)$$

The above sum is equal to zero since the total number of particles is conserved. Using the solutions for $\overline{n}_i^{(0)}$ and $\overline{n}_i^{(1)}$, and dividing through by t_s, we simplify Eq. (3.5) to:

$$\partial_t d - \partial_\alpha\left[\frac{l_s^{\,2}}{8t_s}\sum_{i=1}^{4} c_{i\alpha}c_{i\beta}\partial_\beta d\right] = 0 \,, \qquad (3.6)$$

where $\beta = 1,2$ is a second index over the two spatial dimensions. Since each velocity $\vec{c}_i$ only has a non-zero component in one of the two spatial dimensions, the sum $\sum_{i=1}^{4} c_{i\alpha} c_{i\beta} = 2\delta_{\alpha\beta}$, where $\delta_{\alpha\beta}$ is the Kronecker delta. Therefore we can write Eq. (3.6) as follows:

$$\partial_t d + \nabla \cdot [-D \nabla d] = 0,$$

here D is the diffusion coefficient:

$$D = \frac{l_s^{\,2}}{4 t_s}.$$

This section provided an analytical view of the microdynamics of diffusion in two-dimensional lattice gas automata model of diffusion. The next section describes how the above diffusion rule is implemented in combination with a reaction rule governing the attachment and detachment of particles to a simulated nucleating/growing crystal.

3.2 Two-dimensional LGA model of Nucleation and Growth

The model operates on a set of distinct computational arrays. The "diffusion" lattice handles the diffusion of solute particles in a background solvent, while a variable number of "crystal" lattices store the nucleating/growing crystals. While, in principle, the model can be used to accommodate multiple crystals growing at the same time, for this study it was restricted to permit only one crystal at a time to grow. In this way, the equilibrium concentration, C_{eq}, can be obtained, following the procedure explained in chapter 4.

Each simulation begins with a pre-determined quantity of solute particles distributed randomly among the diffusion lattice nodes and among the four directional positions at each node. This establishes the initial concentration of the system. Then, diffusion is allowed to take place and collision of solute particles eventually leads to the attachment together of two solute particles, in the formation of a first nucleus of the crystal phase. The particles constituting this nucleus are removed from the diffusion lattice and added to the crystal lattice. While the nucleus persists, it is linked to the diffusion lattice node (called the "seed" node) at which it formed. Other solute particles may be incorporated into the crystal phase if they diffuse onto the seed node, as explained in section 3.2.2, below. Any particle that dissolves from the crystal phase is replaced onto the diffusion lattice at the seed node. For the simulation results presented in this thesis, the seed node was preset as the centre node of the diffusion lattice.

Particles may be present on any node of the diffusion lattice, pointing in one of the four cardinal directions (north, east, south, and west), as per the standard D2Q4 geometry explained in section 3.1.1 [Chopard 1998, Wolf-Gladrow 2005]. The exclusion principle of LGA modeling is applied as explained in that section, as well.

The simulation proceeds by repeating a sequence of four steps: streaming, attachment, rotation, and detachment. Each sequence of four simulation steps occurs during one simulation time step of unit t_s. The simulation is ended either after a set number of time steps have elapsed or once the first crystal of a set maximum size has formed, depending on the simulation data required.

3.2.1 Streaming step

During the streaming step, each particle on each node of the diffusion lattice is moved ("streamed") from its current lattice node to the adjacent node in the direction that the particle is pointing. Therefore, a particle pointing east will move from its present node to the node directly to the right and occupy the east-pointing position on the new node. Every particle on every non-boundary node is streamed in this manner. As the diffusion lattice is a square, two-dimensional lattice of constant lattice spacing of unit l_s, the particles move with a constant speed $c = l_s / t_s$.

Particles streaming toward the boundary are handled differently depending on the adopted boundary condition: with a reflective (i.e., zero mass flux) boundary condition in place, a particle that streams toward the boundary is reflected backwards and remains on the same node at which it began, but will end up pointing in the opposite direction. Therefore, an east-pointing particle on a node next to the eastern boundary of the diffusion lattice will remain on the same node following the streaming step, but will occupy the west-pointing position on that node.

With a constant concentration boundary condition in place, any particle that streams onto a boundary node is removed from the simulation after the detachment step and before the subsequent streaming step. Immediately following the removal of the boundary-node particles, and before the next streaming step occurs, the constant boundary concentration is enforced all along the diffusion lattice boundary by randomly distributing the appropriate number of particles among the boundary nodes and among the four directional positions on each boundary node.

3.2.2 Attachment step

The attachment step follows. At this stage, particles that have streamed to the seed node of the diffusion lattice are evaluated for attachment to the crystal lattice. If there is no crystal existing on the crystal lattice (e.g. initially, or following complete dissolution of a crystal), pairs of particles present at the seed node on the diffusion lattice are evaluated for attachment to each other. If a pair of particles successfully attaches together, then a two-particle crystal is placed at the centre of the crystal lattice. On the other hand, if a particle diffuses onto the seed node and a crystal is already present on the crystal lattice, then the particle may attach to one of the sites on the crystal surface that is accessible to the incoming particle. These sites are the crystal lattice nodes representing crystal surface edges having normal vectors opposite in direction to the incoming particle's velocity, and which are not screened from the path of the particle by other crystal particles. Fig. 3.2 shows an example of the accessible sites on an existing crystal for attachment of a particle streaming toward the crystal from the west (i.e. the approaching particle has an east-pointing velocity).

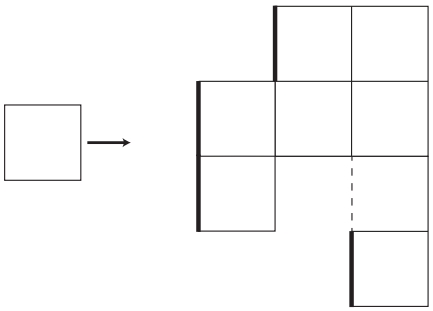

FIG. 3.2. Example of accessible sites for solute particle attachment on a simulated crystal. Solid, darkened lines represent accessible sites on an existing crystal for attachment of a solute particle streaming toward the crystal from the west. Dashed line represents a site which is screened by a portion of the crystal – the site is inaccessible for attachment by the incoming solute particle.

The evaluation for success or failure of attachment makes use of the bonding energy input parameters for solid-to-solid bonds, solid-to-water bonds, and next-to-nearest neighbour bonds. Solute (unattached) particles are considered to have each of their four bonding sites (one per cardinal direction) occupied by solid-to-water bonds with bonding energy E_{sw}. Upon attachment to a crystal, a solid-to-water bond is replaced by one solid-to-solid bond with bonding energy E_{ss} for each cardinal direction where the newly added particle touches the crystal. Therefore, there may be one, two, or three new solid-to-solid bonds replacing solid-to-water bonds between the newly added particle and the crystal face at the attachment location (see Fig. 3.3). Next-to-nearest neighbour bonds to the crystal edge (along the diagonal directions) are considered to be solid-to-solid bonds of a bonding energy ηE_{ss}, where $0 \leq \eta \leq 1$ is an input parameter that quantifies the proportion of the solid-to-solid bond energy contained in each next-to-nearest neighbour bond. The parameter η can be interpreted as a measure of the range of the solid-to-solid interaction. The total free energy of a crystal is then:

$$E = N_{ss}E_{ss} + N_{sw}E_{sw} + \eta N_{nn}E_{ss}, \qquad (3.7)$$

where N_{ss}, N_{sw}, and N_{nn} are respectively the numbers of solid-to-solid, solid-to-water, and next-to-nearest neighbour bonds of the particles making up the crystal. In practice, only the change in the direct interaction energy, ΔE, needs to be calculated. Note that, as the temperature T is held constant in the model, all energy parameters are scaled by k_BT, where k_B is the Boltzmann constant. Also note that a parameter η_{sw} quantifying the range of the solid-to-water interaction could also be considered in the model. This would add a term of the form $\eta_{sw}(4N - 2N_{nn})E_{sw}$ to Eq. (3.7) where N is the total number of particles in the crystal. Here, we take $\eta_{sw} = 0$ due to the presumably small range of the solid-to-water interaction. This also has the benefit of reducing the parameter space, for simplicity.

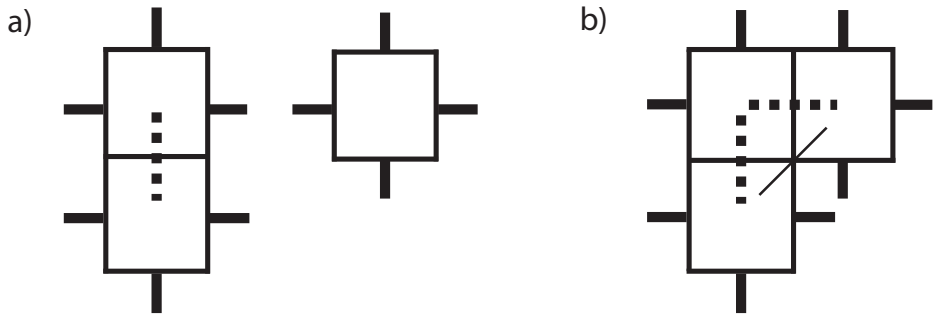

FIG. 3.3. Schematic of an attachment event. (a) A two-particle crystal is held together by one solid-to-solid bond (vertical dashed bar) and has six solid-to-water bonds at its surface (solid bars). A solute particle with four solid-to-water bonds is evaluated for attachment at the eastern attachment site of the top particle of the crystal. (b) The solid particle has attached to the crystal and formed a new solid-to-solid bond (horizontal dashed bar) replacing two solid-to-water bonds. A next-to-nearest neighbour bond to the lower crystal particle is also formed (thin solid bar).

A Metropolis calculation is used to evaluate the success or failure of an attachment attempt [Chopard 1998]. Therefore, a decrease in total energy (negative ΔE) between the case where the incoming particle has attached to the crystal (hypothetical final state) and the original case where the incoming particle is separate from the crystal (initial state) results in automatic addition of the incoming particle to the crystal. However, an increase in total energy (positive ΔE) means that the particle can only be attached to the crystal following a probability determined by the Boltzmann distribution: $p = \exp(-\Delta E)$. Therefore, the probability of attachment, p, is calculated and compared to a uniformly distributed random number, q, between 0 and 1. If $q < p$ the attachment succeeds, but if $q > p$ the attachment fails.

3.2.3 Rotation step

The rotation step is implemented to simulate collisions between diffusing solute particles, as mentioned in section 3.1.1. At every node on the diffusion lattice, a random number is generated which determines the angular rotation of all particles at that node. In order to achieve an isotropic diffusion field, we choose an equal probability for each of the four rotation options ($\pi/2$, π, $3\pi/2$ or 2π rad), resulting in a diffusion coefficient $D = l_s^{\,2} / 4t_s$, as we saw in the previous section [Chopard 1998].

3.2.4 Detachment step

The detachment process is the inverse of the attachment step, where particles may be removed from the crystal lattice and replaced on the corresponding seed node of the diffusion

lattice. For each available cardinal direction on the seed node (in a random order), one crystal surface particle facing in the given direction is evaluated for detachment. The first requirement for detachment is an unoccupied directional position at the associated seed node of the diffusion lattice, in the direction of detachment. If this requirement is met, then a crystal surface particle is randomly chosen from among the crystal surface particles with normal vectors pointing in the available direction on the diffusion lattice which are not screened by other portions of the crystal (similar to the choice of an attachment location, see section 3.2.2 and Fig. 3.2). Evaluation for detachment is then executed, following the same Metropolis scheme as for the attachment step, but with reversed tentative initial and final states.

As a matter of simplification, the model does not permit a crystal to split into multiple pieces. Any single particle that bridges two groups of contiguous particles must therefore remain in place, and does not form part of the set of surface crystal particles eligible for detachment. This avoids the extra calculations that would be involved in modeling inter-crystal particle exchange and aggregation and ripening taking place on a single crystal lattice.

A final dissolution is possible during the detachment step if the crystal on the crystal lattice is composed of only two particles. Given at least two unoccupied positions on the seed node, upon successful dissolution the final two particles are removed from the crystal lattice and placed on the diffusion lattice in distinct directions chosen randomly from among the unoccupied directions available at the seed node.

The above sequence of four steps constitutes the LGA model of nucleation and growth. Fig. 3.4 provides some examples of crystals formed with the same values of E_{ss}, E_{sw},

and the supersaturation, $S = C_{in} / C_{eq}$, and with different values of η. In the next chapter, we will look at the equations used to analyze the simulated nucleation and growth processes.

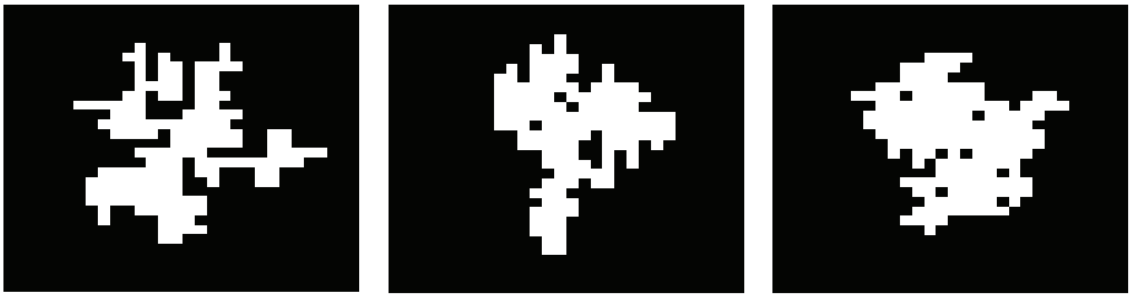

FIG. 3.4. Examples of crystals during the growth phase for parameters Ess = -0.7, Esw = -0.1, S = 3.29 and (a) η = 0, (b) η = 0.5, and (c) η = 1.0.

Chapter 4

Analytical Results Pertaining to the Simulations

The equations that are used in the verification of the simulation and in the analysis of the simulation data are presented here. To begin with, let us define a few dimensionless quantities that will be used frequently in this chapter: $\rho = R/\sqrt{a}$ represents a crystal's effective radius *R*, scaled by the square root of the area, *a*, of a crystal particle; $\Sigma = \sigma\sqrt{a}/kT$ is the radius-dependent (non-classical) surface tension scaled by units of energy divided by length, and; $\Delta g = \Delta G/kT$ is the scaled free energy of the crystal.

This chapter beings with a derivation of the exact form of the Tolman expression, $f(\rho) = \sigma/\sigma_0 = \Sigma/\Sigma_0$, describing surface tension variation as a function of cluster radius in the two-dimensional case, where σ_0 and Σ_0 represent the surface tension (non-scaled and scaled, respectively) in the Classical Nucleation Theory.

In section 4.1, we replace Σ_0 with the radius-dependent surface energy term, $\Sigma = \Sigma_0 f(\rho)$, in the nucleation free energy, ΔG, allowing us to derive the nucleation rate, J, the energy barrier to nucleation, ΔG^*, and critical nucleus size, R^* in the non-classical case.

Section 4.2 contains the analytical results related to crystal growth. We derive expressions for the solute concentration as a function of space and time, $C(r,t)$, under constant concentration boundary and no-flux boundary conditions. From the no-flux boundary condition result, we are able to obtain the equilibrium concentration of the system, $C_{eq}(t)$, which is required in order to determine the supersaturation, S. We also consider the derivations of the crystal's effective radius, $R(t)$, under the two boundary conditions, and see how these results are used to verify the simulation.

4.1 Surface Tension Dependence on Cluster Size

In 1949, Tolman presented a thermodynamic derivation of the surface tension, σ, of a small spherical cluster of a new phase (a liquid droplet in his case) as a function of its radius, introducing the "Tolman length", δ, as a parameter in this function which can be interpreted as a measure of the degree of diffuseness of the cluster's surface [Tolman 1949]. As discussed in Chapter 2, Dillmann and Meier [Dillman 1989, 1991] have previously incorporated an approximation of the Tolman expression as an extension to the CNT in three dimensions.

We adapt this approach in two dimensions in order to obtain Eq. (4.1), the exact form of the Tolman expression relating the dimensionless size-dependent (non-classical) surface

tension, $\Sigma = \sigma\sqrt{a}/kT$, to the dimensionless size-independent (classical) surface tension $\Sigma_0 = \sigma_0\sqrt{a}/kT$. We can interpret the parameter Σ_0 as being the surface tension between two flat faces in the case of an infinitely large planar crystal. However, in the general case of a crystal of arbitrary size having a rough surface, Σ_0 must be interpreted as a macroscopic approximation of the microscopic effects that cause detachment of surface particles (e.g. collisions between solute molecules and crystal surface molecules). The derivation of Tolman does not provide further explanation of Σ_0 in microscopic terms.

We derive the two-dimensional form of the Tolman expression in Appendix B. The result presented there is as follows:

$$f(\rho) = \frac{\Sigma}{\Sigma_0} = \left(1 + \frac{\delta}{\rho} + \frac{\delta^2}{2\rho^2}\right)^{-1/2} \exp(\pi/4) \exp\left(-\tan^{-1}\left(1 + \frac{\delta}{\rho}\right)\right), \qquad (4.1)$$

where $\rho = R/\sqrt{a}$ is the dimensionless crystal radius. Similarly, we will later use $\rho^* = R^*/\sqrt{a}$, the dimensionless radius of a critical nucleus. As expected, the surface tension approaches its classical value as δ goes to 0. $f(\rho)$ is shown in Fig. 4.1 for two values of δ.

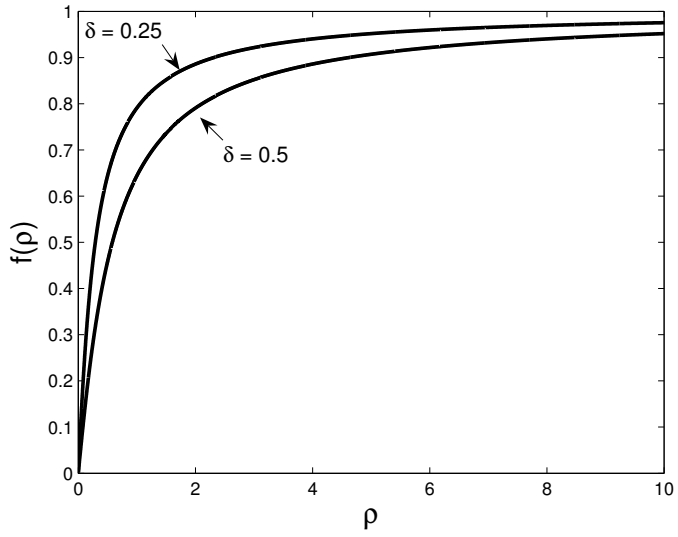

FIG. 4.1. Plot of Eq. (4.1) for $\delta = 0.25$ and $\delta = 0.5$.

As can be seen in Fig. 4.1, Eq. (4.1) predicts a surface tension during the nucleation phase that is lower than the surface tension for a large crystal. Since the nucleation rate depends on the negative exponential of Σ_0 (see Eq. (2.16) with (2.6)), a surface tension smaller than the bulk value of Σ_0 leads to a larger nucleation rate. This feature is promising because, as noted in Chapter 1, a principal concern regarding the CNT is that its predictions for crystal nucleation rates are too low by several orders of magnitude when compared to experiments.

A word about the physical interpretation of the δ parameter would be helpful at this point. δ is defined as the radial distance from the perimeter (located at a distance R from the crystal centre), of a simulated crystal to a hypothetical sharp interface located at a point where the difference in the total amount of matter in the actual system and the sharp interface system, per unit surface (i.e. circumference), is zero (see Fig. 4.2 and Appendix B). The size of δ therefore depends on the crystal density profile in the regions $r < R$ and $r > R$. For

example, a crystal that is densely packed in the region $r < R$ but which spreads out sparsely at distances greater than R will have a larger value of δ. On the other hand, for a crystal with the same low density at distances greater than R but that is less compact for $r < R$, the value of δ will be smaller (see Fig. 4.3).

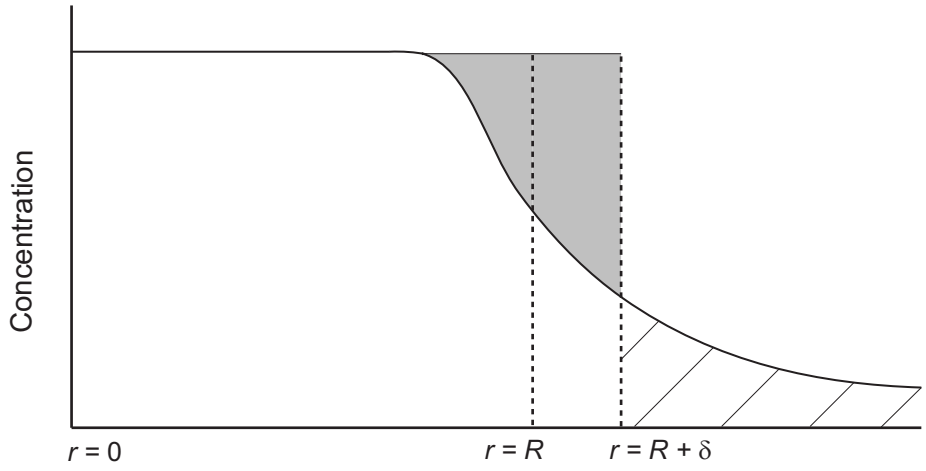

FIG. 4.2. Schematic graph of a concentration vs. radial position curve: δ is the distance from the effective radius, R, to a hypothetical sharp interface located at the position where the total difference in bulk concentration and system concentration up to that point (grey fill) is equal to the difference in system concentration and solute concentration from that point on (diagonal hatching).

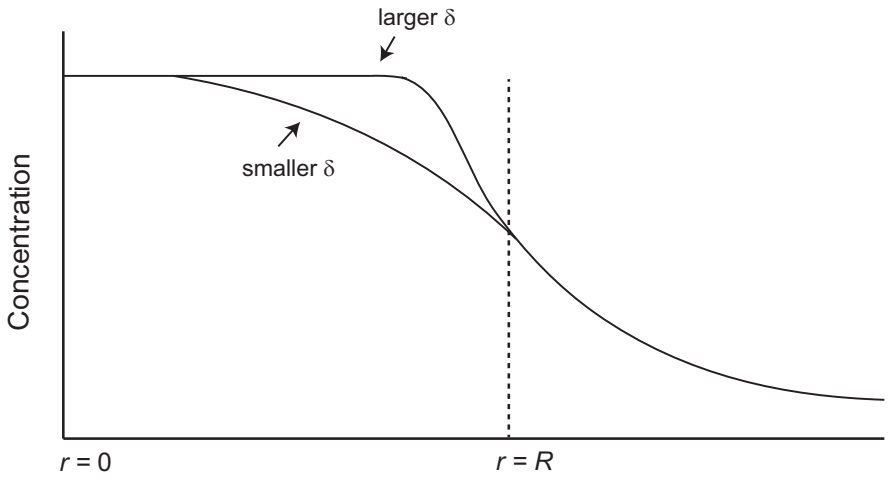

FIG. 4.3. Schematic graph of two concentration vs. radial position curves having the same density profiles at distances greater than the effective radius, but different concentration profiles up to the position of the effective radius. The value of δ is larger for the upper curve.

4.1.1 Derivation of the Non-classical Nucleation Rate

We now determine the nucleation rate, *J*, assuming a size-dependent surface tension as per Eq. (4.1). *J* is proportional to the exponential of a supersaturated system's free energy barrier to nucleation, ΔG^* as in Eq. (2.16), from Chapter 2:

$$J = C_{in}\omega^* Z \exp\left(-\frac{\Delta G^*}{kT}\right). \tag{4.2}$$

The change in ΔG when a crystal precipitates out of the solution is (Eqs. (2.3) and (2.4)):

$$\Delta G = -\Delta\mu N + 2\pi R\sigma = -\Delta\mu\frac{\pi R^2}{a} + 2\pi R\sigma, \tag{4.3}$$

where $\Delta\mu$ is the difference in chemical potential between the dissolved and solid phases. Dividing through by kT scales Eq. (4.3) in terms of the dimensionless variables ρ, Σ, and $\Delta g = \Delta G / kT$. Considering that $\Delta\mu = kT \log(S)$, we have:

$$\Delta g = -\log(S)\pi\rho^2 + 2\pi\rho\Sigma. \tag{4.4}$$

The critical radius is defined by setting $\mathrm{d}\Delta g / \mathrm{d}\rho\big|_{\rho^*} = 0$. Then, replacing Σ with $\Sigma_0 f(\rho^*)$ allows us to obtain an implicit expression for the critical nucleus size ρ^*:

$$\rho^* = \frac{\Sigma_0 f(\rho^*)}{\log(S) - \Sigma_0 f'(\rho^*)}, \tag{4.5}$$

where $f'(\rho^*)$ is the derivative of $f(\rho)$ with respect to ρ, evaluated at ρ^*. Substituting Eq. (4.5) into Eq. (4.4) gives us the scaled free energy difference at the critical nucleus size:

$$\Delta g^* = \frac{\pi\Sigma_0^{\,2} f(\rho^*)^2}{\log(S)} \frac{(1 - 2\Sigma_0 f'(\rho^*)/\log(S))}{(1 - \Sigma_0 f'(\rho^*)/\log(S))^2}. \tag{4.6}$$

In the classical case, $\Delta g_0^* \equiv \pi\Sigma_0^{\,2} / \log(S)$, as can be seen by substituting $f(\rho) = 1$ into Eq. (4.6). By analogy with the CNT, we therefore have the following non-classical expression for Δg^*:

$$\Delta g^* = \frac{\pi\Psi^2}{\log(S)},$$

where the variable Ψ is related to the non-classical surface tension Σ:

$$\Psi = \Sigma_0 f(\rho^*) \frac{(1 - 2\Sigma_0 f'(\rho^*)/\log(S))^{1/2}}{(1 - \Sigma_0 f'(\rho^*)/\log(S))},$$

and is equal to Σ to first order:

$$\Psi = \Sigma\left(1 + O\left(\Sigma_0 f'(\rho^*)/\log(S)\right)^2\right).$$

Now, in Eq. (4.2), the prefactor includes the equilibrium concentration, C_{eq}, the Zeldovich factor Z, and the rate of attachment of incoming particles to the crystal surface, ω^*. Following [Markov 2003], and referring to Appendix C, we have:

$$Z = \frac{1}{2\pi\rho^*}\left[\log(S) - 2\Sigma_0 f' - \frac{{\Sigma_0}^2 f f''}{\log(S) - \Sigma_0 f'}\right]^{1/2} \times\left(1 - \frac{\Sigma_0}{16\pi}\frac{4f''' + f^{iv} f \Sigma_0/\left(\log(S) - \Sigma_0 f'\right)}{\left(\log(S) - 2\Sigma_0 f' - \rho^* \Sigma_0 f''\right)^2}\right) \tag{4.7}$$

and

$$\omega^* = 2\pi\rho^* a C_{in} \frac{D}{{l_s}^2} \tag{4.8}$$

A final challenge is the high level of noise in the data for ρ*, which precludes us from using Eq. (4.7) and Eq. (4.8) directly with Eq. (4.2) in the analysis. We instead consider a third order expansion of Ψ and Z via an expansion of ρ* in terms of the small parameter δ. This eliminates ρ* in favour of S and leaves us with a systematic expansion of log(J) to third order in log(S):

$$\log(J) \approx \alpha - \frac{\pi\Sigma_0^{\,2}}{\log(S)} + \frac{1}{2}\log(\log(S)) + 2\log(S) + \delta^2\left(-\frac{3\pi}{2}\log(S) - \frac{3(\log(S))^2}{4\Sigma_0^{\,2}} - \frac{9(\log(S))^3}{8\pi\Sigma_0^{\,4}}\right) + \delta^3\left(\frac{5\pi(\log(S))^2}{6\Sigma_0} + \frac{5(\log(S))^3}{4\Sigma_0^{\,3}} + \frac{25(\log(S))^4}{8\pi\Sigma_0^{\,5}}\right), \tag{4.9}$$

where $\alpha = \log\left(C_{eq}^{\,2} Da / l_s^{\,2}\right) + 2\pi\delta\Sigma_0$ is a constant. Eq. (4.9) is then used to fit the data for log(J) as a function of 1/log(S) in order to obtain the parameters δ and Σ_0. Application of this result to simulation data is shown in Chapter 6.

As a side note, we can make an observation about the relationship between ρ^* and δ. Expanding Eq. (4.5) to second order in δ gives us, with the help of Eq. (4.1):

$$\rho^* \approx \rho_0 - \frac{3\delta^2}{4\rho_0}$$

where $\rho_0 = \Sigma_0 / \log(S)$ is the classical dimensionless value of the critical radius. The non-classical theory presented here thus predicts, to second order, that the critical radius decreases with increasing δ. This behaviour was also predicted by the Cahn-Hilliard density functional theory model of Gránásy [Gránásy 1999b] and observed in the molecular dynamics simulation of Báez and Clancy [Báez 1995].

4.2 Crystal Growth: Some Analytical Results

In order to make use of Eq. (4.9), we must know the value of the supersaturation, S, of the simulated system at the given bonding strengths. Since $S = C_{in}/C_{eq}$, where the spatially homogeneous initial concentration of the system, C_{in}, is chosen by the user, we must determine the equilibrium concentration, C_{eq}.

4.2.1 Constant concentration boundary condition

The system's equilibrium concentration, C_{eq}, is the concentration at which crystal growth no longer occurs, on the average. In other words, C_{eq} is the average system concentration for which the average number of crystal particles does not change in time.

First we will examine the concentration of solute $C(r,t)$ as a function of time, t, and the distance, r, from the crystal center in the circularly symmetric case of a crystal with effective radius $R(t)$ growing in a diffusion field with constant concentration at the system's boundaries. The boundary condition far from the crystal and the initial condition can be written as $C(\infty,t) = C(r,0) = \hat{C}$, where $\hat{C} = C_{in}$ is the (constant) concentration at the system's boundary, equal to the initial concentration. The continuity of flux at the growing surface provides a second boundary condition at the surface: $a^{-1}V = D\left.\frac{\partial C}{\partial r}\right|_R + VC(R,t)$, where D is the diffusion coefficient, and V is the growth rate of the crystal. The analytical result for the solute concentration at the surface of the crystal, valid for large time, is:

$$C(R,t) \approx C_{eq}\left(1 + A_0 \frac{1}{\sqrt{t}}\right), \tag{4.10}$$

where A_0 is a constant. A derivation is given in Appendix D. We fit Eq. (4.10) to simulation data for $C(R,t)$ up to a time of 3000 t_s in Fig. 4.4 with the boundary concentration held constant. Results were averaged over 1000 realisations. Although the fit is qualitatively good, the data contains significant fluctuations since it is recorded at a single node of the diffusion lattice (the single "seed node" as described in Chapter 3). Furthermore, we observe that the asymptotic descent of $C(R,t) \rightarrow C_{eq}$ is very slow, such that the fit of Eq. (4.10) does not provide a reliable measure of C_{eq}.

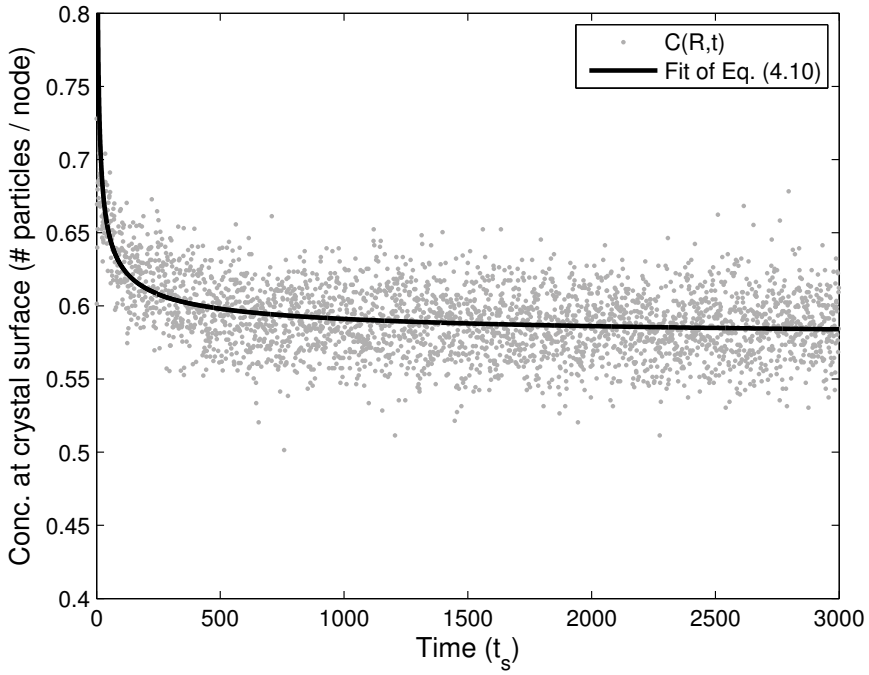

FIG. 4.4. $C(R,t)$ with boundaries held at constant concentration: fit of Eq. (4.10) for $C_{in} = 0.75$ and for parameters $E_{ss} = -1.3$, $E_{sw} = -0.1$, $\eta = 0$.

In the constant boundary condition case, for large times, the effective radius as a function of time, $R(t)$ has the following form, as shown in Appendix D:

$$R(t) = 2\sqrt{A_1 t} \tag{4.11}$$

Fig. 4.5 shows a fit of Eq. (4.11) to the data for effective radius vs. time for the same simulation shown in Fig. 4.4, but up to 18 000 t_s. The fit is considered satisfactory.

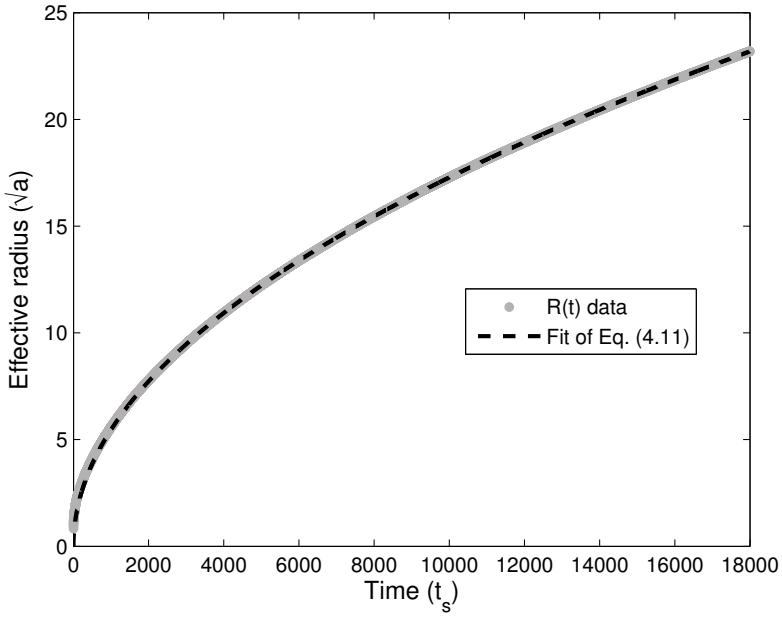

FIG. 4.5. $R(t)$ with boundaries held at constant concentration, large time: fit of Eq. (4.11) for $C_{in} = 0.75$ and for parameters $E_{ss} = -1.3$, $E_{sw} = -0.1$, $\eta = 0$.

For intermediate times, the equations for $C(R,t)$ and $R(t)$ are as follows (a derivation is shown in Appendix D):

$$C_0 \approx C_{eq}\left(1 + A_2 \frac{e^{-B_0 t}}{\sqrt{t \ln(t / 2B_0)}}\right), \tag{4.12}$$

and

$$R \approx A_3 e^{-B_0/t} \sqrt{\frac{t}{\ln(t/2B_0)}}, \tag{4.13}$$

where A_2, A_3, and B_0, are constants. Fig. 4.6 shows that the logarithmic corrections are non-trivial in the intermediate time case, and that the results are consistent with the simulations. The cross-over from the intermediate time result (fit of Eq. 4.13) to the large time result (fit of Eq. 4.11) is well illustrated. These results were presented to show the validity of the algorithm, however, we will not use these simulation results explicitly. Instead we will look at another boundary condition: the no-flux case.

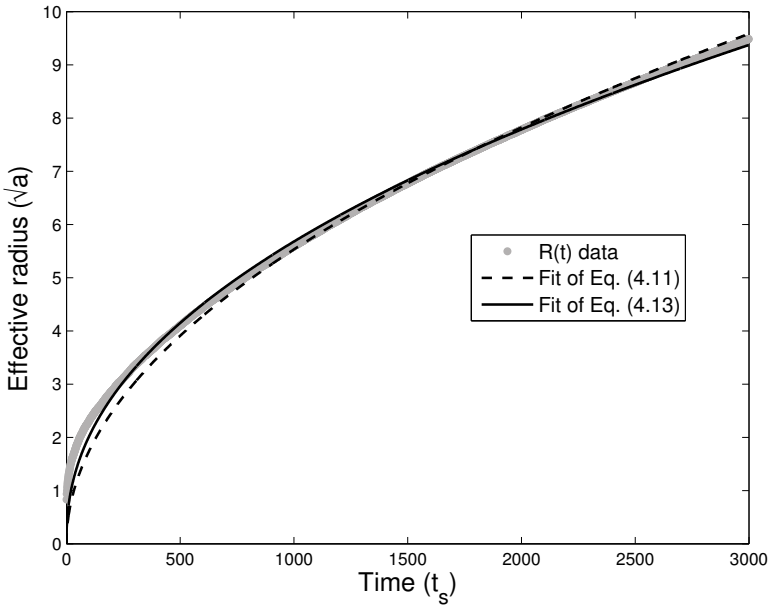

FIG. 4.6. $R(t)$ with boundaries held at constant concentration, intermediate time: fit of Eq. (4.11) and Eq. (4.13) for C_{in} = 0.75 and for parameters E_{ss} = -1.3, E_{sw} = -0.1, $\eta = 0$.

4.2.2 No-flux boundary condition

In the circularly symmetric case of a crystal with radius $R(t)$ growing in a diffusion field, the analytical result for the concentration of solute $C(r,t)$ as a function of time and of the distance, r, from the crystal center with reflective boundary conditions is shown in Eq. (4.14):

$$C(r,t) \approx k_1 \left[J_0\left(r\sqrt{b/D}\right) + k_2 Y_0\left(r\sqrt{b/D}\right) \right] \exp(-bt) + C_{eq}. \qquad (4.14)$$

Here, J_0 and Y_0 are the Bessel functions of order zero, b controls the rate of decay of the concentration over time, and k_1, k_2 are constants that can be determined given the value of b. A derivation is given in Appendix E.

If we take a spatial average of Eq. (4.14), we obtain a simplified equation for the time dependent concentration, $C(t)$, under reflective boundary conditions:

$$C(t) = A_4 \exp(-bt) + C_{eq}, \qquad (4.15)$$

where A_4 is a constant. We observe that the asymptotic descent of $C(t) \rightarrow C_{eq}$ occurs more quickly with reflective boundaries than with constant concentration boundaries. This provides a much more efficient method for us to measure C_{eq} than in the constant concentration boundary case.

A measurement of C_{eq} was performed by allowing the system to evolve to large times (40 000 t_s) with reflective boundary conditions, such that the solute particle concentration spatially averaged over the diffusion lattice became stationary in time. Results were averaged over 100 realisations. A fit was then made to the data using Eq. (4.15). As a test of

the algorithm, we measured the system's equilibrium concentration, C_{eq}, for various initial concentration values, C_{in}, for set input parameters E_{ss}, E_{sw}, and η. As can be seen in Fig. 4.7, the value of C_{eq} is independent of the C_{in} values, as it should be.

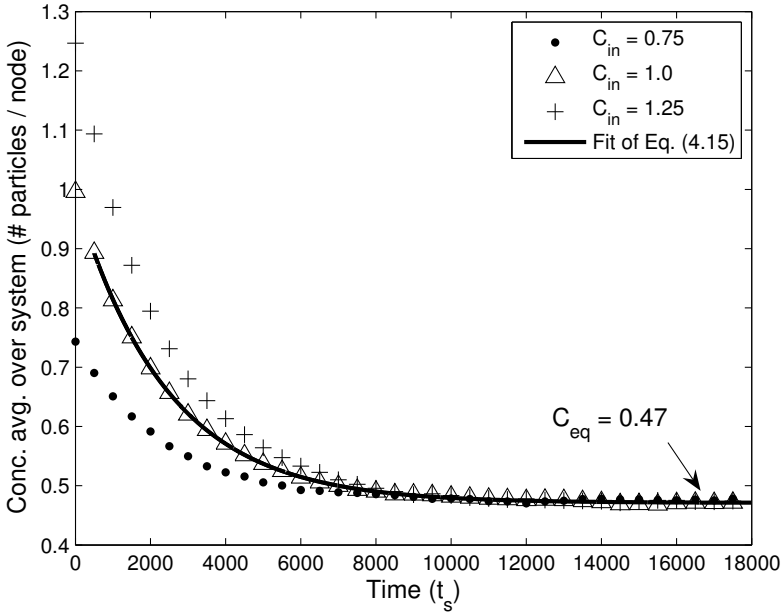

FIG. 4.7. Spatially averaged concentration vs. time: approach to C_{eq} for different values of C_{in} and for parameters E_{ss} = -1.3, E_{sw} = -0.1, η = 0.

As a further test of the algorithm, measurements of $R(t)$ vs. time are shown in Fig. 4.8 It is seen that the curves can be fitted with the analytical result in Eq. (4.16), where A_5 is a constant coefficient and R_∞ is the crystal radius at large time:

$$R(t) \cong -A_5 \exp(-bt) + R_\infty . \tag{4.16}$$

Eq. (4.16) comes from Eq. (4.17) below:

$$R(t) \cong R_\infty - \frac{\beta k_1}{C_{eq} b}\left[J_0\left(R_\infty \sqrt{b/D}\right) + k_2 Y_0\left(R_\infty \sqrt{b/D}\right)\right] \exp(-bt). \tag{4.17}$$

Appendix E offers a derivation.

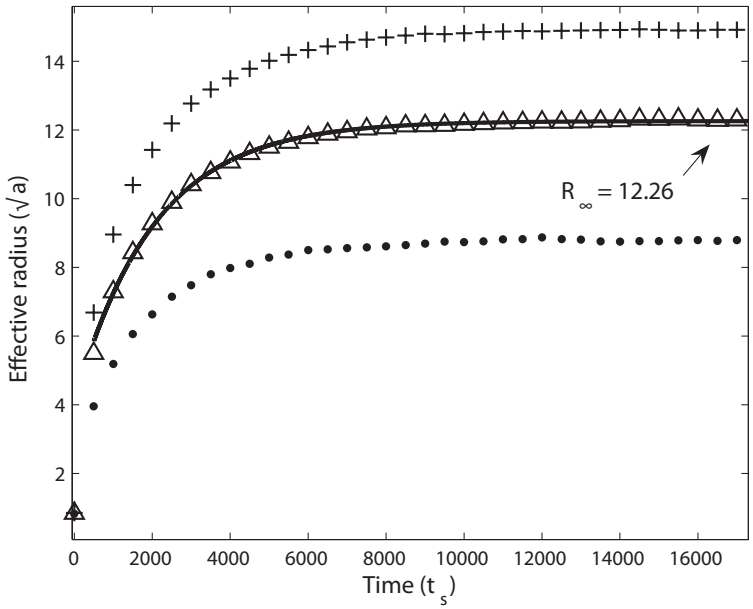

FIG. 4.8. Effective crystal radius vs. time: approach to R_∞ for different values of C_{in} and for parameters E_{ss} = -1.3, E_{sw} = -0.1, η = 0. The fit is done for large time data only ($t > 500\ t_s$).

In this chapter, we have presented the analytical results related to nucleation and growth. Eq. (4.9) is used in the discussion of the results of the simulation in Chapter 6, and Eq. (4.15) is used to determine C_{eq}. In the next chapter, we explain the mean first-passage time technique that is used to obtain the nucleation rate, J, from the simulation data, which is required for the analysis of non-classical nucleation effects using Eq. (4.9).

Chapter 5

Mean First-Passage Time Method to Obtain Nucleation Parameters

A key problem in the computational simulation of nucleation is the determination of the nucleation rate, J, without first knowing the critical nucleus size, N^*, of a nucleating cluster. Furthermore, since nucleation events occur rarely, it is not practical to attempt to observe nucleation in a simulation directly. Several different methods exist for handling this problem, such as the umbrella sampling approach used by Frenkel and co-workers [ten Wolde 1994], and methods that require setting a threshold value for the number of particles in a cluster that is assumed to be significantly greater than N^*, such as the Yatsuoka-Matsumoto method [Chkonia 2009].

Wedekind et. al have recently developed an alternative data analysis technique that uses the mean-first passage times (MFPT) of cluster nucleation through a range of cluster sizes to determine J and N^* [Wedekind 2007]. An important advantage of this technique is

that it uses only the kinetic information of the system produced by the computational simulation, and does not require the use of an unknown threshold parameter or the implementation of artificial constraints or tempering of system temperature or cluster size to observe nucleation events. In addition to providing the required information on the nucleation rate and the critical cluster size, the MFPT technique also allows one to obtain the magnitude of the free energy barrier to nucleation, ΔG^*.

Several authors have indicated that Wedekind et al.'s approach in nucleation modeling provides a valid assessment of the nucleation process and serves as a useful and efficient method for determining J and N^* in simulations of nucleation [Romer 2007, Chkonia 2009, Lundrigan 2009]. This chapter presents the MFPT technique of Wedekind et. al, and demonstrates how it can be used to obtain information on the parameters J and N^*, and to discriminate between the nucleation and growth regimes of the cluster.

5.1 Fokker-Planck Equation and the MFPT

The Fokker-Planck equation is used to determine how the probability-density function of a stochastic process changes in time. This equation is often applied to describe the dynamics of activated processes in terms of the reaction coordinate x, which in the case of nucleation is the number of particles, N, in a nucleating or growing cluster [Gardiner 1990]. For an activated process in general, the Fokker-Planck equation has the form:

$$\frac{\partial P(x,t)}{\partial t} = \frac{\partial}{\partial x}\left[U'(x)P(x,t)\right] + D\frac{\partial^2 P(x,t)}{\partial x^2}$$

where $P(x,t)$ is the probability distribution function of the reaction coordinate, D is the diffusion coefficient in reaction coordinate space, $U(x)$ is the free energy barrier of the activated process, and $\beta_B = 1/k_BT$ where k_B is the Boltzmann constant and T is the temperature.

The MFPT is a statistical quantity that can be determined from the Fokker-Planck equation. It describes the average time that an activated system described by the Fokker-Planck equation will remain within a certain domain of the reaction coordinate. An activated process with a single reaction coordinate can be thought of as a system which resides within a domain $x = [x_a, x_b]$, where x_a is a reflecting barrier and x_b is an absorbing point located at a position beyond the free energy barrier. In this case, the MFPT, $\tau(x_0; x_a,x_b)$, is the average time that it takes for the system with initial state x_0 to cross the barrier and escape from the domain $[x_a, x_b]$ by moving past the point x_b for the first time. Fig. 5.1 shows a representation of a free energy barrier-crossing process and the corresponding MFPT, where x^* is the location of the peak of the energy barrier. [Gardiner 1990].

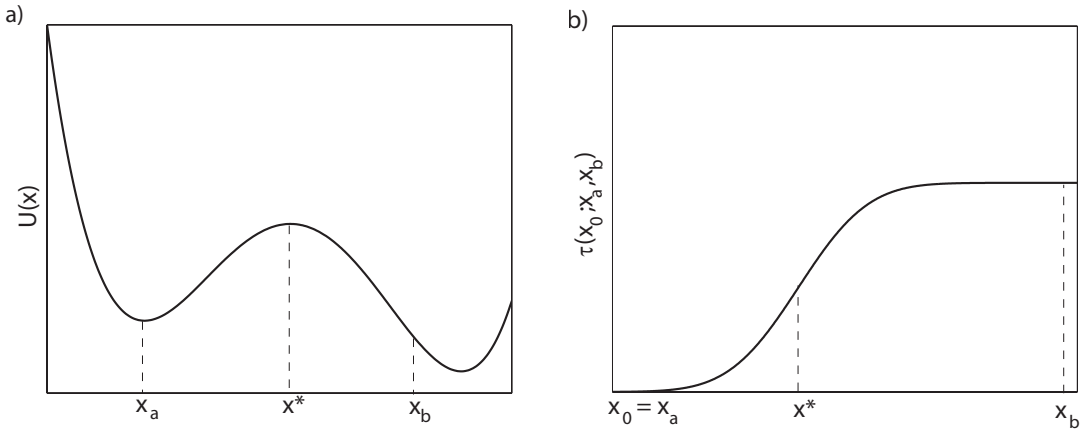

FIG. 5.1. Representation of (a) the energy barrier for an activated process, and (b) the associated MFPT (reproduced from [Gardiner 1990]).

5.1.1 MFPT applied to nucleation

Turning to the process of nucleation, let us consider the number of particles in a nucleating cluster, N, as the reaction coordinate, in place of the parameter x_0 above. For a nucleating system, the point x_a corresponds to $N = 0$. The point x_b corresponds to a point $N > N^*$, located after the free energy barrier to nucleation, $\Delta G(N^*)$, has been crossed. The initial condition x_0 corresponds to an initial number of cluster particles, N_0. The boundary condition is reflecting at $N = 0$ and absorbing at $x_b = N > N^*$. With these boundary conditions, the MFPT for an arbitrary number of cluster particles can be written in the following form:

$$\tau(N_0;0,N) = \int_{N_0}^{N} \frac{1}{D} d\bar{y} e^{\beta \Delta G(\bar{y})} \int_{0}^{\bar{y}} d\bar{z} e^{-\beta \Delta G(\bar{z})}. \qquad (5.1)$$

A derivation of Eq. (5.1) is available in [Gardiner 1990].

In a nucleating system where a free energy barrier exists, the nucleation rate, J, is the rate at which the free energy barrier is crossed. As explained by Wedekind et. al [Wedekind 2007], the rate of barrier crossing can be related to the MFPT as follows: the MFPT for the critical nucleus size N^* is $\tau(N^*)$, which represents the average time it takes for a cluster to grow to the critical nucleus size for the first time. Since there is a probability of ½ that a cluster of critical size will either increase in size or decrease in size, the nucleation rate is equal to:

$$J = \frac{1}{2\tau(N^*)L^2}, \qquad (5.2)$$

where L is the system size and L^2 is the total area of the system.

5.1.2 Error function approximation of MFPT

The technique developed by Wedekind et. al makes use of the sigmoidal shape of the MFPT function to propose the following approximation, based on the error function:

$$\tau(N) = \frac{\tau_J}{2}[(1 + \mathrm{erf}(N - N^*)z)], \tag{5.3}$$

where we have defined $\tau(N_0;0,N) \equiv \tau(N)$ for simplicity. A derivation of this expression is reproduced from Wedekind et al. [Wedekind 2007] in Appendix F, for reference. When Eq. (5.3) is fitted to the MFPT data, the parameters N^* and $\tau_J = 1/JL^2$ can be extracted. The fitting parameter z represents the curvature at the top of the free energy barrier, which is related to the second derivative of the free energy barrier evaluated at the critical nucleus size $\Delta G''(N^*)$ as follows:

$$z = \sqrt{\frac{|\Delta G''(N^*)|}{2kT}}$$

and also to the Zeldovitch factor, Z, (defined in section 2.1.2) [ter Horst 2003]:

$$Z = \frac{z}{\sqrt{\pi}}.$$

5.2 Implementation of the MFPT Method

In order to implement the technique described above, we first must obtain the MFPT profiles for cluster nucleation and growth under the desired bonding strength parameters E_{ss}, E_{sw}, and η (defined in Chapter 3) then apply Eq. (5.3) to determine the corresponding N^* and J values.

5.2.1 Obtaining the MFPT from the simulation data

The first step to obtaining the MFPT, $\tau(N)$, from the nucleation and growth simulation is to create a set of arrays of cluster size vs. time data, $N(t)$. During the simulation, an $N(t)$ array is generated by recording the number of particles in a cluster (if a cluster is present) after each simulation time step. This process is repeated for many realisations, producing a set of $N(t)$ arrays.

An array of first-passage times is obtained from each $N(t)$ array by recording the time of the first appearance of each cluster of size N in the $N(t)$ array. Due to the fact that up to four particles can join a cluster in a single discrete time step, a first-passage time for a given cluster size, N, will often have the same value as for the cluster size $N \pm i$, where $i = (1,2,3)$. This is a side-effect of the discreteness of the model, which is minimized by averaging over many realisations. Table 5.1 gives an example of $N(t)$ data for which this occurs (Table 5.1(a)), and the corresponding first-passage time array (Table 5.1(b)):

Table 5.1: Example of a First-Passage Time Calculation

Table 5.1(a)

Time, t (t_s)	1	2	3	4	5
Cluster size, $N(t)$ (# of particles)	2	2	4	5	5

Table 5.1(b)

Cluster size, $N(t)$ (# of particles)	1	2	3	4	5
First-passage time, (t_s)	1	1	3	3	4

The first-passage times are computed for each realisation, then averaged over the number of realisations to obtain the MFPT, $\tau(N)$. We note that due to the nature of the model used in this study, the smallest possible cluster is composed of two particles, and therefore we do not obtain data for $\tau(N < 2)$.

5.2.2 Fitting criterion for Eq. (5.3)

In order to apply Eq. (5.3) to the MFPT data, we must determine the number of MFPT data points that will be used in the fit calculation. We use the adjusted *R*-square statistic as the criterion on which to base this decision, and take the number of MFPT points for which the adjusted *R*-square value for the fit of Eq. (5.3) is maximized.

The adjusted *R*-square is a statistic that describes the "goodness of fit" as a measure of the difference $y_i - \hat{y}_i$ between the data points, y_i, and the fitted points, $\hat{y}_i$ [Mathworks Inc. 2012]. This difference is called the residual. Two sums are required in order to compute the adjusted *R*-square: the sum of squares due to error (SSE) and the total sum of squares (SST).

The SSE is the sum of squares of the residual multiplied by a weighting coefficient, w_i, for each point:

$$\mathrm{SSE} = \sum_{i=1}^{M_d} w_i (y_i - \hat{y}_i)^2 ,$$

where M_d is the number of data points. The SST is the sum of squares of the data points minus the mean of the data, $\langle y_i \rangle$:

$$\mathrm{SST} = \sum_{i=1}^{M_d} w_i (y_i - \langle y_i \rangle)^2 .$$

The adjusted *R*-square also accounts for the residual degrees of freedom $\nu = M_d - M_p$, where M_p is the number of fitting parameters used, such that:

$$\text{adjusted R} - \text{square} = 1 - \frac{(M_d - 1)\mathrm{SSE}}{\nu\,\mathrm{SST}}$$

Maximizing the adjusted *R*-square provides the most consistent and reliable criterion for making the sigmoidal fit to $\tau(N)$. An alternative method to determine the number of data points for use in the fit of Eq. (5.3) is to take the number of points for which the difference in fitted values of N^* is minimized. This method did not function as consistently as maximizing the adjusted R-square, and was not used to obtain the results of this thesis.

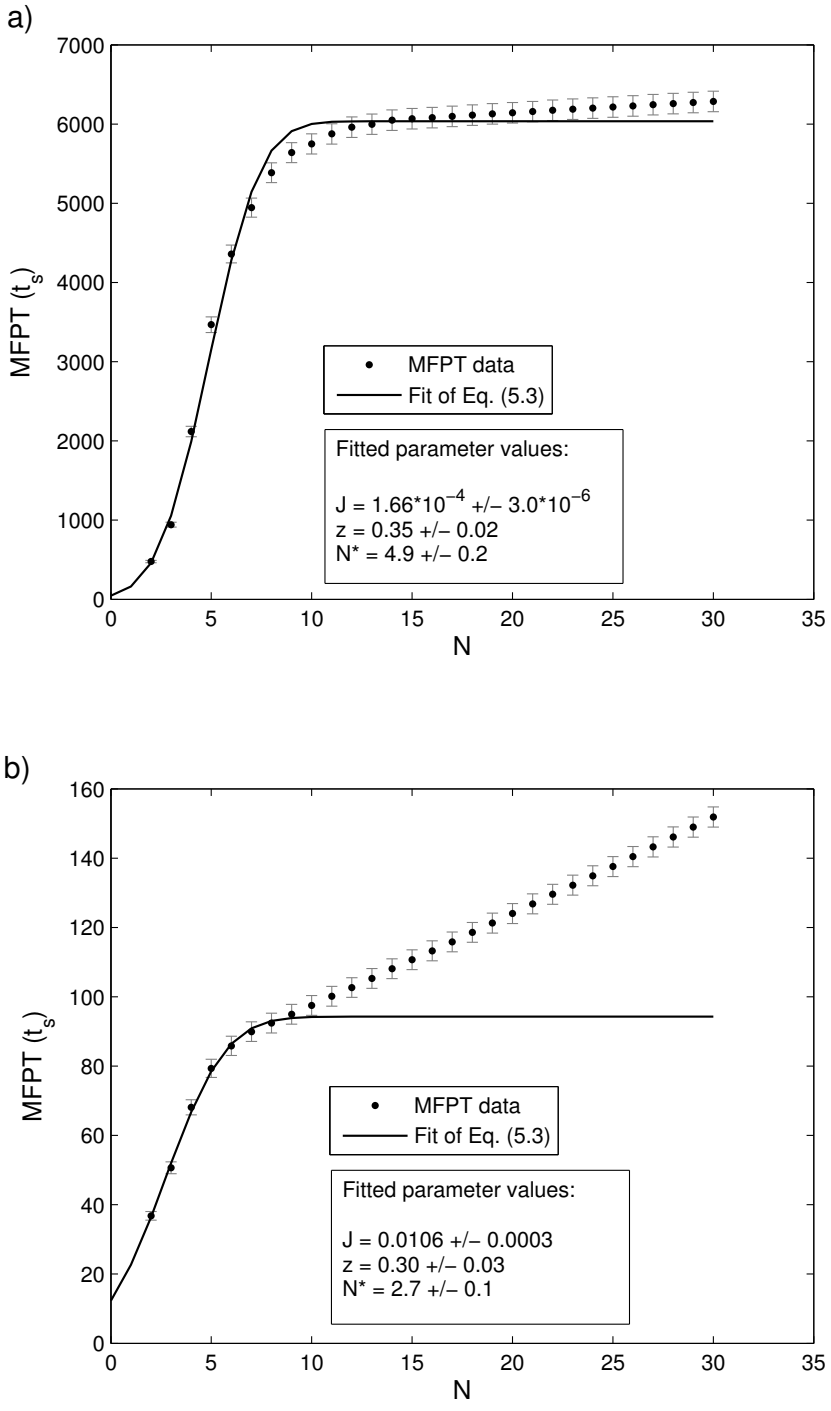

FIG. 5.2. Mean First-Passage Time vs. Cluster Size: Determination of J and N^* for parameters E_{ss} = -1.5, E_{sw} = -0.5, η = 1.0, and (a) S = 3.8, (b) S = 10.6. The error bars are calculated as the standard error on the mean of each data point. 1000 realisations were performed.

5.2.3 Example of application of MFPT technique to simulation data

Fig. 5.2 provides an example of the determination N^* and J via the MFPT method. Fig. 5.2(a) presents a case for which the supersaturation is low and therefore the energy barrier, ΔG^*, is large. With a large barrier to nucleation, the nucleation and growth stages are well separated from one another. In this case, each cluster must successfully complete the nucleation stage before it is capable of growing to larger sizes. This is indicated on the MFPT plot by the flat plateau at large values of N.

In contrast, Fig. 5.2(b) shows the effect of an increased supersaturation on the nucleation of a crystal having the same bonding strength parameters. In this case ΔG^* is reduced, and nucleation and growth can occur on the same timescale, making the distinction between the nucleation and growth processes less pronounced. This is indicated by the lack of a flat plateau at large values of N. For some data sets with very large supersaturations, application of Eq. (5.3) using the method described in section 5.2.2 did not function adequately to identify a plateau in the MFPT plot, and a value for the nucleation rate was not obtained.

5.2.4 Interpretation of error bars in Fig. 5.2

The error bars in Fig. 5.2 are calculated by taking the standard error on the mean of each data point. Because we adopt the method outlined in [Wedekind 2007], for which each first-passage time data set is generated for all cluster sizes, N, before reinitiating the simulation and beginning a new realisation, the first-passage time arrays are always monotonically increasing functions of N. This choice of how to produce the simulation data

creates an inherent bias in the data. For this reason, the error bars in Fig. 5.2 do not represent independent random error on each data point, but rather delimit the range within which MFPT curves are expected to fall on subsequent measurements.

As a verification of this interpretation of the error bars, Fig. 5.3 shows a plot of the MFPT for each of three distinct sets of 1000 realisations of the simulation, for the same bonding strength and supersaturation parameters as those used in Fig. 5.2(b). As can be seen, all of the MFPT curves fall within the error bars calculated for one of the curves (Data-1).

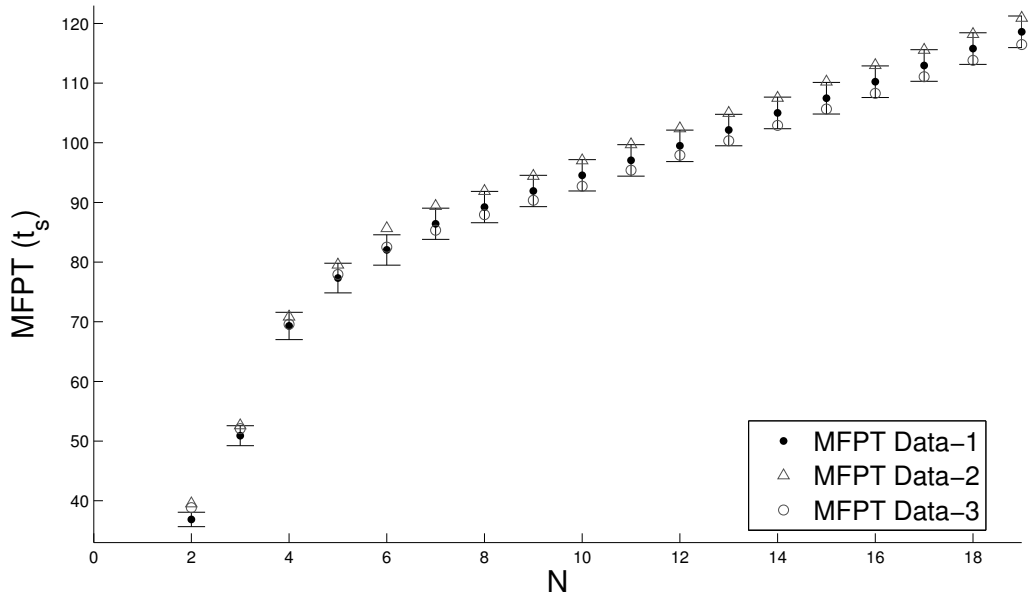

FIG. 5.3. Validation of error bar interpretation. MFPT for four distinct data sets of 1000 realisations each. The error bars on the first data set (Data-1) delimit the range within which subsequent MFPT measurements are expected to be placed.

In order to obtain independent random error bars on the MFPT data points, it would be necessary to generate an independent first-passage time data set for every size, *N*, for

every realisation. This would require restarting the simulation before generating each first-passage time data set for each size, N. A verification of this method to achieve independent random error on the MFPT data points is demonstrated in Fig. 5.4. However, we considered this approach to take an excessive amount of time, and so we chose to implement the method of Wedekind et al. with the error bars interpreted as above.

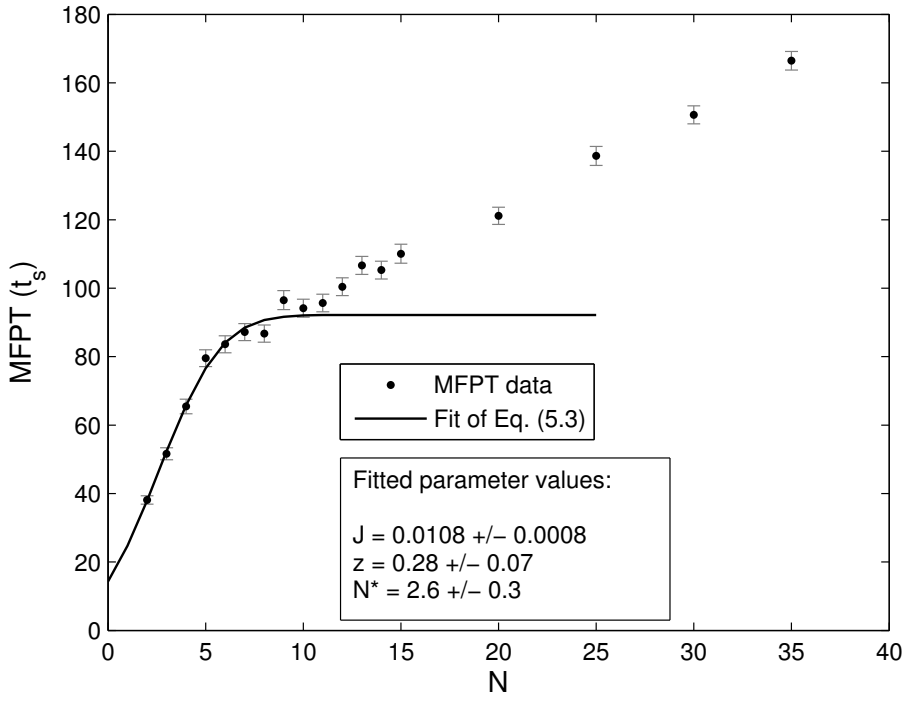

FIG. 5.4. Mean First-Passage Time vs. cluster size: determination of J and N^* for parameters E_{ss} = -1.5, E_{sw} = -0.5, η = 1.0, S = 10.6. The error bars are calculated as the standard error on the mean of each data point and represent independent random error of each data point. 1000 realisations were performed. The fitted parameter values compare well with those of Fig. 5.2(b).

Chapter 6

Results and Discussion

In this chapter, the results of the nucleation and growth simulations described in Chapter 3 are presented and analyzed following the methods outlined in Chapters 4 and 5. First, the implementation of the simulations is described, and examples are shown of plots of the number of particles as a function of time, $N(t)$, for a single nucleating crystal (Fig. 6.1) and for several nucleating crystals generated on separate realisations of the simulation (Fig. 6.2). Next, in section 6.2, we look at plots of the critical nucleus size, N^*, and the nucleation rate J, as functions of the supersaturation, S. This data is produced by a fit of Eq. (5.3). In Section 6.3, we see an application of the fit of Eq. (4.9) to the logarithm of the nucleation rate, $\log(J)$, and the reciprocal of the logarithm of the supersaturation, $1/\log(S)$. This is done in order to determine the Tolman parameter, δ, controlling the non-classical, radius-dependence of the surface tension, σ, and the value of the scaled constant surface tension, Σ_0, of the CNT. Plots of δ and Σ_0 vs. bonding energy are shown. A discussion of these results follows.

6.1 Examples of Simulated Nucleating Crystals

The modeling approach was described in Chapter 3. The simulations are set up as follows: the input parameters are the solid-to-solid bonding energy, E_{ss}, the solid-to-water bonding energy, E_{sw}, the next-to-nearest neighbour bonding strength coefficient in the solid, η, and the initial concentration of the system, C_{in}. The diffusion lattice is implemented on a square array of side length $s = 30$ nodes. One designated seed node, at which the crystal will grow, is set at the position (s/2, s/2). The size of the crystal lattice is chosen large enough to allow the crystal to grow without touching the boundary, and small enough to reduce computational requirements. As this size depends on the values of the input parameters, it may be adjusted as needed before commencing a trial run.

In order to evaluate the nucleation rate, J, many realisations of the simulations must be performed. To begin with, though, let us look at the output of the simulation for a single realisation. Fig. 6.1 shows a plot of the number of particles comprising a crystal, $N(t)$ as a function of time. As can be seen, $N(t)$ can fluctuate up or down over time, leading to the crystal's nucleation and subsequent growth, or to complete dissolution of the crystal. In the plot shown in Fig. 6.1, a new crystal forms and dissolves completely three times, then a fourth crystal forms and attains a much larger size, possibly reaching the critical nucleation size, N^*. However, as explained in Chapter 5, the MFPT method is used to determine the value of N^*, and this requires a large number of realisations.

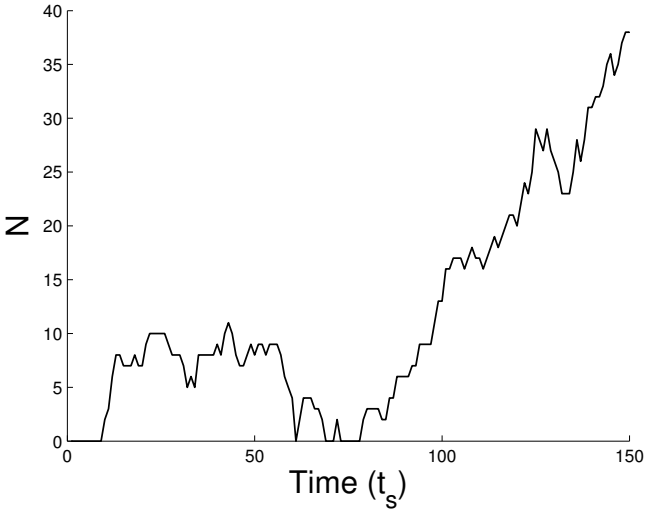

FIG. 6.1. Number of crystal particles as a function of time (single crystal) for bonding strength parameters E_{ss} = -1.8, E_{sw} = -0.625, η = 0, with S = 1.42.

Fig. 6.2 shows $N(t)$ for several simulation runs. Some crystals nucleate and enter the growth stage more quickly than others. An averaging of $N(t)$ arrays such as these would produce a plot similar to Fig. 4.8, under reflective boundary conditions and for large times.

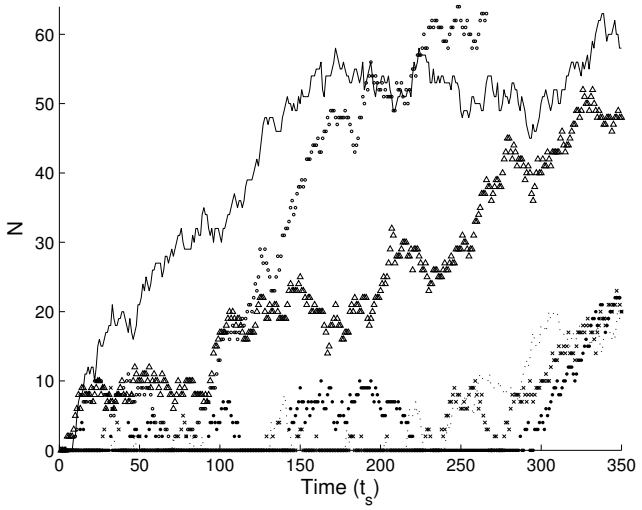

FIG. 6.2. Number of crystal particles as a function of time for bonding strength parameters E_{ss} = -1.8, E_{sw} = -0.625, η = 0, with S = 1.42.

6.2 N^* and J as Functions of Supersaturation

This section shows the simulation data for the critical nucleus size, N^*, and the nucleation rate, J, versus supersaturation S. The N^* and J data are produced using Eq. (5.3) from the Mean First-Passage Time (MFPT) method described in Chapter 5.

Fig. 6.3 is an example of a plot of N^* vs. S, for bonding strength parameters E_{ss} = -1.5, E_{sw} = -0.5, and η = 1.0. The data for N^* for most combinations of bonding energy parameters contains significant fluctuations, such that it is not included in the analysis, as mentioned in section 4.1. However, we see that N^* decreases with increasing S, as expected considering Eq. (2.5) ($R^* = \sigma_0 a / \Delta\mu$) and recalling that $N^* = \pi R^2 / a$ and $\Delta\mu = k_B T \ln(S)$.

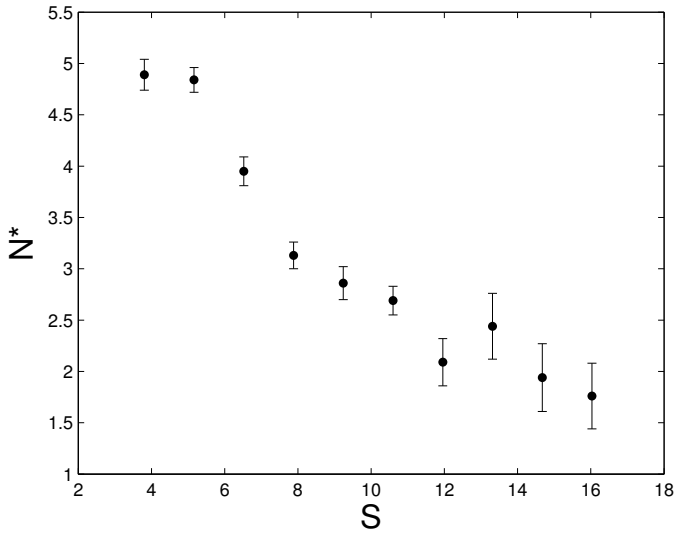

FIG. 6.3. N^* vs. S for bonding strength parameters E_{ss} = -1.5, E_{sw} = -0.5, and η = 1.0.

Fig. 6.4 shows a plot of the nucleation rate, J, as a function of supersaturation. As expected, the nucleation rate increases with increasing supersaturation. In the next section,

we will see how the non-classical effects appearing in Eq. (4.9), due to a radius-dependent surface tension, give a more detailed and better analysis of the data for log(J) plotted as a function of $[\log(S)]^{-1}$.

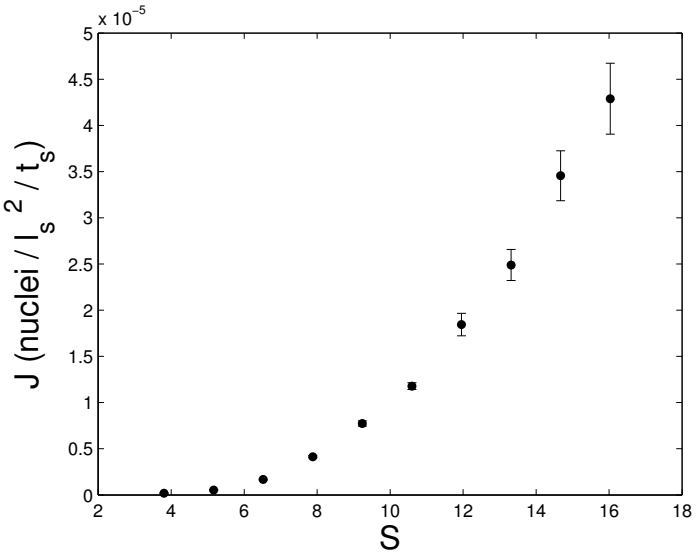

FIG. 6.4. J vs. S for bonding strength parameters E_{ss} = -1.5, E_{sw} = -0.5, and η = 1.0.

6.3 Results for the Tolman length (δ) and CNT Surface Tension (Σ_0)

This section begins with an illustration of the fit of Eq. (4.9) to the data for log(J) and log(S), including a comparison to the fit in the CNT case. This is followed by a presentation of the main results of the thesis: the values of the parameters δ and Σ_0 as functions of the bonding energies E_{ss}, E_{sw}, and η.

6.3.1 Non-classical nucleation compared to the CNT

Fig. 6.5 shows a plot of $\log(J)$ vs. $(\log(S))^{-1}$, for one set of bond energy parameters. The constant surface tension case of CNT is compared with the non-classical, radius-dependent surface tension case by fitting Eq. (4.9) to the data.

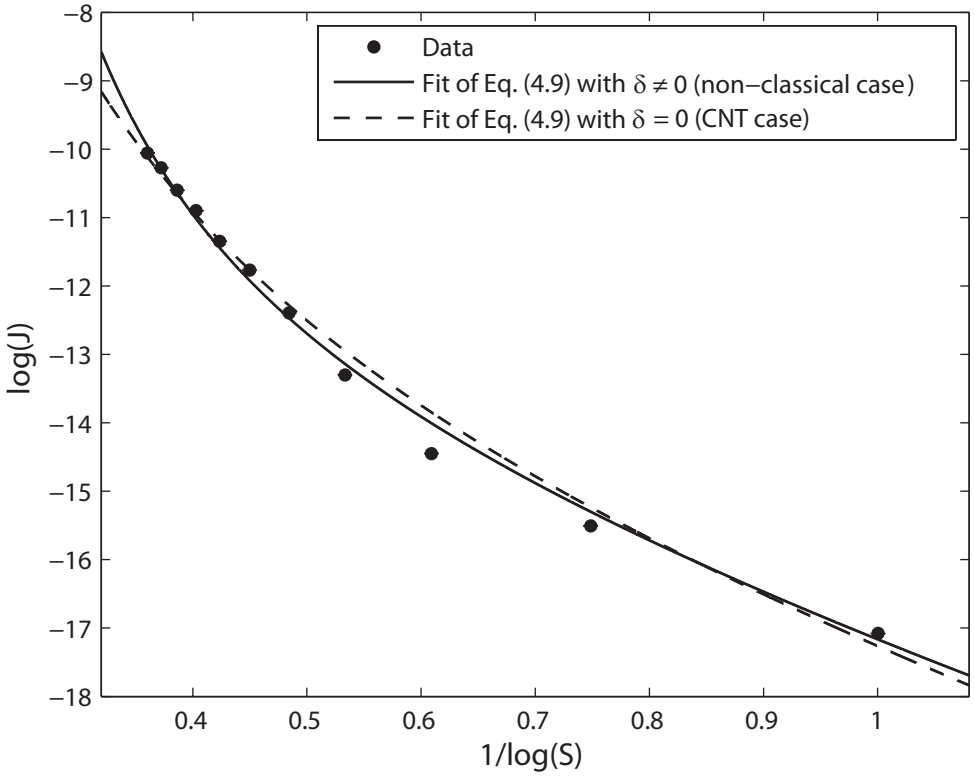

FIG. 6.5. Comparison of fits of Eq. (4.9) to J data for parameters E_{ss} = -1.5, E_{sw} = -0.5, η = 1.0. The second term on the right hand side of Eq. (4.9) is the dominant behaviour and corresponds to a straight line of slope $-\pi\Sigma_o^2$. Error bars are smaller than the symbols marking the data points.

The systematic correction to the curvature indicates that the fit to the nucleation rate data is improved in the non-classical case as compared to the classical case. Applying the fit

of Eq. (4.9) to log(J) vs. log(S)$^{-1}$ data for a range of bonding strength parameters allows us to obtain a picture of how δ and Σ_0 vary as functions of the bonding strengths. We note that the error bars in the figures in this chapter do not represent precise confidence intervals, but rather serve as indicators of how well a given fitted parameter is constrained relative to the other parameter values in the plots. The reason for this is that the MFPT method used did not generate points with independent random errors (see section 5.2.4).

6.3.2 Results for δ and Σ_0 as functions of bonding energies

δ is the Tolman length, the parameter influencing the radius-dependence of the surface tension in the non-classical case. Below, we present the results for δ as a function of bonding strengths. Figs. 6.6(a-c) show the results when E_{sw} is held constant and E_{ss} is varied, for three different values of E_{sw} and three values of η, whereas Fig. 6.7 shows some results when E_{ss} is held constant and E_{sw} is varied, for a value of E_{ss} = -1.8 and the three values of η.

Σ_0 is the value of the surface tension in the classical case, that is, in the case where $\delta = 0$, such that the Tolman expression, $f(\rho) = 1$. As explained in Chapter 4, Σ_0 remains as a parameter in the non-classical nucleation theory, which has a radius-dependent surface tension, $\Sigma = f(\rho)\Sigma_0$. Following Figs. 6.6 and 6.7, we present the results for Σ_0 as a function of the bond energy parameters. Figs. 6.8(a-c) show the results when E_{sw} is held constant and E_{ss} is varied, for three different values of E_{sw}, and Figs. 6.9(a-b) show the results when E_{ss} is held constant and E_{sw} is varied, for a value of E_{ss} = -1.8. Three values of η are considered for

each case. Due to insufficient statistics in certain cases, points were not obtained for a few combinations of bonding strength parameters in Figs. 6.6-6.9.

In all plots in Figs. 6.6-6.9, "square" markers indicate data for which $\eta = 0$, "x" markers indicate $\eta = 0.5$, and "dot" markers indicate $\eta = 1.0$.

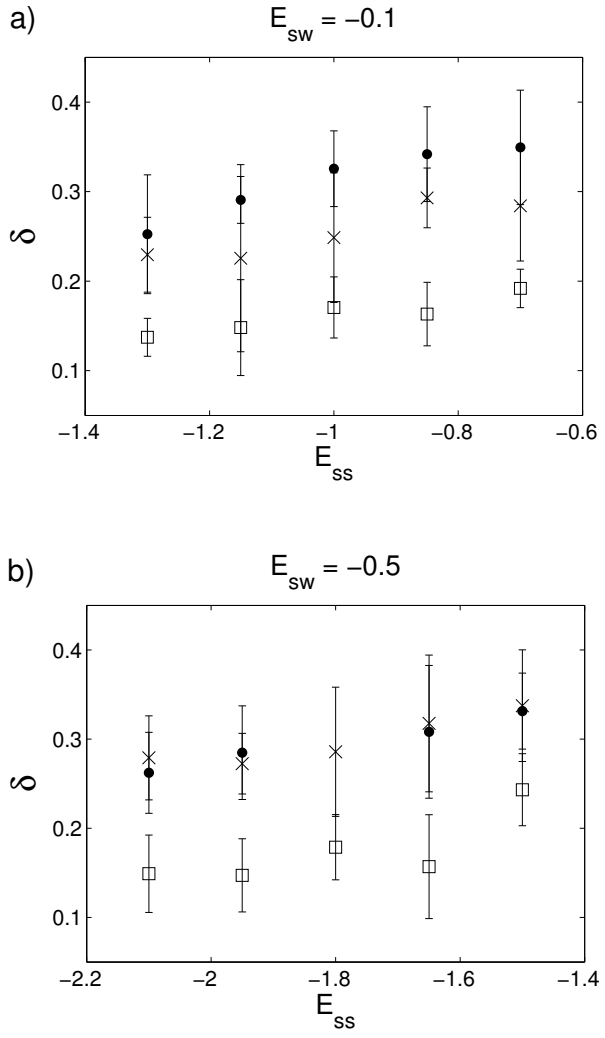

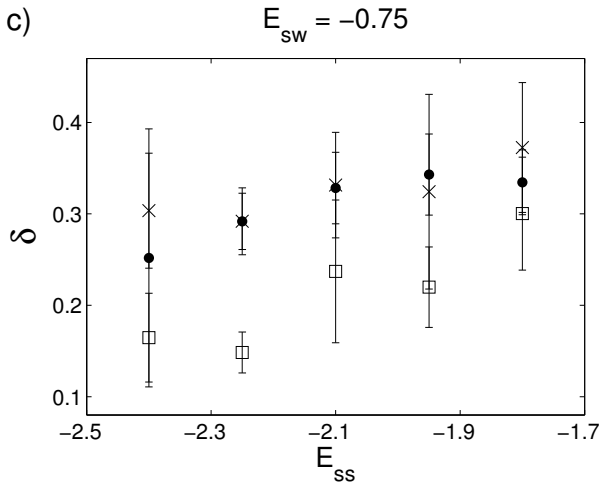

FIG. 6.6. Plots of δ for various E_{ss} while maintaining E_{sw} constant. The point for E_{ss} = -1.8, E_{sw} = -0.5, η = 1.0 in (b) was not obtained due to insufficient statistics.

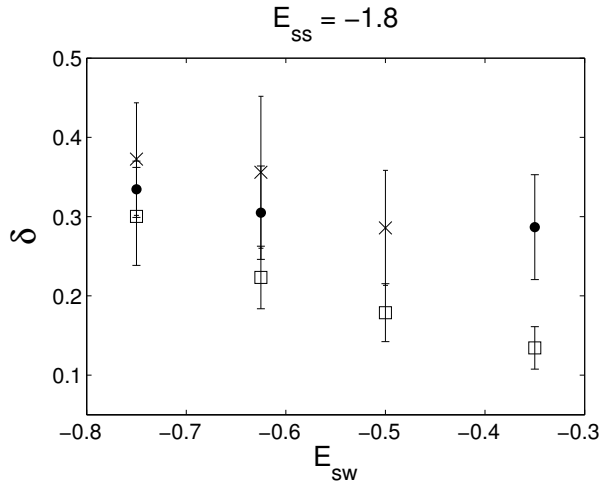

FIG. 6.7. Plots of δ for various E_{sw} while maintaining E_{ss} constant.

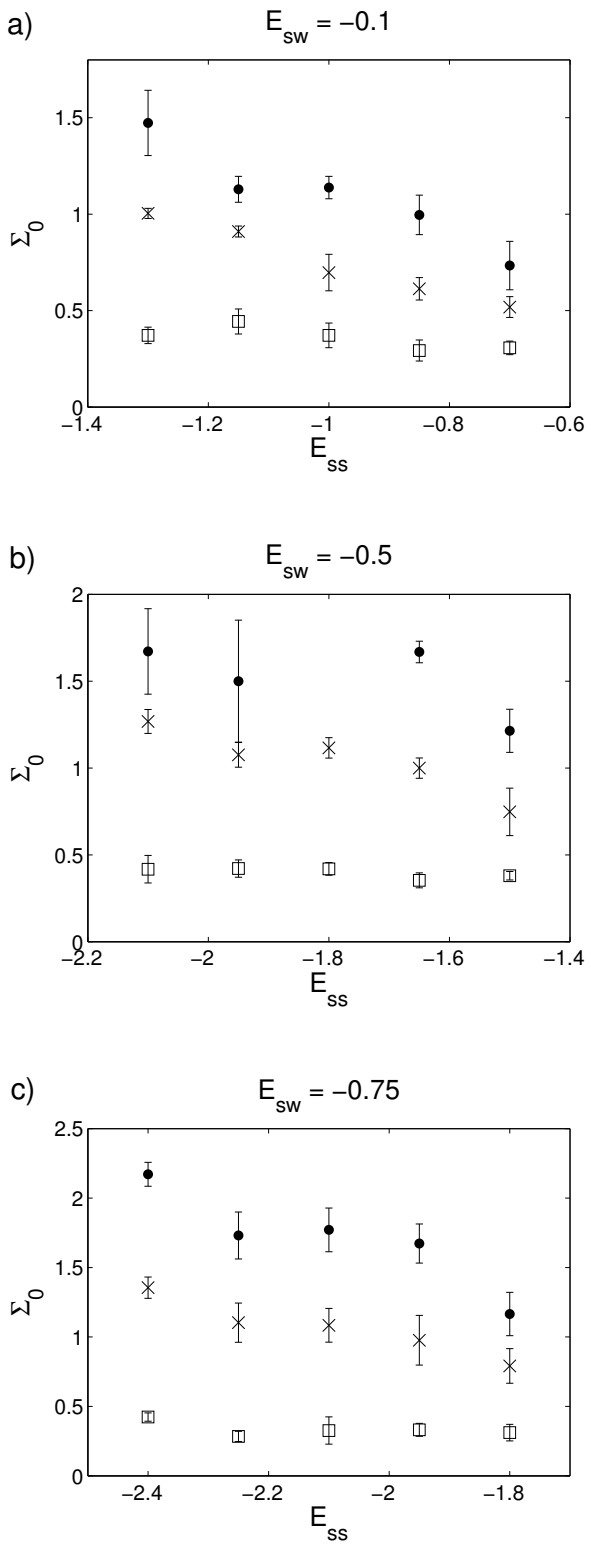

FIG. 6.8. Plots of Σ_0 for various E_{ss} while maintaining E_{sw} constant. The point for E_{ss} = -1.8, E_{sw} = -0.5, η = 1.0 in (b) was not obtained due to insufficient statistics.

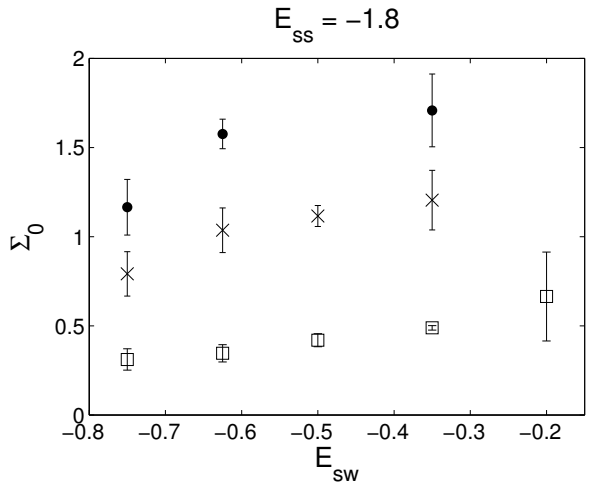

FIG. 6.9. Plots of Σ_0 for various E_{sw} while maintaining E_{ss} constant

6.4 Discussion of Results

In this model, $\delta > 0$, which results in a decrease in the surface tension with respect to its classical value [Gránásy 1999a]. We find that δ tends to decrease with increasing magnitude of E_{ss} at a fixed E_{sw}. This is illustrated in Fig. 6.6. Correspondingly, as shown in Fig. 6.7, the value of δ tends to increase with increasing magnitude of E_{sw} at fixed values of E_{ss}. $E_{ss} - 2E_{sw}$ is the value of ΔE for any single attachment event when $\eta = 0$. Figs. 6.6 and Fig. 6.7 indicate that an increase in the magnitude of the difference in bonding energies $E_{ss} - 2E_{sw}$ leads to a decrease in δ.

The value of δ is larger when the next-to-nearest neighbour bonding energy parameter, η, is equal to 0.5 or 1 compared to its value when $\eta = 0$. For E_{sw} = -0.1 (Fig. 8(a)), the values of δ are also larger in the $\eta = 1.0$ case compared to the $\eta = 0.5$ case,

however, for larger magnitudes of E_{sw} (Figs. 8(c) and (e)) there is no clear difference between the δ values for η = 0.5 and η = 1.

The radius-dependence of the surface tension is controlled by δ, as per Eq. (4.1) and, as explained in section 4.1 and Appendix B, the value of δ depends on the shape of the concentration profile extending along the radial direction, r, from the centre of the nucleating crystal (r = 0), through the position defined by its effective radius, (r = R), and into the surrounding solution to $r = \infty$. It is possible that the bonding strength parameters E_{ss} and η control crystal density to different degrees in the regions $r < R$ and $r > R$, resulting in a contrasting effect between these two parameters on the value of δ. This suggests an explanation for the observation of a decrease in δ with increasing E_{ss} as well as an increase in δ with increasing η. An interesting further work would be to calculate the value of δ directly from the density profiles of simulated crystals under a range of bonding strength parameter values.

Figs. 6.8 and 6.9 show that Σ_0 increases with increasing values of η, increasing magnitude of E_{ss}, and decreasing magnitude of E_{sw}. This can be explained by the fact that surface tension is proportional to the solid-to-solid bonding energy of surface particles over the area that the surface bonds cover. A greater magnitude of E_{ss} (or a smaller magnitude of E_{sw}) means stronger solid-to-solid bonding relative to solid-to-water bonding, which directly results in an increased surface tension. At set values of E_{ss} and E_{sw}, an increase in η increases total bonding energy from any next-to-nearest neighbour solid-to-solid bonds on the crystal surface and therefore results in an increased surface tension.

Eq. (4.1) tells us that Σ_0 is the value of the surface tension Σ when the Tolman expression $f(\rho) = 1$, that is, when $\delta = 0$ or $\rho = \infty$. As stated in section 4.1, in the specific case of a large crystal for which the crystal particles are uniformly packed with maximum density, Σ_0 is the surface tension between two flat faces of that crystal. In such a "bulk" case, therefore, one could calculate Σ_0 by considering the energy released after splitting the crystal into two pieces with flat faces of length $\Delta L = N$, where N is the number of particles along the interface and ΔL has been scaled by $\sqrt{a}$. This leads to a value of

$$\Sigma_0 = \frac{N\,|\,\chi E_{ss} - 2E_{sw}\,|}{2\Delta L} = \frac{|\,\chi E_{ss} - 2E_{sw}\,|}{2} \equiv \left|\Delta E\right| \qquad (6.1)$$

where χ is a coefficient that depends on the value of η (recalling that next-to-nearest neighbour solid-to-water bonds are considered to be negligible in the model):

$$\chi = \begin{cases} 1 \text{ if } \eta = 0 \\ 2 \text{ if } \eta = 0.5 \\ 3 \text{ if } \eta = 1.0 \end{cases}$$

and $|\Delta E|$ is the energy change for an attachment/detachment reaction. Fig. 6.10 shows the results for Σ_0 from Figs. 6.8 and 6.9 plotted as functions of $|\Delta E|$, for the three values of η. The value of Σ_0 in the bulk case (Eq. (6.1)) is represented by a solid straight line.

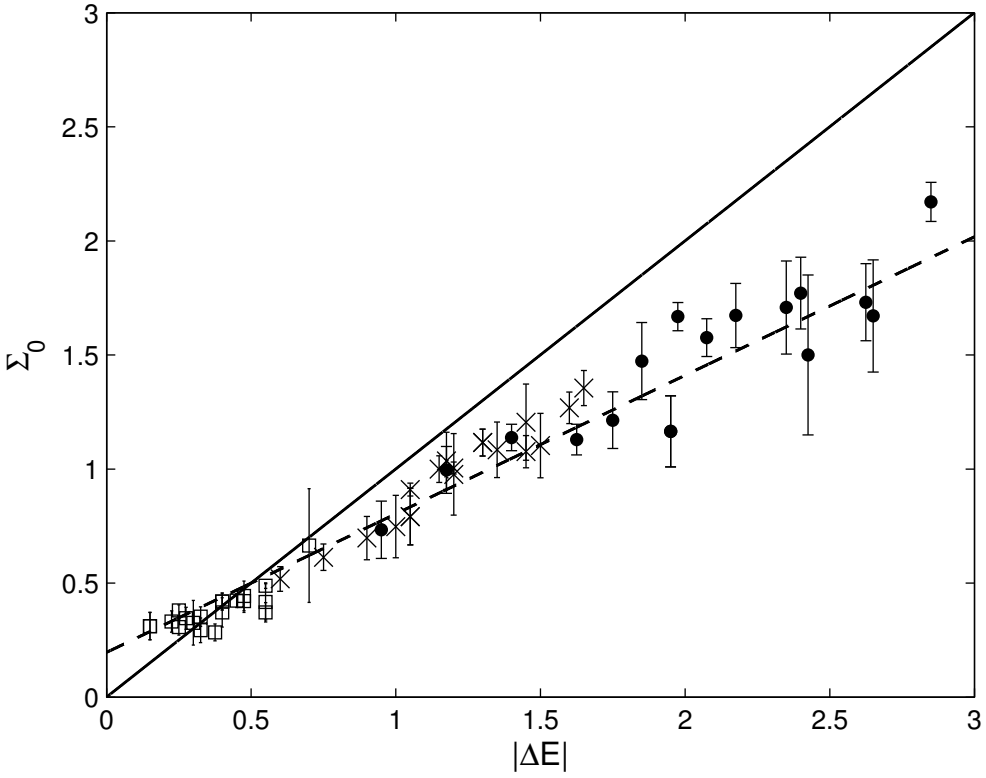

FIG. 6.10. Data for Σ_0 from Figs. 6.8 and 6.9 plotted as a function of the energy difference of an attachment (or detachment) reaction of a solute particle to a cluster. As before, "square" markers indicate data for which $\eta = 0$, "x" markers indicate $\eta = 0.5$, and "dot" markers indicate $\eta = 1.0$. The solid straight line represents the bulk Σ_0 as a function of ΔE according to Eq. (6.1), and the dashed line is a linear fit to the data with slope = 0.61 and an R-square of 0.94.

As can be seen, across the three values of η and for the various values of E_{ss} and E_{sw} considered, Σ_0 for the simulated nucleating crystals is of the same order of magnitude as the bulk Σ_0 for a large, densely packed crystal (solid line in Fig. 6.10) and increases linearly with increasing $|\Delta E|$, although at a slope that is less than that of the bulk case. The crystals that form in this model are not uniformly packed at the maximum possible density and do not attain their bulk planar form under any combination of bonding strength parameters –

consequently, the value of Σ_0 for the simulated nucleating crystals does not equal the value that it would have in the bulk case, and it is not surprising that the plotted values of Σ_0 are generally smaller than the bulk values.

On the other hand, Fig. 6.10 shows that a change in η does not interrupt the linear increase in the plotted Σ_0 values. This indicates that the Σ_0 parameter does not have a special dependence on the strength of the next-to-nearest neighbour bonding interaction. As shown in Fig. 3.4, nucleating clusters become more compact as η is increased – one might expect this increased compactness to cause the fitted Σ_0 values at larger η to approach the predicted values for Σ_0 in the bulk case. However, this does not appear to be the case, as the deviation in the Σ_0 data from the solid line in Fig. 6.10 increases as η increases. One possible explanation for this deviation could be that the next-to-nearest neighbour bonding between solid particles and water particles is significant, especially for crystals which have strong next-to-nearest neighbour bonding in the solid phase. Next-to-nearest neighbour bonding between solid and water particles was expected to have a small range and was considered to be negligible in this study (see section 3.2.2). The behaviour of Σ_0 at very small values of $|\Delta E|$ requires long simulation times and remains to be explored. This hypothesis would require further work to test.

According to Eq. (4.1), the non-classical surface tension, Σ, approaches Σ_0 as the effective radius, $\rho \rightarrow \infty$. Therefore, it would be interesting to have a plot of Σ as a function of ρ. Unfortunately, a significant limitation in this study is the lack of workable data for the critical nucleus size. With reliable data for N^*, one would be able to directly analyze the

non-classical surface tension, Σ as a function of the critical radius, ρ*, using Eq. (4.1) and (4.5). Taking Eq. (4.1) and (4.5) to first order in δ and rearranging for Σ gives:

$$\Sigma \approx \Sigma_0 - \delta \log(S) \tag{6.2}$$

Following from Eq. (6.2), the trends apparent in Fig. 6.6(b-d) and Fig. 6.8(b-d) – i.e. a decrease in δ and increase in Σ_0 with increasing magnitude of E_{ss} at constant values of E_{sw} – point toward an increase in Σ with an increase in the magnitude of E_{ss}. Using the same reasoning, Figs. 6.7 and 6.9 indicate an increase in Σ with a decrease in the magnitude of E_{sw}, We cannot make a similar prediction regarding the behaviour of Σ vs. η, since the trends in Σ_0 and δ have opposite effects on Σ as η is increased from 0 to 1 – i.e. both Σ_0 and δ increase with increasing values of η in Figs. 6.6-6.9.

A further discussion point concerns the lattice geometry used in this study. The choice of a D2Q4 diffusion lattice is sufficient for an isotropic model of diffusion [Chopard 1998]. Neither momentum nor energy is conserved: rather, these quantities are presumed to be absorbed by the background medium that constitutes the solvent in this model. One drawback of the D2Q4 setup is that, with only four available occupation sites at each diffusion lattice node, a maximum of four particles can attach or detach from the crystal to the seed node(s) of the diffusion lattice in any given time step. This may provide an artificial barrier to the nucleation rate that could be reduced using a multi-particle model. That being said, we find that the nucleation rate obtained in the model at varying supersaturation behaves adequately close to expectations for use in this study, as illustrated in Fig. 6.5.

Chapter 7

Conclusion

The goal of this thesis was to investigate nucleation phenomena beyond the limits of the CNT. In order to accomplish this, a D2Q4 Lattice Gas Automaton model of crystal nucleation in a supersaturated thermodynamic system was implemented, and the simulation data evaluated using a non-classical nucleation theory which incorporates surface tension dependence on radius via the Tolman parameter, δ. The input parameters in the model are the microscopic bonding energies for nearest and next-to-nearest neighbour solid-to-solid bonding and nearest neighbour solid-to-water bonding, and the initial concentration of solute in the system. The model is presented in Chapter 3.

Needed analytical results for the non-classical nucleation theory, as well as for the solute concentration as a function of space and time and the crystal's effective radius under different boundary conditions were derived in Chapter 4 and the relevant appendices. The mean-first passage time (MFPT) technique was used to obtain the nucleation rate, J, and

critical nucleus size, N^*, from the simulation data. This method is described in Chapter 5, with supplementary details in Appendix F.

The approach presented here illustrates with a simple method that non-classical nucleation phenomena can be quantified via the variation of the parameters δ and Σ_0 vs. bonding energy, as obtained from the simulation data. The CNT surface tension, Σ_0, increases (decreases) with increasing solid-to-solid (solid-to-water) bonding strength, as expected. A decrease in the Tolman length, δ, with increasing (decreasing) magnitude of E_{ss} (E_{sw}) was observed in most cases. These two trends together indicate an increase in the radius-dependent surface tension, Σ, with respect to increasing magnitude of E_{ss} relative to the magnitude of E_{sw}. Both δ and Σ_0 increased with increasing next-to-nearest neighbour solid-to-solid bonding energy, η, at fixed values of E_{ss} and E_{sw}. Σ_0 increases linearly as a function of the change in energy during an attachment or detachment reaction, $|\Delta E|$, however with a slope less than that predicted for a crystal that is uniformly packed at maximum density. These results are presented and discussed in Chapter 6.

For future work, a method to obtain an estimate of δ directly from the simulations could be designed and implemented. The results for δ obtained in this way may elucidate the different effects of the bonding energy E_{ss} and the next-to-nearest neighbour bonding strength coefficient, η, on δobserved in the plots shown in Figs. 6.6 and 6.7. In light of the results for Σ_0 vs. $|\Delta E|$ shown in Fig. 6.10, the influence of a next-to-nearest neighbour bonding interaction parameter, η_{sw} on the value of Σ_0 could be explored. This may explain the smaller than expected slope found for the linear fit to the simulated data.

Other next steps that would improve the applicability of the model to a physical nucleation system include extending the model into three dimensions, implementing a more realistic crystal lattice with a greater number of directional bonding site availabilities, allowing surface diffusion of molecules bonded to the crystal surface, and allowing multiple particles to exist at each occupation site in the diffusion lattice. Nevertheless, the method presented in this thesis provides a relatively simple and practical approach to probe nucleation phenomena beyond the classical case. Furthermore, the pedagogical aspect of the approach is a unique feature in comparison to other contemporary techniques, and it provides an intuitive illustration of nucleation and growth phenomena.

Appendix A

Derivation of Eq. (2.11)

The Thompson-Gibbs equation for the formation of a liquid droplet from its vapour in a two-dimensional system is as follows:

$$\mu_v - \mu_l = \sigma_0 \frac{dp}{dN}, \qquad \text{(A.1)}$$

where μ_v and μ_l are the chemical potentials of the vapour and liquid phase, N is the number of particles in the two-dimensional liquid droplet, p is its perimeter, σ_0 is its surface tension. Noting that $p = 2\pi R$ and $N = \pi R^2 / a$ where R is the liquid droplet's radius and a is the area of one liquid particle, we can re-write Eq. (A.1) as:

$$\mu_v - \mu_l = \sigma_0 \frac{d(2\pi R)}{d(\pi R^2 / a)} = \frac{a\sigma_0}{R}.$$

Setting $\Delta\mu = \mu_v - \mu_l$ and using the relationship $\Delta\mu = k_B T \ln(P_R / P_\infty)$, where P_R is the equilibrium vapour pressure of a liquid droplet with radius R and P_∞ is the equilibrium vapour pressure of an infinitely large liquid droplet, we have:

$$k_B T \ln\left(\frac{P*}{P_\infty}\right) = \frac{a\sigma_0}{R*}, \tag{A.2}$$

and

$$k_B T \ln\left(\frac{P_N}{P_\infty}\right) = \frac{a\sigma_0}{R_N}, \tag{A.3}$$

where $R*$ is the critical radius of a liquid droplet, R_N is the radius of a droplet containing N molecules, and $P*$ and P_N are the equilibrium vapour pressures of liquid droplets with these sizes.

According to Markov, the reverse rate of reaction $\omega_N^- \sim P_N$, and the forward rate of reaction $\omega_{N-1}^+ \sim P$, where P is the vapour pressure available in the system. Furthermore, making the assumption that $P \approx P*$ due to the fact that $R*$ is small, we have $\omega_{N-1}^+ \sim P*$. Setting the ratio of rate constants equal to the ratio of Eq. (A.2) and Eq. (A.3) we get:

$$\frac{\omega_N^-}{\omega_{N-1}^+} = \frac{P_N}{P*} = \exp\left[\frac{\sigma_0 a}{k_B T}\left(\frac{1}{R_N} - \frac{1}{R*}\right)\right]. \tag{A.4}$$

Then the product of rate constants term in the sum of Eq. (A.4) can be replaced as follows, recalling that $N = \pi R^2 / a$:

$$\frac{\omega_2^- \omega_3^- \ldots \omega_N^-}{\omega_1^+ \omega_2^+ \ldots \omega_{N-1}^+} = \exp\left[\frac{\sigma_0 \sqrt{a\pi}}{k_B T} \sum_1^N \left(\frac{1}{\sqrt{N}} - \frac{1}{\sqrt{N*}}\right)\right]. \tag{A.5}$$

Invoking the "capillary approximation" ($N^* >> 1$) and integrating the term within the sum in Eq. (A.5) from 0 to N gives us:

$$\frac{\omega_2^- \omega_3^- \ldots \omega_N^-}{\omega_1^+ \omega_2^+ \ldots \omega_{N-1}^+} = \exp\left\{ \frac{\sigma_0}{k_B T} \sqrt{\pi a N^*} \left[2\left(\frac{N}{N^*} \right)^{1/2} - \frac{N}{N^*} \right] \right\} \tag{A.6}$$

The term in the exponential on the right-hand side of Eq. (A.6) is equal to $\Delta G(N)/k_B T$. This can be shown beginning with Eq. (2.3) in the liquid droplet case, and substituting $\Delta\mu = a\sigma_0 / R^* = \sqrt{\pi a \sigma_0^{\,2} / N^*}$:

$$\begin{aligned} \Delta G(N) &= -N(\Delta\mu) + 2\pi R \sigma_0 \\ &= -N(\Delta\mu) + 2\pi\sigma_0 \sqrt{\frac{Na}{\pi}} \\ &= -N\sigma_0 \sqrt{\frac{\pi a}{N^*}} + 2\pi\sigma_0 \sqrt{\frac{Na}{\pi}} \\ &= \sigma_0 \sqrt{\pi a N^*} \left[2\left(\frac{N}{N^*} \right)^{1/2} \frac{-N}{N^*} \right]. \end{aligned} \tag{A.7}$$

Replacing this result in the exponential of Eq. (A.6) gives Eq. (2.11) from the main text:

$$\frac{\omega_2^- \omega_3^- \ldots \omega_N^-}{\omega_1^+ \omega_2^+ \ldots \omega_{N-1}^+} = \exp\left\{ \frac{\Delta G(N)}{k_B T} \right\}.$$

Appendix B

Derivation of Eq. (4.1)

Following the thermodynamic approach of Tolman [Tolman 1949], we can derive the exact expression (Eq. (4.1)) for the surface tension dependence on crystal radius in the two-dimensional case of a crystal precipitating from solution.

Let σ be the two-dimensional surface tension, μ the chemical potential of either dissolved or solid phase, p' the two-dimensional "pressure" (force per unit length) in the dissolved phase, p'' the "pressure" in the solid phase, γ' the surface number density of solute in the dissolved phase, γ'' the surface number density of crystal particles in the solid phase, R the crystal's effective radius (as defined in section 2.1.1), and Γ the number density at the perimeter of the crystal, calculated with respect to the surface of tension. As in [Tolman 1949] we begin with the thermodynamic relationships between these variables:

$$d\sigma = -\Gamma d\mu \tag{B.1}$$

$$d\mu = \frac{dp'}{\gamma'} = \frac{dp''}{\gamma''} \tag{B.2}$$

$$p' - p'' = \frac{\sigma}{R} \tag{B.3}$$

then substitute Eq. (B.2) into Eq. (B.1), to obtain

$$d\sigma = -\left(\frac{\Gamma}{\gamma' - \gamma''}\right) d(p' - p'') \tag{B.4}$$

Differentiating Eq. (B.3) and substituting into Eq. (B.4) gives the term

$$d\sigma = -(\Gamma/(\gamma' - \gamma''))d(\sigma/R) = -(\Gamma/(\gamma' - \gamma''))\left(d\sigma/R - (\sigma/R^2)dR\right),$$

and rearranging leads to:

$$\frac{1}{\sigma}\frac{d\sigma}{dR} = \frac{(1/R^2)(\Gamma/(\gamma' - \gamma''))}{1 + (1/R)(\Gamma/(\gamma' - \gamma''))}. \tag{B.5}$$

We now introduce the coordinates, *x*, the radial distance extending from the crystal surface towards a reference point, and *y*, the radial distance extending from the centre of the crystal towards that point, such that:

$$y = x + R.$$

The actual amount of matter in the system can be written as the integral of the concentration as a function of radial position, $\gamma(y)$, over the area of the system:

$$\int_0^\infty 2\pi y\gamma(y)dy = \int_{-R}^\infty 2\pi(x + R)\gamma(x)dx.$$

Per unit circumference of the crystal, this becomes:

$$\int_{-R}^{\infty} \frac{(x+R)\gamma(x)}{R} dx = \int_{-R}^{\infty} (1+x/R)\gamma(x) dx .$$

In the two-dimensional case, Γ is the difference, per unit length, between the actual amount of material in the system and the amount of material in a system having a Gibbs surface of tension located at $x = 0$ and with thickness $d_1 + d_2$.

$$\Gamma = \int_{-d_1}^{0} (1+x/R)(\gamma-\gamma')dx + \int_{0}^{d_2} (1+x/R)(\gamma-\gamma'')dx \qquad \text{(B.6)}$$

We now introduce the Tolman length $\delta = \Delta/\sqrt{a}$. The length $|\Delta|$ indicates the distance from the (hypothetical) Gibbs surface of tension located at $x = 0$ to another (hypothetical) sharp interface at which $\Gamma = 0$ when calculated with respect to it [Tolman 1949] (see Fig. 6.10). Thus Eq. (B.6) becomes by definition:

$$\begin{aligned} 0 &= \int_{-d_1}^{\Delta} (1+x/R)(\gamma-\gamma')dx + \int_{\Delta}^{d_2} (1+x/R)(\gamma-\gamma'')dx \\ &= \int_{-d_1}^{0} (1+x/R)(\gamma-\gamma')dx + \int_{0}^{\Delta} (1+x/R)(\gamma-\gamma')dx \\ &\quad + \int_{0}^{d_2} (1+x/R)(\gamma-\gamma'')dx - \int_{0}^{\Delta} (1+x/R)(\gamma-\gamma'')dx \end{aligned}$$

This gives us:

$$\Gamma = \int_{0}^{\Delta} (1+x/R)(\gamma-\gamma'')dx - \int_{0}^{\Delta} (1+x/R)(\gamma-\gamma')dx = (\gamma'-\gamma'')\left[\Delta + \Delta^2/2R\right],$$

and

$$\Gamma/(\gamma'-\gamma'') = \Delta[1+\Delta/2R]. \qquad \text{(B.7)}$$

Now we substitute Eq. (B.7) into Eq. (B.5) and integrate from $R = \infty$ (plane surface) to R:

$$\log(\sigma/\sigma_0) = \int_{\infty}^{R} \frac{\Delta/R^2(1+\Delta/2R)}{1+\Delta/R(1+\Delta/2R)} dR .$$

This integral can be solved exactly to produce the Tolman expression in two dimensions:

$$\sigma/\sigma_0 = (1+\Delta/R+\Delta^2/2R^2)^{-1/2} \exp(\pi/4)\exp(-\tan^{-1}(1+\Delta/R)) ,$$

or, in terms of the scaled variables $\Sigma = \sigma a/kT$, $\Sigma_0 = \sigma_0 a/kT$, $\delta = \Delta/\sqrt{a}$, and $\rho = R/\sqrt{a}$,

$$f(\rho) = \frac{\Sigma}{\Sigma_0} = \left(1+\frac{\delta}{\rho}+\frac{\delta^2}{2\rho^2}\right)^{-1/2} \exp(\pi/4)\exp\left(-\tan^{-1}\left(1+\frac{\delta}{\rho}\right)\right),$$

as we had in Eq. (4.1).

Appendix C

Derivation of Eqs. (4.7) and (4.8)

We follow the approach of Becker and Doring, as laid out in [Markov 2003] to obtain the non-classical Zeldovich factor (Eq. (4.7)) beginning with the equation for the steady-state nucleation rate (Eq. (2.10), with $C_1 = C_{eq}$, as explained in Chapter 2):

$$J_{ss} = C_1 \left[\sum_{N=1}^{M-1} \left(\frac{1 \quad \omega_2^- \omega_3^- \ldots \omega_N^-}{\omega_n^+ \, \omega_1^+ \omega_2^+ \ldots \omega_{N-1}^+} \right) \right]^{-1},$$

where M is a number of cluster particles which is significantly greater than N^*, and ω_N^+ and ω_N^- indicate the rate constants of single-particle attachment (forward reaction) and single-particle detachment (reverse reaction) from the cluster. Since nucleation occurs at early time, we assume that the concentration of solute at the cluster surface, is approximately equal to the initial concentration, C_{in}: $C_1(R,t) = C(R,t) \approx C_{in}$, such that we have:

$$J_{ss} = C_{in} \left[\sum_{N=1}^{M-1} \left(\frac{1 \quad \omega_2^- \omega_3^- \ldots \omega_N^-}{\omega_n^+ \, \omega_1^+ \omega_2^+ \ldots \omega_{N-1}^+} \right) \right]^{-1} \qquad \text{(C.1)}$$

In the approach of Becker and Doring, clusters made up of *M* particles are removed from the system and replaced by an equivalent number of dissolved particles in order to maintain a constant concentration.

The product of rate constants in the sum of Eq. (C.1) is related to the cluster free energy Δg (scaled by kT) as follows:

$$\frac{\omega_2^- \omega_3^- \ldots \omega_N^-}{\omega_1^+ \omega_2^+ \ldots \omega_{N-1}^+} = \exp(\Delta g). \qquad \text{(C.2)}$$

Eq. (C.2) results from the relationships between supersaturation, forward and reverse rate constants, chemical potential, and critical nucleus size in the CNT as explained, for example, in [Markov 2003].

In light of Eq. (C.2), we expand Δg about the dimensionless critical cluster radius ρ^*:

$$\Delta g = \Delta g^* + \frac{1}{2}\Delta g''(\rho - \rho^*)^2 + \frac{1}{6}\Delta g'''(\rho - \rho^*)^3 + \ldots$$

Note that derivatives of Δg are evaluated at ρ^* in Eq. (C.2) and in the following. Then, assuming that $\omega_n^+ = \omega_{n^*}^+ \equiv \omega^* = \text{constant}$ as in [Markov 2003] and recognizing that $N = \pi\rho^2$ and therefore $dN/d\rho\big|_{\rho^*} = 2\pi\rho^*$, we write out an integral with respect to $d\rho$ that will replace the sum in Eq. (C.1):

$$\left(\frac{J_{ss}}{C_{in}}\right)^{-1} = \frac{1}{\omega^*}\left(\frac{dN}{d\rho}\right)\Bigg|_{\rho^*} \exp(\Delta g^*)\int_{-\infty}^{\infty} d\rho \exp\left(-\frac{1}{2}\left|\Delta g''\right|(\rho-\rho^*)^2\right)$$
$$\exp\left(\frac{\Delta g'''}{6}(\rho-\rho^*)^3 + \frac{\Delta g^{iv}}{24}(\rho-\rho^*)^4 + \ldots\right)$$

We have extended the integration limits from -∞ to +∞ as in [Markov 2003]. Expanding the exponential terms containing $\Delta g'''$ and Δg^{iv} above gives:

$$\left(\frac{J_{ss}}{C_{in}}\right)^{-1} = \frac{1}{\omega^*} 2\pi\rho^* \exp(\Delta g^*)\int_{-\infty}^{\infty} d\rho \exp\left(-\frac{1}{2}\left|\Delta g''\right|(\rho-\rho^*)^2\right)\left[1+\frac{\Delta g'''}{6}(\rho-\rho^*)^3\right.$$
$$\left. + \frac{\Delta g^{iv}}{24}(\rho-\rho^*)^4 + O(\rho-\rho)^6\right]$$

The integral containing $\Delta g'''$ becomes zero due to symmetry, and we are left with:

$$\left(\frac{J_{ss}}{C_{in}}\right)^{-1} = \frac{2\pi\rho^*}{\omega^*}\exp(\Delta g^*)\sqrt{\frac{2\pi}{\left|\Delta g''\right|}}\left(1+\frac{1}{8}\frac{\Delta g^{iv}}{\left|\Delta g''\right|^2} + O\left(\Delta g^{vi}\Big/\left|\Delta g''\right|^3\right)\right).$$

Rearranging for J_{ss} gives us:

$$J_{ss} = \omega^* C_{in} Z \exp(-\Delta g^*),$$

where the Zeldovich factor is

$$Z = \frac{1}{2\pi\rho^*}\sqrt{\frac{\left|\Delta g''\right|}{2\pi}}\left(1-\frac{1}{8}\frac{\Delta g^{iv}}{\left|\Delta g''\right|^2} + O\left(\Delta g^{vi}\Big/\left|\Delta g''\right|^3\right)\right).$$

Returning to Eq. (4.4) and differentiating with respect to ρ, and evaluating at ρ*, we have:

$$\Delta g = -\log(S)\pi\rho^{*2} + 2\pi\rho^{*}\Sigma_0 f(\rho^{*}),$$
$$\Delta g'' = -2\pi\log(S) + 4\pi\Sigma_0 f'(\rho^{*}) + 2\pi\rho^{*}\Sigma_0 f''(\rho^{*}),$$
$$\Delta g^{iv} = 2\pi\Sigma_0\left[4f'''(\rho^{*}) + \frac{f^{iv}(\rho^{*})f(\rho^{*})\Sigma_0}{\log(S) - \Sigma_0 f'(\rho^{*})}\right],$$

and therefore we recover Eq. (4.7):

$$Z = \frac{1}{2\pi\rho^{*}}\left[\log(S) - 2\Sigma_0 f' - \frac{\Sigma_0{}^2 f f''}{\log(S) - \Sigma_0 f'}\right]^{1/2}\left(1 - \frac{\Sigma_0}{16\pi}\frac{4f''' + f^{iv} f\Sigma_0 / (\log(S) - \Sigma_0 f')}{(\log(S) - 2\Sigma_0 f' - \rho^{*}\Sigma_0 f'')^2}\right)$$

where f and its derivatives are evaluated at ρ^* given by Eq. (4.5).

Eq. (4.8) from the main text is for the frequency of attachment of particles to the critical nucleus, ω^*. To obtain Eq. (4.8), we multiply the frequency of arrival of particles to the surface of a cluster, γ^+, by the number of available sites at the surface, M_a. These terms are:

$$M_a = \frac{2\pi R^{*}}{\sqrt{a}} = 2\pi\rho^{*},$$

and

$$\gamma^{+} = aC\nu e^{-\Delta U_d / kT}.$$

The variables appearing in γ^+ are related to the diffusion coefficient, D:

$$D = \nu l_s{}^2 \exp(-\Delta U_d / kT),$$

where ΔU_d is the energy barrier that a solute particle must overcome in order to break the bonds with other solute particles that will be replaced by bonds to the surface (ΔU_d is called

the desolvation energy), and ν is a frequency factor representing the rate at which a solute particle completes diffusion step that brings it to the cluster surface.

As above, we assume that the concentration in the area near the cluster surface, C, is approximately equal to the initial concentration. Then, multiplying γ^+ by M_a gives us:

$$\omega^* = 2\pi\rho^* a C_{in} \frac{D}{l_s^{\,2}},$$

which is Eq. (4.8).

Appendix D

Derivation of Eqs. (4.10 – 4.13)

In this appendix, we derive Eqs. (4.10-4.13). In addition to the variables defined in the main text, section 4.2.1, let L be the system size, a the molecular area of a crystal particle, and β the growth rate kinetic coefficient of particle attachment to the crystal surface (which is related to the bond-strength parameters). The growth rate, V is equal to the rate of change of the crystal radius, $dR(t)/dt$. For simplicity of notation, let $C = C(r, t)$ and $C_0 = C(R, t)$.

We begin with Fick's law in the area of the system outside of the growing crystal:

$$\frac{\partial C}{\partial t} = \frac{D}{r}\frac{\partial}{\partial r}\left(r\frac{\partial C}{\partial r}\right); \quad r > R(t), \tag{D.1}$$

and consider the flux across the crystal surface:

$$a^{-1}V = D\left.\frac{\partial C}{\partial r}\right|_R + VC_0, \tag{D.2}$$

with the general form of the growth rate, as in Eq. (2.18):

$$V = \beta(C_0 - C_{eq}) / C_{eq}. \qquad \text{(D.3)}$$

The boundaries are held at a constant concentration, $\hat{C}$, which is equal to the uniform concentration in the initial configuration of the system, such that $C(\infty, t) = C(r,0) = \hat{C}$. We introduce the substitution $\varsigma = r^2/4Dt$ and see that:

$$\frac{\partial}{\partial r} = \frac{\partial \varsigma}{\partial r}\frac{d}{d\varsigma} = \frac{r}{2Dt}\frac{d}{d\varsigma} = \sqrt{\frac{\varsigma}{Dt}}\frac{d}{d\varsigma},$$

and:

$$\frac{\partial}{\partial t} = \frac{\partial \varsigma}{\partial t}\frac{d}{d\varsigma} = \frac{-r^2}{4Dt^2}\frac{d}{d\varsigma} = \frac{-\varsigma}{t}\frac{d}{d\varsigma}.$$

This allows us to rewrite Eq. (D.1) as:

$$\varsigma\frac{dC}{d\varsigma} = -\frac{d}{d\varsigma}\left(\varsigma\frac{dC}{d\varsigma}\right). \qquad \text{(D.4)}$$

Let us now define $\delta C = C - \hat{C}$, with $\delta C(\infty,t) = \delta C(r,0) = 0$. Let us also define $w = \varsigma\frac{d(\delta C)}{d\varsigma}$, such that $w = -\frac{dw}{d\varsigma}$, following from Eq. (D.4). We can therefore say that:

$$-\varsigma = \log(w/\alpha_1),$$

where α_1 is a constant. This gives us the equation:

$$w = \alpha_1 e^{-\varsigma} = \varsigma\frac{d\delta C}{d\varsigma},$$

and therefore:

$$\delta C = \alpha_1 \int_{a_2}^{\varsigma} \frac{e^{-\varsigma}}{\varsigma} d\varsigma, \tag{D.5}$$

where α_2 is another constant. Noticing that $r^2/4Dt \to \infty$ when $t \to 0$ or $r \to \infty$, we take $\alpha_2 \to \infty$ in order to have $\delta C \to 0$ when $t \to 0$ or $r \to \infty$ We rewrite the integral in Eq. (D.5) as:

$$\delta C = -\alpha_1 \int_{\varsigma}^{\infty} \frac{e^{-\varsigma}}{\varsigma} d\varsigma. \tag{D.6}$$

The integral in Eq. (D.6) is called the "exponential integral", $E_1(\varsigma)$. We can reexpress Eq. (D.6) as follows:

$$\delta C = -\alpha_1 E_1(r^2/4Dt),$$

or, in other terms:

$$C = \hat{C} - \alpha_1 E_1(r^2/4Dt). \tag{D.7}$$

Eq. (D.7) can be evaluated at $r = R$ and written in terms of C_0 as follows:

$$C_0 = \hat{C} - \alpha_1 E_1(R^2/4Dt), \tag{D.8}$$

and, by evaluating Eq. (D.6) at the crystal radius, R, we can obtain an expression for the derivative of Eq. (D.7) at $r = R$:

$$\left.\frac{\partial C}{\partial r}\right|_{r=R} = 2\alpha_1 \frac{e^{-R^2/4Dt}}{R}.$$

Let us define $\varsigma_R = R^2/4Dt$ for simplicity of notation. Returning to the boundary condition (Eq. D.2), we can determine the rate of growth, V, as a function of C_0:

$$\begin{aligned} V &= aD\left.\frac{\partial C}{\partial r}\right|_{r=R}(1-aC_0)^{-1} \\ &= \frac{2aD\alpha_1}{R}e^{-\varsigma_R}(1-a(\hat{C}-\alpha_1 E_1(\varsigma_R))^{-1}, \end{aligned}$$

where Eq. (D.8) has been substituted in at the second line. Next, we can solve for α_1:

$$\alpha_1 = V(1-a\hat{C})\frac{R}{2aD}e^{\varsigma_R}(1-\frac{VR}{2D}E_1(\varsigma_R)e^{\varsigma_R})^{-1}$$

which, using Eq. (D.8), allows us to write an expression for C_0:

$$C_0 = \left(\hat{C}-\frac{VR}{2aD}e^{\varsigma_R}E_1(\varsigma_R)\right)\left(1-\frac{VR}{2D}E_1(\varsigma_R)e^{\varsigma_R}\right)^{-1}. \qquad \text{(D.9)}$$

Now substituting Eq. (D.9) into the general equation for the growth rate (Eq. (D.3)) and rearranging leaves us with a quadratic equation for V:

$$0 = V^2\frac{R}{2D}E_1(\varsigma_R)e^{\varsigma_R} + V\left[-1+\frac{\beta R}{2D}E_1(\varsigma_R)e^{\varsigma_R} - \frac{\beta R}{2DaC_{eq}}E_1(\varsigma_R)e^{\varsigma_R}\right] + \frac{\beta}{C_{eq}}(\hat{C}-C_{eq}).$$

In solving this equation for V, we find that taking the negative sign in the quadratic formula is the correct choice as it reproduces Eq. (D.3) under interface-controlled where $D \to \infty$, and $C \to \hat{C}$.

At large times ($R^2 << 4Dt$), such that $\varsigma_R \rightarrow 0$, the exponential integral can be approximated as $E_1(\varsigma_R) \rightarrow -\ln(\varsigma_R)$ [Abramowitz 2002]. We therefore obtain the following equation for V at large times:

$$V \approx -\frac{De^{-\varsigma_R}}{R\ln\varsigma_R}\left[1+\frac{\beta R\ln\varsigma_R(aC_{eq}-1)}{2DaC_{eq}e^{-\varsigma_R}}-\left(\left(1+\frac{\beta R\ln\varsigma_R(aC_{eq}-1)}{2DaC_{eq}e^{-\varsigma_R}}\right)^2+\frac{2\beta R\ln\varsigma_R(\hat{C}-C_{eq})}{DC_{eq}e^{-\varsigma_R}}\right)^{1/2}\right].$$

Expanding the above equation gives us:

$$V \approx -\frac{De^{-\varsigma_R}}{R\ln\varsigma_R}\left[\begin{array}{l}-\dfrac{\beta R\ln\varsigma_R(1-aC_{eq})}{2DaC_{eq}e^{-\varsigma_R}}+1+\dfrac{\beta R(1-aC_{eq})\ln\varsigma_R}{2DaC_{eq}e^{-\varsigma_R}}\times \\ \left(1-\dfrac{4DaC_{eq}e^{-\varsigma_R}}{\beta R\ln\varsigma_R(1-aC_{eq})}+\dfrac{8Da^2C_{eq}(\hat{C}-C_{eq})e^{-\varsigma_R}}{\beta R\ln\varsigma_R(1-aC_{eq})^2}+\dfrac{4D^2a^2{C_{eq}}^2e^{-2\varsigma_R}}{\beta^2R^2(\ln\varsigma_R)^2(1-aC_{eq})^2}\right)^{1/2}\end{array}\right]$$

To simplify this equation, we first neglect the last term containing $1/(\ln\varsigma_R)^2$ because it decreases more rapidly than the other terms. Next we approximate the remaining terms under the square root following the series $\sqrt{1+x}=1+x/2+O(x^2)$, and simplify to finally arrive at:

$$V \approx -\frac{2aD}{R\ln\varsigma_R e^{\varsigma_R}}\frac{(\hat{C}-C_{eq})}{(1-aC_{eq})}. \qquad \text{(D.10)}$$

For large times, let us propose the ansatz $R(t)=2\sqrt{A_1 t}$, which is Eq. (4.11) from the main text. The corresponding growth rate is $V=dR/dt=\sqrt{A_1/t}$. Substitution of this proposed solution and its derivative into Eq. (D.10) shows that the constant A_1 is indeed independent of time:

$$A_1 = -\frac{aD}{\ln(A_1/D)e^{A_1/D}}\left(\frac{\hat{C}-C_{eq}}{1-aC_{eq}}\right).$$

A_1 can then be found by solving this transcendental equation. This means that the proposed solution for $R(t)$ at large time is self-consistent. Now we can obtain the concentration at the crystal surface using Eq. (D.3) in the large time case, and recover Eq. (4.10):

$$C_0 = C(R,t) \approx C_{eq}\left(1 + A_0 \frac{1}{\sqrt{t}}\right),$$

where

$$A_0 = \frac{\sqrt{A_1}}{\beta}.$$

For intermediate times, we can obtain a solution to Eq. (D.10) by assuming that the $R(t)$ does not change significantly in time, such that $R(t) \approx R_0$ where R_0 is the crystal's size at $t = 0$. Under this assumption, we propose Eq. (4.13), the solution for $R(t)$, as an ansatz:

$$R \approx 2e^{-R_0^2/8Dt}\sqrt{\frac{aDt}{\ln(4Dt/R_0^2)}\frac{(\hat{C}-C_{eq})}{(1-aC_{eq})}} = A_3 e^{-B_0/t}\sqrt{\frac{t}{\ln(t/2B_0)}}, \qquad \text{(D.11)}$$

where

$$A_3 = 2\sqrt{aD\frac{(\hat{C}-C_{eq})}{(1-aC_{eq})}},$$

and

$$B_0 = \frac{R_0^{\,2}}{8D}.$$

Differentiating the ansatz Eq. (D.11) provides us with an equation for V:

$$\begin{aligned} V = \frac{dR}{dt} &= A_3 B_0 e^{-B_0/t}\left(\frac{1}{2}\sqrt{\frac{1}{t\ln(t/2B_0)}} - \frac{1}{2}\sqrt{\frac{1}{t\ln(t/2B_0)^3}} + \sqrt{\frac{\ln(t/2B_0)}{t^3}}\right) \\ &\approx \frac{A_3}{2} e^{-B_0/t}\sqrt{\frac{1}{t\ln(t/2B_0)}}, \end{aligned} \tag{D.12}$$

where second and third terms under the square roots in the first line can been neglected in comparison to the first term under the square root. Substituting Eq. (D.12) into Eq. (D.3) allows us to obtain an expression for C_0 for intermediate times, which is Eq. (4.12) from the main text:

$$C_0 \approx C_{eq}\left(1 + A_2 \frac{e^{-B_0 t}}{\sqrt{t\ln(t/2B_0)}}\right),$$

where

$$A_2 = \frac{A_3}{2\beta}.$$

Appendix E

Derivation of Eqs. (4.14- 4.17)

In this appendix, we derive Eqs. (4.14-4.17). In addition to the variables defined in the main text, section 4.2.1, let L be the system size, a the molecular area of a crystal particle, and β the growth rate kinetic coefficient of particle attachment to the crystal surface (which is related to the bond-strength parameters). The growth rate, V is equal to the rate of change of the crystal radius, $dR(t)/dt$. For simplicity of notation, let $C = C(r, t)$ and $C_0 = C(R, t)$.

We begin with Fick's law in the area of the system outside of the growing crystal:

$$\frac{\partial C}{dt} = \frac{D}{r}\frac{\partial}{\partial r}\left(r\frac{\partial C}{\partial r}\right); \quad r > R(t), \tag{E.1}$$

and consider the flux across the crystal surface:

$$a^{-1}V = D\left.\frac{\partial C}{\partial r}\right|_R + VC_0,$$

with the growth rate $V = \beta(C_0 - C_{eq})/C_{eq}$. We take reflective (no-flux) boundary conditions, where $\partial C/\partial r\big|_L = 0$, and a uniform initial concentration condition where $C(r, 0) = \hat{C}$. C will approach C_{eq} asymptotically as time goes on. We let $C = C_{eq} + \varepsilon C_1(r, t)$ and

$V = (\beta/C_{eq})\,\varepsilon C_1(R, t)$, where εC_1 is small.

Now we assume that the concentration decays over time in the form $\varepsilon C_1(r, t) = X(r)\exp(-bt)$, where b is a constant controlling the rate of exponential decay of the concentration. Under Fick's law this becomes:

$$-bX = \frac{D}{r}\frac{d}{dr}\left(r\frac{dX}{dr}\right) = D\frac{d^2X}{dr^2} + \frac{D}{r}\frac{dX}{dr},$$

or,

$$\frac{d^2X}{dr^2} + \frac{1}{r}\frac{dX}{dr} + \frac{b}{D}X = 0.$$

Making the substitution $\nu = r\sqrt{b/D}$ and differentiating X with respect to ν gives:

$$X'' + \frac{X'}{\nu} + X = 0,$$

which is a form of the Bessel equation with solutions $J_0(\nu)$ and $Y_0(\nu)$. Thus, the solution of Eq. (E.1) is a superposition of products of functions exponentially decaying in time with $J_0(\nu)$ or $Y_0(\nu)$. The boundary condition gives a relation between the decay constant and the parameters defining the problem. If we keep only the slowest decaying mode, the solution has the form of Eq. (4.14):

$$C(r,t) \approx k_1\left[J_0\left(r\sqrt{b/D}\right)+k_2 Y_0\left(r\sqrt{b/D}\right)\right]\exp(-bt)+C_{eq}, \qquad \text{(E.2)}$$

where k_1 and k_2 are constants. Eq. (4.15) results from a spatial averaging of Eq. (E.2).

Next, let us look at behavior of $R(t)$ under reflective boundary conditions. The growth of the crystal radius is:

$$R(t) = R_0 + \int_0^t V(t')dt',$$

where R_0 is the crystal radius at $t = 0$. We can add and subtract the time integral of the rate as follows:

$$R(t) = R_0 + \int_0^\infty V(t')dt' - \int_0^\infty V(t')dt' + \int_0^t V(t')dt',$$

where $R_\infty = \int_0^\infty V(t')dt'$ is the radius at $t = \infty$ and $-\int_0^\infty V(t')dt' + \int_0^t V(t')dt' = -\int_t^\infty V(t')dt'$, giving us

$$R(t) = R_\infty - \int_t^\infty V(t')dt'.$$

We substitute $V(t') = (\beta/C_{eq})\,\varepsilon C_1(R,t')$ into this equation and integrate to obtain:

$$\begin{aligned} R(t) &= R_\infty - \frac{\beta}{C_{eq}}\int_t^\infty \varepsilon C_1(R,t')dt' \\ &\approx R_\infty - \frac{\beta}{C_{eq}}\left(k_1\left[J_0\left(R_\infty\sqrt{b/D}\right)+k_2 Y_0\left(R_\infty\sqrt{b/D}\right)\right]\right)\int_t^\infty \exp(-bt')dt' \\ &= R_\infty - \frac{\beta k_1}{bC_{eq}}\left[J_0\left(R_\infty\sqrt{b/D}\right)+k_2 Y_0\left(R_\infty\sqrt{b/D}\right)\right]\exp(-bt) \end{aligned}$$

as in Eq. (4.17). Eq. (4.16) is obtained by representing the coefficient on the exponential in the above equation as a constant, A_5.

Appendix F

Derivation of Eq. (5.3)

This appendix reproduces the derivation of Eq. (5.3) from Eq. (5.1) from the paper of Wedekind et al. [Wedekind 2007]. We begin with Eq. (5.1):

$$\tau(N_0;0,N) = \int_{N_0}^{N} \frac{1}{D} d\bar{y} e^{\Delta G(\bar{y})/kT} \int_{0}^{\bar{y}} d\bar{z} e^{-\Delta G(\bar{z})/kT}. \qquad \text{(F.1)}$$

If the free energy barrier is high, such that $\Delta G(N^*)/kT >> 1$, then the first exponential in the integrand of Eq. (F.1) will have a sharp peak near the maximum of $\Delta G(\bar{y})$. This allows us to expand $\Delta G(\bar{y})$ around the critical nucleus size, N^*:

$$\Delta G(\bar{y}) \approx \Delta G(N^*) - \frac{1}{2}\left|\Delta G''(N^*)\right|(\bar{y} - N^*)^2,$$

where $\Delta G''(N^*)$ is the second derivative of the free energy evaluated at the critical nucleus size (the first derivative is zero at the maximum of ΔG). We also make the assumption that the diffusion coefficient, D, is constant and equal to its value at the critical nucleus size: $D =$

$D(N^*)$. Since we focus on the region around the peak of the free energy barrier, we can replace the upper integration limit on the second integral in Eq. (F.1) with N^*, and get the expression:

$$\tau(N) = \frac{1}{D(N^*)} \int_{N_0}^{N} d\bar{y} \exp[\Delta G(N^*)/kT] \exp[-\frac{1}{2}|\Delta G''(N^*)|(\bar{y} - N^*)^2/kT] \times \int_{0}^{N^*} d\bar{z} \exp[-\Delta G(\bar{z})/kT]. \quad \text{(F.2)}$$

Next, we make the substitution $u = \bar{y} - N^*$, which turns the lower integration limit in the first integral into $N_0 - N^* \approx -\infty$ due to the sharpness of the free energy peak. Then, we break up the first integral into two parts, such that:

$$\int_{-\infty}^{N-N^*} = \int_{-\infty}^{0} + \int_{0}^{N-N^*},$$

where the integral with integration limits $-\infty$ and 0 is a Gaussian integral and equals to a constant, and the other integral can be written in terms of the error function:

$$\text{erf}(\bar{x}) = \frac{2}{\sqrt{\pi}} \int_{0}^{\bar{x}} \exp[-\bar{x}^2] d\bar{x}.$$

Then, factoring out the exponential containing $\Delta G(N^*)$, we can write Eq. (F.2) as follows:

$$\tau(N) = \frac{\exp[\Delta G(N^*)/kT]}{D(N^*)} \left(\int_{0}^{N^*} d\bar{z} \exp[-\Delta G(\bar{z})/kT] \right) \times \frac{1}{2} \sqrt{\frac{2\pi kT}{|\Delta G''(N^*)|}} \left(1 + \text{erf}\left(\sqrt{\frac{|\Delta G''(N^*)|}{2kT}} (N - N^*) \right) \right). \quad \text{(F.3)}$$

At the critical nucleus size, the MFPT is as follows, using the fact that erf(0) = 0 and recalling Eq. (5.2):

$$\tau(N = N^*) = \frac{\exp[\Delta G(N^*)/kT]}{D(N^*)}\left(\int_0^{N^*} d\bar{z}\exp[-\Delta G(\bar{z})/kT]\right)\frac{1}{2}\sqrt{\frac{2\pi kT}{|\Delta G''(N^*)|}} \equiv \frac{1}{2JL^2}.$$

Following from the previous step, Eq. (F.3) becomes Eq. (5.3):

$$\tau(N) = \frac{\tau_J}{2}[(1+\mathrm{erf}(N-N^*)z)],$$

where $\tau_J = 1/JL^2$ and $z = \sqrt{|\Delta G''(N^*)|/2kT}$.

Appendix G

Code

```
!!!!!!!!!!!!!!!!!!!!!!!!!!!! GLOBAL PARAMETERS !!!!!!!!!!!!!!!!!!!!!!!!!!!!

MODULE global_params
! S1:# of 'j' indices in diffusion lattice, S2: # of 'i' indices of
! diffusion lattice, G1:# of 'j' indices in crystal lattice, G2: # of 'i'
! indices of crystal lattice.
! Effective size of the diffusion lattice is (S1-1)x(S2-1) because 1 row
! and column  at each side is used to handle boundary condition.
! cnum_max: number of crystals that my form at one time (limited to 1 in
! thesis results).
! t_final: maximum number of time steps for a given realisation.
! realisations: maximum number of realisations.
INTEGER, PARAMETER :: S1=32, S2=32, G1=S1, G2=S1, cnum_max=1
INTEGER, PARAMETER :: t_final = 15000, realisations = 1000, n_max = 30
! Set MFPT_run = 1 to generate data for MFPT analysis, set MFPT_run = 0
! otherwise
INTEGER, PARAMETER :: MFPT_run = 1
! Ess: solid-solid bonding strength, Esw: solid-water bonding strength,
! eta: next-to-nearest neighbour bonding strength
REAL, PARAMETER :: Ess = -1.5, Esw = -0.5, eta = 1.0
! C_init: initial concentration of solute in system
REAL, PARAMETER :: C_init = 0.350
! Glattice: crystal lattice, stores nucleating/growing clusters
INTEGER :: GLattice(cnum_max,G1,G2)
INTEGER ::  used(4*G1,2), used_counter
! Slattice: diffusion lattice, handles diffusion of solute particles
INTEGER :: SLattice(2,S1,S2,4), NOW, PAST, sFlags(S1,S2), restart
! rand: stores random number
REAL :: rand
END MODULE global_params

!!!!!!!!!!!!!!!!!!!!!!!!!!!!!!!! MAIN PROGRAM !!!!!!!!!!!!!!!!!!!!!!!!!!!!!!
```

```
PROGRAM LGA_Nucleation

USE global_params
! Variables used generally in main program
INTEGER :: r,t,i,j
INTEGER :: temp,inv,Init
REAL :: conc_glob, conc_counter
! Variables used in “streaming” step
INTEGER :: inv_directions(4),Ex(4),Ey(4)
! Variables used in “attachment” and “detachment” steps
INTEGER :: i2,j2,gFlags(S1,S2), k_counter, k_store(4)
INTEGER :: found_i, found_j, site_type, cnum, cnum_counter, tot_en
INTEGER :: attach_success, detach_allowed, num_particles
INTEGER :: num_particles_streaming, two_particles
INTEGER :: cnum_store(cnum_max)
INTEGER, PARAMETER :: set_j = (S1)/2, set_i = (S2)/2
! Variables used in “rotation” step
INTEGER :: Rot(4), ang
! Variables used for MFPT generation
INTEGER :: size_sample(t_final), size_max, size_current, t_index

! Initiate random number generator with new random seed
call RANDOM_SEED

! Open file for parameter value storage
open(unit = 7, file="./Data/params.txt", status="replace", action="write")
! Open file to record number of particles vs. t
open(unit = 8, file="./Data/n_p.txt", status="replace", action="write")
! Open file for globally averaged concentration data
open(unit = 9, file="./Data/conc_glob.txt", status="replace",
action="write")
! Open file for data used in MFPT and Pst calculation
open(unit = 10, file="./Data/size_sample.txt", status="replace",
action="write")

! D2Q4 specific vector directions, and their inverse directions.
! The “origin” (0,0) of the streaming lattice is located in its top-left
! corner.
Ex=[1, 0, -1, 0]
Ey=[0, -1, 0, 1]
inv_directions=[3,4,1,2]
! Used to store current and past SLattice
NOW=1
PAST=2

! Output parameter values
write(7,*) MFPT_run, realisations, t_final, Ess, Esw, eta, C_init, n_max

! Begin loop over all realisations
do r = 1,realisations

! Continue from here if simulation needs to be restarted (if crystal
! touches edge of crystal lattice, or if the nmax is not obtained when
! MFPT_run=1).
```

```
5 continue

t=0
! Reset array of cluster sizes vs. time
size_sample = 0
! Re-initialize diffusion lattice and crystal lattice parameters
sFlags=0
gFlags=0
SLattice=0
GLattice=0
cnum=0
cnum_counter=0
used_counter=0
cnum_store=0
two_particles=0
tot_en=0
attach_success=0

! Choose initialization (set Boundary Condition (using “flags” value).
Init = 1
! Set up sFlags to give each SLattice node a type: sFlags = 1 is used for
! reflective or constant-concentration boundary, sFlags = 2 for fluid
! cells, sFlags = 3 for wrap-around boundary (not used in thesis).
if (Init.eq.1) then
call SetFlag1
else if (Init.eq.2) then
call SetFlag2
end if

! Fill Slattice at initial concentration, C_init.
call Initial_Concentration

! Output initial # of particles in crytal lattice (zero particles)
do cnum = 1,cnum_max
num_particles = sum(GLattice(cnum,:,:))
write(8, '(1X, I5)', ADVANCE="YES") num_particles
end do

! Output initial concentration measurement, averaged
! over all non-boundary cells of diffusiion lattice.
conc_glob = sum(SLattice(PAST,2:S1-1,2:S2-1,:))/real((S1-2)*(S2-2))
write(9,*) conc_glob

! If MFPT_run = 1, then loop continues until cluster reaches size n_max:
! if n_max is not reached by t_final, this realisation is restarted.
! If MFPT_run = 0, then loop until t = t_final and stop at that point.

do t=1,t_final

! Initialize restart variable (if set =1 then this realisation restarted
restart=0

! Reset boundary to C_init by calling “Boundary_Concentration” subroutine
! if constant concentration boundaries are desired:
! call Boundary_Concentration
```

```
!!!!!! Streaming Step !!!!!!

do i=S2-1,2,-1
do j=S1-1,2,-1
do k =1,4,1
inv=inv_directions(k)

!Stream to non-boundary cells
if(sFlags(j+Ey(inv),i+Ex(inv)).eq.2) then
SLattice(NOW,j,i,k)=SLattice(PAST,j+Ey(inv),i+Ex(inv),k)
end if

!Reflective boundary
if((sFlags(j+Ey(inv),i+Ex(inv)).eq.1)) then
SLattice(NOW,j,i,k)=SLattice(PAST,j,i,inv)
end if

!Wrap-around boundary (not used in thesis)
if(sFlags(j+Ey(inv),i+Ex(inv)).eq.3) then
if(Ey(k).eq.0) then
jnew=j
inew=S2+1-i
end if
if(Ex(k).eq.0) then
inew=i
jnew=S1+1-j
end if
SLattice(NOW,j,i,k)=SLattice(PAST,jnew,inew,k)
end if

end do
end do
end do

! Output # of particles in cluster(s)
do cnum = 1,cnum_max
num_particles = sum(GLattice(cnum,:,:))
write(8, '(1X, I5)', ADVANCE="YES") num_particles
end do

! Output globally averaged concentration
conc_glob = sum(SLattice(NOW,2:S1-1,2:S2-1,:))/real((S1-2)*(S2-2))
write(9,*) conc_glob

!!!!!! Attachment Step !!!!!!

! For attachment, site_type = 1
! For detachment (below), site_type = 2
site_type = 1
do i = 2, S2-1
do j = 2, S1-1

!!! Solid Creation !!!
```

```
! When only one cluster is permitted to form, as was done for the data
! analyzed in the thesis, the cluster is restricted to forming at the
! specific location (set_j,set_i), e.g. the centre node of the diffusion
! lattice (Slattice).
if (j == set_j .and. i == set_i) then

! In order for a crystal to form, there must be no crystal present
! at the corresponding node in the Glattice.
if (gFlags(j,i).eq.0 .and. sum(cnum_store) < cnum_max) then

! Determine # of particles streaming to this Slattice node. There must be
! at least two particles for solid creation to take place.
num_particles_streaming = sum(SLattice(NOW,j,i,:))
if (num_particles_streaming >= 2) then
two_particles = 1

! If num_particles == 2 or num_particles == 3, do this process once.
! But if num_particles == 4 and attach_success still equals 0, two
! attempts are made.
call Energy_Calc(cnum, found_i, found_j, site_type, two_particles,
attach_success)
if (num_particles_streaming == 4 .and. attach_success == 0) then
call Energy_Calc(cnum, found_i, found_j, site_type, two_particles,
attach_success)
end if

! If a two-particle cluster successfully forms,
if (attach_success == 1) then
! Randomly choose and remove 2 (solute) particles from this node of the
! Slattice.
do i2 = 1,2
num_particles_streaming = sum(SLattice(NOW,j,i,:))
do while (int(sum(SLattice(NOW,j,i,:)))-num_particles_streaming == 0)
call RANDOM_NUMBER(rand)
if (rand < 0.25 .and. SLattice(NOW,j,i,1) == 1) SLattice(NOW,j,i,1) = 0
if (rand >= 0.25 .and. rand < 0.5 .and. SLattice(NOW,j,i,2) == 1)
SLattice(NOW,j,i,2) = 0
if (rand >= 0.5 .and. rand < 0.75 .and. SLattice(NOW,j,i,3) == 1)
SLattice(NOW,j,i,3) = 0
if (rand > 0.75 .and. SLattice(NOW,j,i,4) == 1) SLattice(NOW,j,i,4) = 0
end do
end do

! Tag this cluster with next available cluster number in cnum_store array
!(when only 1 cluster is permitted to grow, as in thesis, cnum_max=1).
do i2 = 1, cnum_max
if (cnum_store(i2) == 0) then
cnum = i2
cnum_store(i2) = 1
exit
end if
end do

! Place the two-particle cluster in the centre of the Glattice.
GLattice(cnum,(G2+1)/2,(G1+1)/2) = 1
```

```
GLattice(cnum,(G2+1)/2,(G1+1)/2+1) = 1
! Identify the Slattice node as a “seed node,” where a attachment to or
! detachment from a cluster may take place, and assign a number to this
! cluster.
gFlags(j,i) = cnum

end if
end if
end if
end if

!!! Attachment to an existing cluster !!!

used_counter=0
used=0
do k_counter = 1,4
if (k_counter == 1) k_store(:) = 0
call Pick_Direction(k, k_store)

! If this SLattice node is a “seed node” and there are solute particles
! that have streamed to this node, then proceed.
if (gFlags(j,i).ne.0 .and. SLattice(NOW,j,i,k).eq.1) then
! Specify cluster
cnum = gFlags(j,i)
two_particles = 0

! Find an attachment site on the cluster surface accessible to the solute
! particle based on its incoming direction.
call Find_Site_and_Test(k, cnum, found_j, found_i, two_particles,
site_type, attach_success)

! Realisation may need to be restarted if Glattice boundary is touched.
if (restart == 1) GO TO 5

! If attachment of solute particle is successful, remove it from Slattice
! and insert on Glattice at selected attachment site.
if (attach_success == 1) then
GLattice(cnum,found_j,found_i) = 1
SLattice(NOW,j,i,k)=0
end if
end if
end do
end do
end do

!!!!!! Rotation Step !!!!!!

do i = 2, S2
do j = 2, S1

! There must be at least one particle at this Slattice node for rotation
! of particles to proceed.
if (sum(SLattice(NOW,j,i,:)) > 0) then
CALL RANDOM_NUMBER(rand)
```

```
! Decide counter-clockwise rotation angle.
if (rand <= 0.25) ang = 0
if (rand > 0.25 .and. rand <= 0.5) ang = 3
if (rand > 0.5 .and. rand <= 0.75) ang = 2
if (rand > 0.75 .and. rand <= 1) ang = 1
! Do the rotation.
do k = 1,4
if ((k-ang) < 1) then
Rot(k) = SLattice(NOW,j,i,k-ang+4)
else
Rot(k) = SLattice(NOW,j,i,k-ang)
end if
end do
SLattice(NOW,j,i,1:4) = Rot(1:4)
end if
end do
end do

!!!!!! Detachment Step !!!!!!

! site_type = 2 for detachment.
! site_type = 1 for attachment (above).
site_type = 2
do i = 2, S2-1
do j = 2, S1-1
do k_counter = 1,4
if (k_counter == 1) k_store(:) = 0
call Pick_Direction(k, k_store)

! If this Slattice node contains a solid cluster and has a vacancy for
! an additional solute particle, then proceed:
if (gFlags(j,i).ne.0 .and. SLattice(NOW,j,i,inv_directions(k)).eq.0) then
cnum = gFlags(j,i)

! Determine the number of particles in the cluster.
num_particles = sum(GLattice(cnum,:,:))
! If the cluster only has two particles, then detachment will result in
! complete dissolution.
if (num_particles == 2) then

! Determine if there are two positions available in the Slattice for
! detached solute particles.
vacancy = 0
if (SLattice(NOW,j,i,1) == 0) vacancy = vacancy + 1
if (SLattice(NOW,j,i,2) == 0) vacancy = vacancy + 1
if (SLattice(NOW,j,i,3) == 0) vacancy = vacancy + 1
if (SLattice(NOW,j,i,4) == 0) vacancy = vacancy + 1
if (vacancy > 1) then
call RANDOM_NUMBER(rand)
two_particles = 1
call Energy_Calc(cnum, found_i, found_j, site_type, two_particles,
attach_success)

! If detachment was successful, add the 2 particles to the Slattice.
if (attach_success == -1) then
```

```
! Place the first detached particle on the current Slattice node,
! with velocity pointing in the direction used to find the detachment
site.
SLattice(NOW,j,i,k) = 1
! Place the second detached particle at a different, randomly chosen,
! available site at this Slattice node.
num_particles_streaming = sum(SLattice(NOW,j,i,:))
do while (sum(SLattice(NOW,j,i,:))-num_particles_streaming == 0)
call RANDOM_NUMBER(rand)
if (rand < 0.25 .and. SLattice(NOW,j,i,1) == 0) SLattice(NOW,j,i,1) = 1
if (rand >= 0.25 .and. rand < 0.5 .and. SLattice(NOW,j,i,2) == 0)
SLattice(NOW,j,i,2) = 1
if (rand >= 0.5 .and. rand < 0.75 .and. SLattice(NOW,j,i,3) == 0)
SLattice(NOW,j,i,3) = 1
if (rand > 0.75 .and. SLattice(NOW,j,i,4) == 0) SLattice(NOW,j,i,4) = 1
end do

! Remove the two particles from the Glattice (final dissolution).
GLattice(cnum,:,:) = 0
! Reset this cluster number to allow a new cluster to receive this tag
! at a later time.
cnum_store(cnum) = 0
gFlags(j,i) = 0
end if
end if

! Otherwise, if the cluster is composed of more than two particles,
! proceed by attempting single particle detachment:
else if (num_particles > 2) then
two_particles  = 0
call Find_Site_and_Test(k, cnum, found_j, found_i, two_particles,
site_type, attach_success)
if (restart == 1) GO TO 5
if (attach_success == -1) then
GLattice(cnum,found_j,found_i) = 0
SLattice(NOW,j,i,inv_directions(k))=1
end if
end if
end if
end do
end do
end do

! Output data used in MFPT calculation
if (MFPT_run == 1) then
t_index = t
size_max = 0
do i = 1, cnum_max
size_current = sum(GLattice(i,:,:))
if (size_current > size_max) then
size_max = size_current
end if
end do
if (size_max < n_max) then
size_sample(t_index) = size_max
```

```
! If the size limit has been reached, skip to the end of this realisation.
else if (size_max .ge. n_max) then
size_sample(t_index) = n_max
GO TO 6
end if
end if

! Used to transfer current SLattice to past SLattice.
temp=PAST
PAST=NOW
NOW=temp

! End loop through “t.”
end do
! End loop through “r.”
! If generating MFPT data and the maximum cluster size was not reached,
! restart this realisation.
if (MFPT_run == 1) then
if (maxval(size_sample) < n_max) then
GO TO 5
end if
end if
6 CONTINUE
! Output MFPT data.
if (MFPT_run == 1) then
write(10,*) size_sample
end if
end do

!!!!!!!!!!!!!!!!!!!!!!!!!!! End of Main Program !!!!!!!!!!!!!!!!!!!!!!!!!!!

END PROGRAM LGA_Nucleation

!!!!!!!!!!!!!!!!!!!!!!!!!!!!!!! Subroutines !!!!!!!!!!!!!!!!!!!!!!!!!!!!!!!

SUBROUTINE SetFlag1
USE global_params

!Reflective boundary on all sides,
!Fluid cells in bulk
!No solid initially

sFlags(1:S1,1:S2)=2

sFlags(1:S1,1)=1
sFlags(1:S1,S2)=1
sFlags(1,1:S2)=1
sFlags(S1,1:S2)=1

END SUBROUTINE SetFlag1

SUBROUTINE SetFlag2
USE global_params

!Wrap-around boundary on all sides (not used in thesis),
```

```
!Fluid cells in bulk
!No solid initially

sFlags(1:S1,1:S2)=2

sFlags(1:S1,1)=3
sFlags(1:S1,S2)=3
sFlags(1,1:S2)=3
sFlags(S1,1:S2)=3

END SUBROUTINE SetFlag2

SUBROUTINE Initial_Concentration
! Set initial concentration of SLattice

USE global_params
INTEGER :: n_counter, num_particles_init, num_particles_left, n, i, j
INTEGER :: num_bins_j, num_bins_i
REAL :: bin_size_i, bin_size_j

! Clear SLattice
SLattice(NOW,:,:,:) = 0
SLattice(PAST,:,:,:) = 0
! Initialize variables
n_counter = 0
num_particles_init = C_init*(S1-2)*(S2-2)
! Check for error of having too many particles
if (num_particles_init > 4*(S1-2)*(S2-2)) then
STOP "max number of particles exceeded"
end if

num_particles_left = num_particles_init

num_bins_j = S1-2
num_bins_i = S2-2

bin_size_j = 1./real(num_bins_j)
bin_size_i = 1./real(num_bins_i)

! Insert all particles into SLattice, at randomly chosen nodes, in
randomly chosen directions.
do while (num_particles_left > 0)
n_counter = n_counter + 1
! Find j and i coordinates of node (may not be on outer boundary)
10 CONTINUE

call RANDOM_NUMBER(rand)
do i = 2, S2-1
if (rand >= (i-2)*bin_size_i .and. rand < (i-1)*bin_size_i) then
exit
end if
end do

call RANDOM_NUMBER(rand)
do j = 2, S2-1
```

```
if (rand >= (j-2)*bin_size_j .and. rand < (j-1)*bin_size_j) then
exit
end if
end do

! No room left at this node if there are already 4 particles present.
if (sum(SLattice(PAST,j,i,:)) == 4) then
! Pick another node.
GO TO 10
end if

! Choose direction at selected node (direction must not be already
! occupied).
20 CONTINUE

call RANDOM_NUMBER(rand)
! Decide counter-clockwise rotation angle.
if (rand <= 0.25) k = 1
if (rand > 0.25 .and. rand <= 0.5) k = 2
if (rand > 0.5 .and. rand <= 0.75) k = 3
if (rand > 0.75 .and. rand <= 1) k = 4

if (SLattice(PAST,j,i,k) == 0) then
SLattice(PAST,j,i,k) = 1
else if (SLattice(PAST,j,i,k) == 1) then
! If node is occupied in this direction, try until an available
! direction is found.
GO TO 20
end if
num_particles_left = num_particles_left - 1
end do
SLattice(NOW,:,:,:) = SLattice(PAST,:,:,:)

END SUBROUTINE Initial_Concentration

SUBROUTINE Boundary_Concentration
! Used to keep boundary at constant concentration, if desired.

USE global_params
INTEGER :: i, j, k, t, num_particles_init, num_particles_left, num_nodes,
n
INTEGER :: num_bins
REAL :: bin_size

! # of cells along boundary.
num_nodes = (S2-2)*2+(S1-4)*2

! calculate # of particles corresponding to constant concentration at
! boundary.
num_particles_left = C_init*num_nodes
! Set boundary nodes to 0
SLattice(PAST,2,2:S2-1,:) = 0
SLattice(PAST,S1-1,2:S2-1,:) = 0
SLattice(PAST,3:S1-2,2,:) = 0
SLattice(PAST,3:S1-2,S1-1,:) = 0
```

```
do n = 1,abs(num_particles_left)

11 CONTINUE

! Pick i or j as first coordinate of chosen boundary cell to be defined.
i = 0
j = 0
call Random_Number(rand)
if (rand < 0.5) then
call Random_Number(rand)
if (rand < 0.5) then
j = 2
else if (rand >= 0.5) then
j = S1-1
end if
else if (rand >=0.5) then
call Random_Number(rand)
if (rand < 0.5) then
i = 2
else if (rand >= 0.5) then
i = S2-1
end if
end if

! Pick second coordinate (random choice along row or column specified
! above).
call Random_Number(rand)
if (j == 0) then
num_bins = S1-3
bin_size = 1.0/real(num_bins)
if (i == 2) then
do j = 2, S1-2
if (rand >= (j-2)*bin_size .and. rand < (j-1)*bin_size) then
exit
end if
end do
else if (i == S2-1) then
do j = 3, S1-1
if (rand >= (j-3)*bin_size .and. rand < (j-2)*bin_size) then
exit
end if
end do
end if
else if (i == 0) then
num_bins = S2-3
bin_size = 1.0/real(num_bins)
if (j == 2) then
do i = 3, S2-1
if (rand >= (i-3)*bin_size .and. rand < (i-2)*bin_size) then
exit
end if
end do
else if (j == S1-1) then
do i = 2, S2-2
```

```
if (rand >= (i-2)*bin_size .and. rand < (i-1)*bin_size) then
exit
end if
end do
end if
end if

! No room left at this node if there are already 4 particles there.
if (sum(SLattice(PAST,j,i,:)) == 4) then
! Pick another node.
GO TO 11
end if
! Choose direction at selected node (must not be already occupied).
21 CONTINUE
call RANDOM_NUMBER(rand)
! Decide counter-clockwise rotation angle.
if (rand <= 0.25) k = 1
if (rand > 0.25 .and. rand <= 0.5) k = 2
if (rand > 0.5 .and. rand <= 0.75) k = 3
if (rand > 0.75 .and. rand <= 1) k = 4

if (SLattice(PAST,j,i,k) == 0) then
SLattice(PAST,j,i,k) = 1
else if (SLattice(PAST,j,i,k) == 1) then
! If node is occupied in this direction, try until an available direction
! is found.
GO TO 21
end if
end do

END SUBROUTINE Boundary_Concentration

SUBROUTINE Find_Site_and_Test(k, cnum, found_j, found_i, two_particles,
site_type, attach_success)
! Site location subroutine for use in attachment/detachment processes:

! Find available crystal sites in GLattice for attachment (site_type=1) or
! for detachment (site_type=2).
! If site_type=2, determine if a particle is permitted to be removed from
! this site (call Detachment_Permission subroutine), then determine if
! particle is actually removed (call Energy_Calc subroutine).
! Variable “attach_success” is passed back to MAIN PROGRAM
! (for attachment, attach_success=1, for detachment, attach_success=-1).

USE global_params
INTEGER :: k, cnum
INTEGER:: num_avail, num_bins, found_i, found_j, site_type, i, j, m, n
INTEGER:: two_particles, detach_allowed, attach_success
! “availables” variable holds available positions, from among which a
random
! site selection is made.
INTEGER, DIMENSION(:,:), allocatable :: availables
INTEGER:: allocate_status, availables_holder(G1,2)
REAL :: bin_size
```

```
num_avail = 0
availables_holder = 0
found_j = 0
found_i = 0
attach_success = 0

if (k == 1) then
! Particle is entering from / leaving towards the west:
! scan GLattice from left to right, row by row.
do j = 2,G1-1
do i = 2,G2-1
if (GLattice(cnum,j,i).eq.1) then
num_avail = num_avail + 1
availables_holder(num_avail,1) = j
if (site_type == 1) then
availables_holder(num_avail,2) = i-1
else if (site_type == 2) then
availables_holder(num_avail,2) = i
end if
exit
end if
end do
end do

else if (k == 2) then
! Particle entering from / leaving towards south:
! scan GLattice from bottom to top, column by column.
do i = 2,G2-1
do j = G1-1,2,-1
if (GLattice(cnum,j,i).eq.1) then
num_avail = num_avail + 1
if (site_type == 1) then
availables_holder(num_avail,1) = j+1
else if (site_type == 2) then
availables_holder(num_avail,1) = j
end if
availables_holder(num_avail,2) = i
exit
end if
end do
end do

else if (k == 3) then
! Particle entering from / leaving towards east:
! scan GLattice from right to left, row by row.
do j = 2,G1-1
do i = G2-1,2,-1
if (GLattice(cnum,j,i).eq.1) then
num_avail = num_avail + 1
availables_holder(num_avail,1) = j
if (site_type == 1) then
availables_holder(num_avail,2) = i+1
else if (site_type == 2) then
availables_holder(num_avail,2) = i
end if
```

```
exit
end if
end do
end do

else if (k == 4) then
! Particle entering from / leaving towards north:
! scan GLattice from top to bottom, column by column.
do i = 2, G2-1
do j = 2, G1-1
if (GLattice(cnum,j,i).eq.1) then
num_avail = num_avail + 1
if (site_type == 1) then
availables_holder(num_avail,1) = j-1
else if (site_type == 2) then
availables_holder(num_avail,1) = j
end if
availables_holder(num_avail,2) = i
exit
end if
end do
end do
end if

allocate (availables(num_avail,2), STAT = allocate_status)
if (allocate_status /= 0) STOP "*** Not enough memory ***"

do i = 1,num_avail
availables(i,1) = availables_holder(i,1)
availables(i,2) = availables_holder(i,2)
end do

num_bins = num_avail
bin_size = 1./real(num_bins)

! For attachment: Pick one of the available sites at random, call
! Energy_Calc subroutine to determine if attachment reaction is
! successful.
if (site_type == 1) then
call RANDOM_NUMBER(rand)
do i = 1, num_bins
if (rand >= (i-1)*bin_size .and. rand < i*bin_size) then
found_j = availables(i,1)
found_i = availables(i,2)
end if
end do

! Must restart realisation if GLattice boundary is reached.
if (found_i == 1 .or. found_i == G2 .or. found_j == 1 .or. found_j == G1)
then
attach_success = 0
write(*,*) "Crystal lattice boundary reached"
restart = 1
else
```

```
call Energy_Calc(cnum, found_i, found_j, site_type, two_particles,
attach_success)
end if

! For detachment: Pick one of the available sites at random, decide if it
! is permitted to be removed (call Detachment_Permission subroutine).  If
! permitted, call Energy_Calc subroutine to determine if detachment
! reaction is successful.
else if (site_type == 2) then

call RANDOM_NUMBER(rand)
do i = 1, num_bins
if (rand >= (i-1)*bin_size .and. rand < i*bin_size) then
if (availables(i,1).ne.0 .and. availables(i,2).ne.0) then
found_j = availables(i,1)
found_i = availables(i,2)
end if
end if
end do

call Detachment_Permission(cnum, found_i, found_j, detach_allowed)

if (detach_allowed == 1) then
call Energy_Calc(cnum, found_i, found_j, site_type, two_particles,
attach_success)
end if

end if

! Deallocate “availables.”
deallocate (availables, STAT = allocate_status)
if (allocate_status /= 0) STOP "*** Not enough memory ***"

END SUBROUTINE Find_Site_and_Test

SUBROUTINE Energy_Calc(cnum, found_i, found_j, site_type, two_particles,
attach_success)
! Performs Metropolis energy calculation to determine if attachment or
! detachment reaction is successful.

USE global_params
INTEGER :: found_i, found_j, cnum, two_particles, site_type,
attach_success
REAL :: a_s_bonds, a_w_bonds, inc
REAL :: boltz_fac, en_diff, tot_en, tot_en_hyp

! Initialize attach_success variable.
attach_success = 0

if (two_particles == 0) then

tot_en_hyp = 0

! Initialize additional solid-solid bonds variable (a_s_bonds)
! Initialize additional solid-water bonds variable (a_w_bonds)
```

```
a_s_bonds = 0
a_w_bonds = 0

! Set increment value to add to a_s_bonds and a_w_bonds, depending on
! reaction type.
if (site_type == 1) then
inc = 1
else if (site_type == 2) then
inc = -1
end if

! Calculate a_s_bonds and a_w_bonds in hypothetical case where
! the reaction is successful.
if (GLattice(cnum,found_j,found_i+1) == 1) then
a_s_bonds = a_s_bonds + inc
a_w_bonds = a_w_bonds - inc
end if
if (GLattice(cnum,found_j-1,found_i) == 1) then
a_s_bonds = a_s_bonds + inc
a_w_bonds = a_w_bonds - inc
end if
if (GLattice(cnum,found_j+1,found_i) == 1) then
a_s_bonds = a_s_bonds + inc
a_w_bonds = a_w_bonds - inc
end if
if (GLattice(cnum,found_j,found_i-1) == 1) then
a_s_bonds = a_s_bonds + inc
a_w_bonds = a_w_bonds - inc
end if

! Include next-to-nearest neighbour solid-solid bonds.
if (GLattice(cnum,found_j+1,found_i+1) == 1) then
a_s_bonds = a_s_bonds + eta*inc
end if
if (GLattice(cnum,found_j-1,found_i-1) == 1) then
a_s_bonds = a_s_bonds + eta*inc
end if
if (GLattice(cnum,found_j+1,found_i-1) == 1) then
a_s_bonds = a_s_bonds + eta*inc
end if
if (GLattice(cnum,found_j-1,found_i+1) == 1) then
a_s_bonds = a_s_bonds + eta*inc
end if

! Calculate total change in energy for hypothetical state after reaction.
en_diff = a_s_bonds*Ess + 2*a_w_bonds*Esw
tot_en_hyp = tot_en + en_diff

else if (two_particles == 1) then
! en_diff is always the same for two-particle cluster creation or
! dissolution.
if (site_type == 1) en_diff = Ess - 2*Esw
if (site_type == 2) en_diff = -Ess + 2*Esw

end if
```

```
! Metropolis accept/reject condition.
if (en_diff < 0) then
! If en_diff negative, accept change: reaction successful.
if (site_type == 1) then
attach_success = 1
else if (site_type == 2) then
attach_success = -1
end if
tot_en = tot_en_hyp
else if (en_diff >= 0) then
! If en_diff positive, calculate Boltzmann factor:
boltz_fac = exp(-en_diff)
call RANDOM_NUMBER(rand)
! Accept change (reaction successful) with probability = Boltzmann factor.
if (rand < boltz_fac) then
if (site_type == 1) then
attach_success = 1
else if (site_type == 2) then
attach_success = -1
end if
tot_en = tot_en_hyp
end if
end if

END SUBROUTINE Energy_Calc

SUBROUTINE Detachment_Permission(cnum, found_i, found_j, detach_allowed)
! Verify if particle selected with Find_Site_and_Test subroutine can be
! detached from the cluster without breaking the cluster into two or more
! pieces.
USE global_params
INTEGER :: found_i, found_j, cnum, detach_allowed
INTEGER :: n, m, n_final
INTEGER :: neighbour(4,2), start_neighbour(2), second_neighbour(2),
third_neighbour(2)
INTEGER :: new_particle(2), old_particle(2), second_neighbour_found,
third_neighbour_found
INTEGER :: num_particles, num_bonds

! Initialize variables.
detach_allowed = 0
num_bonds = 0
neighbour = 0
start_neighbour = 0
second_neighbour = 0
third_neighbour = 0
second_neighbour_found = 0
third_neighbour_found = 0

! Determine # of solid-solid bonds at selected particle.
! Found particle has neighbour to the east:
if (GLattice(cnum, found_j, found_i+1) == 1) then
num_bonds = num_bonds + 1
neighbour(1,1) = found_j
```

```
neighbour(1,2) = found_i+1
end if

! Found particle has neighbour to the north:
if (GLattice(cnum, found_j-1, found_i) == 1) then
num_bonds = num_bonds + 1
neighbour(2,1) = found_j-1
neighbour(2,2) = found_i
end if

! Found particle has neighbour to the west:
if (GLattice(cnum, found_j, found_i-1) == 1) then
num_bonds = num_bonds + 1
neighbour(3,1) = found_j
neighbour(3,2) = found_i-1
end if

! Found particle has neighbour to the south:
if (GLattice(cnum, found_j+1, found_i) == 1) then
num_bonds = num_bonds + 1
neighbour(4,1) = found_j+1
neighbour(4,2) = found_i
end if

! One-bond case.  Particle can be detached without splitting up cluster.
! Permission for detachment granted.
if (num_bonds == 1) detach_allowed = 1

! Two-bond and three-bond case. Create hypothetical cluster by removing
! selected particle.  Following steps will evaluate if hypothetical
! cluster is one piece or it is split into multiple pieces.
GLattice(cnum, found_j, found_i) = 0

! Find neighbours of selected particle in case where it has 2 solid-to-
! solid bonds.
if (num_bonds == 2) then

do n = 1,4
if (sum(neighbour(n,:)).ne.0) then
start_neighbour = neighbour(n,:)
exit
end if
end do

do n = 4,1,-1
if (sum(neighbour(n,:)).ne.0) then
second_neighbour = neighbour(n,:)
exit
end if
end do

! Find neighbours of selected particle in case where it has 3 solid-to-
! solid bonds.
else if (num_bonds == 3) then
```

```
do n = 1,4
if (sum(neighbour(n,:)).ne.0) then
start_neighbour = neighbour(n,:)
exit
end if
end do

do m = (n+1),4
if (sum(second_neighbour(:)).eq.0) then
if (sum(neighbour(m,:)).ne.0) then
second_neighbour = neighbour(m,:)
end if
else if (sum(second_neighbour(:)).ne.0) then
if (sum(neighbour(m,:)).ne.0) then
third_neighbour = neighbour(m,:)
end if
end if
end do

end if

old_particle = start_neighbour

if (num_bonds == 2 .or. num_bonds == 3) then

num_particles = sum(GLattice(1,:,:))

! Set “n_final” (number of interations to try in tracking procedure
! below). Functions below based on test of number of iterations needed to
! properly identify a particle is permissible for detachment 99% of the
! time.
if (num_bonds == 2) n_final = 0.043*num_particles**2 + 15*num_particles
if (num_bonds == 3) n_final = num_particles*20 + 100

! Track particles through cluster, starting at “start_neighbour” and
! ending at “end_neighbour.”  If a path can be followed from one crystal
! particle to the next from the start_neighbour to _end_neighbour, after
! removing the selected particle, then the cluster will be guaranteed to
! remain intact upon removal of the selected particle.
do n  = 1, n_final

call Pick_Neighbour(new_particle, old_particle)

if (GLattice(cnum, new_particle(1), new_particle(2)) == 1) then
old_particle = new_particle
end if

! If tracking procedure lead from first neighbour to other neighbours,
! then detachment is permissible.
if (new_particle(1) == second_neighbour(1) .and. new_particle(2) ==
second_neighbour(2)) then
if (num_bonds == 2) then
detach_allowed = 1
exit
else if (num_bonds == 3) then
```

```
second_neighbour_found = 1
if (third_neighbour_found == 1) then
detach_allowed = 1
exit
end if
end if
end if
if (num_bonds == 3) then
if (new_particle(1) == third_neighbour(1) .and. new_particle(2) ==
third_neighbour(2)) then
third_neighbour_found = 1
if (second_neighbour_found == 1) then
detach_allowed = 1
exit
end if
end if
end if
end do
end if

! Replace particle in the GLattice, (Energy_Calc subroutine will then be
! used to determine if it will in fact be removed).
GLattice(cnum, found_j, found_i) = 1

END SUBROUTINE Detachment_Permission

SUBROUTINE Pick_Neighbour(new_particle, old_particle)
! Subroutine to pick one of the neighbours of the selected particle, used
! in the Detachment_Permission subroutine.

INTEGER ::  new_particle(2), old_particle(2)

call RANDOM_NUMBER(rand)

if (rand < 0.25) then
new_particle(1) = old_particle(1)
new_particle(2) = old_particle(2) + 1
else if (rand > 0.25 .and. rand <= 0.5) then
new_particle(1) = old_particle(1) - 1
new_particle(2) = old_particle(2)
else if (rand > 0.5 .and. rand <= 0.75) then
new_particle(1) = old_particle(1)
new_particle(2) = old_particle(2) - 1
else if (rand > 0.75) then
new_particle(1) = old_particle(1) + 1
new_particle(2) = old_particle(2)
end if

END SUBROUTINE Pick_Neighbour

SUBROUTINE Pick_Direction(k, k_store)
! Picks a random value of “k” (direction on SLattice).

INTEGER :: k, i, k_store(4)
```

```
do i = 1, 10000

call Random_Number(rand)
if (rand < 0.25) k = 1
if (rand >= 0.25 .and. rand < 0.5) k = 2
if (rand >= 0.5 .and. rand < 0.75) k = 3
if (rand >= 0.75 .and. rand < 1) k = 4

if (k_store(k).ne.1) then
k_store(k)=1
exit
end if

end do

! This stop contingency was never enacted in generating thesis data.
if (i >= 1000) STOP "k-direction could not be chosen in 1000 tries."

END SUBROUTINE Pick_Direction
```

References

[Abramovitz 2002] M. Abramowitz and I.A. Stegun, *Handbook of Mathematical Functions with Formulas, Graphs, and Mathematical Tables* (U.S. Department of Commerce, Washington D.C.).

[Báez 1995] L. A. Báez and P. Clancy, "The kinetics of crystal growth and dissolution from the melt in LennardJones systems." *J. Chem. Phys.* **102**, 8138.

[Becker 1935] R. Becker and W. Döring, "Kinetische Behandlung der Keimbildung in übersättigten Dämpfen." *Annalen der Physik*, **416**(8), 719-752.

[Bonabeau 2002] E. Bonabeau, "Agent-based modeling: Methods and techniques for simulating human systems." *PNAS*, **99**, 7287.

[Burton 2002] W.K. Burton, N. Cabrera, F.C. Frank, "The Growth of Crystals and the Equilibrium Structure of their Surfaces." *Philosophical Transactions of the Royal Society of London. Series A, Mathematical and Physical Sciences*, **243**(866), 299-358.

[Chkonia 2009] G. Chkonia, J. Wölk, R. Strey, J. Wedekind, and D. Reguera, "Evaluating nucleation rates in direct simulations." *J. Chem. Phys.* **130**, 064505.

[Chopard 1998] B. Chopard and M. Droz, *Cellular Automata Modeling of Physical Systems* (Cambridge University Press, Cambridge).

[Courtney 1961] W.G. Courtney, "Remarks on Homogeneous Nucleation." *J. Chem. Phys.* **35**, 2249.

[Dillmann 1989] A. Dillmann and G.E.A. Meier, "Homogeneous Nucleation of Supersaturated Vapors." *Chem. Phys. Lett.* **160**, 71.

[Dillmann 1991] A. Dillmann and G.E.A. Meier, "A refined droplet approach to the problem of homogeneous nucleation from the vapor phase." *J. Chem. Phys.* **94**, 3872.

[Djikaev 2004] Y.S. Djikaev, I. Napari, A. Laaksonen, "On the closure conjectures for the Gibbsian approximation model of a binary droplet." *J. Chem. Phys.* **120**, 9752.

[Fillion 2011] L. Fillion, R. Ni, D. Frenkel, and M. Dijkstra, "Simulation of nucleation in almost hard-sphere colloids: The discrepancy between experiment and simulation persists." *J. Chem. Phys.* **134**, 134901.

[Flageollet 1980] C. Flageollet, M. Dinh Cao, and P. Mirable, "Experimental study of nucleation in binary mixtures: The methanol–water and npropanol–water systems." *J. Chem. Phys.* **72**, 544.

[Frenkel 1955] Y.I. Frenkel, *Kinetic Theory of Liquids*, (Dover, New York).

[Frenkel 2006] D. Frenkel, "Colloidal Crystals: Plenty of Room at the Top." *Nat. Mat.* **5**, 85.

[Frisch 1986] U. Frisch, B. Hasslacher, and Y. Pomeau, "Lattice-Gas Automata for the Navier-Stokes Equation." *Phys. Rev. Lett.* **56**(14), 1505-1508.

[Gardiner 1990] C.W. Gardiner, *Handbook of Stochastic Methods for Physics, Chemistry, and the Natural Sciences*, 2nd Edition (Springer-Verlag, Berlin).

[Ghosh 2011] S. Ghosh and S.K. Ghosh, "Homogeneous nucleation in vapor-liquid phase transition of Lennard-Jones fluids: A density functional theory approach." *J. Chem. Phys.* **134**, 024502.

[Gibbs 1928] J.W. Gibbs, *On the Equilibrium of Heterogeneous Substances, Collected Works*, (Longmans, Green, & Co., New York).

[Girschick 1990] S.L. Girschick and C. Chiu, "Kinetic nucleation theory: A new expression for the rate of homogeneous nucleation from an ideal supersaturated vapor." *J. Chem. Phys.* **93**, 1273.

[Gonzalez-Oliver 1980] C.J.R. Gonzalez-Oliver and P.F. James, "Crystal Nucleation and Growth in a Na2O2CaO.3SiO2 Glass." *J. Non-Crys. Sol.* **38 & 39**, 699-704.

[Goodrich 1963] F.C. Goodrich, "Nucleation Rates and the Kinetics of Particle Growth. II. The Birth and Death Process." *Proc. Roy. Soci. Lond. Ser. A, Math. Phys. Sci.*, **277**(1369), 167-182.

[Gránásy 1993] L. Gránásy, "Diffuse interface theory of nucleation." *J. Non-Cryst. Sol.* **162**, 301-303.

[Gránásy 1994] L. Gránásy, "Nucleation theory for diffuse interfaces." *Mat. Sci. Eng. A* **178**, 121-124.

[Gránásy 1996] L. Gránásy, “Diffuse interface theory for homogeneous vapor condensation.” *J. Chem. Phys.* **104**, 5188.

[Gránásy 1999a] L. Gránásy, “Non-classical theory of crystal nucleation: application to oxide glasses: review.” *J. Non-Crys. Sol.* **253**, 210.

[Gránásy 1999b] L. Gránásy, “Cahn–Hilliard-type density functional calculations for homogeneous ice nucleation in undercooled water.” *J. Mol. Struct.* **485-486** 523-536.

[Hardy 1976] J. Hardy, O. de Pazzis, and Y. Pomeau, “Molecular dynamics of a classical lattice gas: Transport properties and time correlation functions.” *Phys. Rev. A* **13**, 1949-1961.

[Haymet 1981] A.D.J. Haymet and D.W. Oxtoby, “A molecular theory for the solid–liquid interface.” *J. Chem. Phys.* **74**, 2559.

[Kalikmanov 1993] V.I. Kalikmanov, “Self-consistent cluster approach to the homogeneous kinetic nucleation theory.” *Phys. Rev. E.* **47**(5), 3532-3539.

[Kaschiev 2000] D. Kashchiev, *Nucleation: Basic Theory with Applications*, (Butterworth-Heinemann, Oxford).

[Katsev 2002] S. Katsev, *Pattern Formation in Geochemical Systems*. PhD thesis, Dept. of Physics, University of Ottawa.

[Laaksonen 1995] A. Laaksonen, V. Talanquer, and D.W. Oxtoby, “Nucleation: Measurements,Theory, and Atmospheric Applications.” *Ann. Rev. Phys. Chem.* **46**, 489.

[L'Heureux 2007] I. L’Heureux, “A new model of volatile bubble growth in a magmatic system: Isobaric case.” *J. Geophys. Res.* **112**, B12208.

[Lundrigan 2009] S. Lundrigan and I. Saika-Voivod, “Test of classical nucleation theory and mean first-passage time formalism on crystallization in the Lennard-Jones liquid.” *J. Chem. Phys.* **131**, 104503.

[Lutsko 2008] J. F. Lutsko, “Density functional theory of inhomogeneous liquids. III. Liquid-vapor nucleation.” *J. Chem. Phys.* **129**, 244501.

[MacFarlane 1983] D.R. MacFarlane, R.K. Kadiyala, and C.A. Angell, “Homogeneous nucleation and growth of ice from solutions. TTT curves, the nucleation rate, and the stable glass criterion.” *J. Chem. Phys.* **79**, 3921.

[Marchand 2009a] P. Marchand and D. Rancourt, "General model for the aqueous precipitation of rough-surface nanocrystals and application to ferrihydrite genesis." *Amer. Min.* **94**, 1428.

[Marchand 2009b] P. Marchand, *Modèle général de la précipitation aqueuse des solides à surface rugeuse, appliqué à la ferrihydrite*. M.Sc. thesis, Dept. of Physics, University of Ottawa.

[Markov 2003] I.V. Markov, *Crystal Growth for Beginners* (World Scientific Publishing, Singapore).

[Mathworks Inc. 2012] Mathworks, "Evaluating the Goodness of Fit", Matlab Help, Retrieved February 9, 2012 at: http://www.mathworks.com/help/toolbox/curvefit/bq_6zzm.html

[McCabe 1929] W.L. McCabe, "Crystal growth in aqueous solutions: I. Theory." *Ind. Eng. Chem.* **21**(1), 30-33.

[Miyazawa 1974] Y. Miyazawa and G.M. Pound, "Homogeneous Nucleation of Crystalline Gallium from Liquid Gallium." *J. Cryst. Growth* **23**, 45.

[Nielsen 1969] A.E. Nielsen, "Nucleation and Growth of Crystals at High Supersaturation." *Kristall und Technik* **4**(1), 17-38.

[Nielsen 1971] A.E. Nielsen and O. Söhnel, "Interfacial tensions electrolyte crystal-aqueous solution, from nucleation data." *J. Crys. Growth* **11**(3), 233-242.

[Nielsen 1980] A.E. Nielsen, "Transport control in crystal growth from solution." *Croatia Chemica Acta* 53, 255-279.

[Nowakowski 1991] B. Nowakowski and E. Ruckenstein, "Homogeneous nucleation in gases: A three-dimensional Fokker-Planck equation for evaporation from clusters." *J. Chem. Phys.* **94**, 8487.

[Oxtoby 1988] D.W. Oxtoby and R. Evans, "Nonclassical nucleation theory for the gas–liquid transition." *J. Chem. Phys.* **89**, 7521.

[Oxtoby 2003] D.W. Oxtoby, "Crystal Nucleation in Simple and Complex Fluids." *Phil. Trans.: Math. Phys. Eng. Sci.*, **361**(1804), 419-428.

[Pavlovska 1971] A. Pavlovska, D. Nenow, "Experimental investigation of the surface melting of equilibrium form faces of diphenyl." *Surf. Sci.* **27**(1), 211-217.

[Rancourt 2005] D.G. Rancourt, P.-J. Thibault, D. Mavrocordatos, and G. Lamarche, "Hydrous ferric oxide precipitation in the presence of nonmetabolizing bacteria: Constraints on the mechanism of a biotic effect." *Geo. Cosmo. Acta.* **69** 553-577.

[Romer 2007] F. Romer and T. Kraska, "Homogeneous nucleation and growth in supersaturated zinc vapor investigated by molecular dynamics simulation." *J. Chem. Phys.* **127**, 234509.

[Ruckenstein 1990] E. Ruckenstein and B. Nowakowski, "A Kinetic Theory of Nucleation in Liquids." *J. Coll. Inter. Sci.* **137**, 583-592.

[Ruckenstein 2005] E. Ruckenstein and Y.S. Djikaev, "Recent developments in the kinetic theory of nucleation." *Adv. Coll. Int. Sci.* **188**, 51 (2005).

[Saika-Voivod 2011] I. Saika-Voivod, F. Romano, and F. Sciortino, "Nucleation barriers in tetrahedral liquids spanning glassy and crystallizing regimes." *J. Chem. Phys.* **135**, 124506.

[Shevchenko 2006] E. Shevchenko, D.V. Talapin, N.A. Kotov, S. O'Brien, and C.B. Murray, "Structural diversity in binary nanoparticle superlattices." *Nature*, **439**, 51 (2006).

[Talanquer 1994] V. Talanquer and D.W. Oxtoby, "Dynamical density functional theory of gas–liquid nucleation." *J. Chem. Phys.* **100**, 5190.

[ten Wolde 1994] P.R. ten Wolde, M.J. RuizMontero, and D. Frenkel, "Numerical calculation of the rate of crystal nucleation in a LennardJones system at moderate undercooling." *J. Chem. Phys.* **104**, 9932.

[ter Horst 2003] J.H. ter Horst and D. Kaschiev, "Determination of the nucleus size from the growth probability of clusters." *J. Chem. Phys.* **119**, 2241.

[Thibault 2009] P-J Thibault, D.G. Rancourt, R.J. Evans, and J.E. Dutrizac, "Mineralogical confirmation of a near-P:Fe = 1:2 limiting stoichiometric ratio in colloidal P-bearing ferrihydrite-like hydrous ferric oxide." *Geo. Cosmo. Acta.* **73**, 364-376.

[Tolman 1948] R.C. Tolman, "The Effect of Droplet Size on Surface Tension." *J. Chem. Phys.* **17**(3), 333-337.

[Torrie 1974] G.M. Torrie and J.P. Valleau, "Monte Carlo Free Energy Estimates using Non-Boltzmann Sampling: Application to the Sub-Critical Lennard-Jones Fluid." *Chem. Phys. Lett.* **28**(4), 578-581.

[Turnbull 1952] D. Turnbull, "Kinetics of Solidification of Supercooled Liquid Mercury Droplets." *J. Chem. Phys.* **20**, 411.

[van Duijneveldt 1992] J.S. van Duijneveldt and D. Frenkel, "Computer simulation study of free energy barriers in crystal nucleation." *J. Chem. Phys.* **96**, 4655.

[Wedekind 2007] J. Wedekind, R. Strey, and D. Reguera, "New method to analyze simulations of activated processes." *J. Chem. Phys.* **126**, 134103.

[Wilemski 1995] G. Wilemski, "The Kelvin equation and selfconsistent nucleation theory." *J. Chem. Phys.* **103**, 1119.

[Wolf-Gladrow 2005] D.A. Wolf-Gladrow, *Lattice-Gas Cellular Automata and Lattice Boltzman Models – An Introduction* (Springer, Berlin).

[Wolfram 1986] S. Wolfram, "Cellular Automata Fluids 1: Basic Theory." *J. Stat. Phys.* **45**(3/4), 471-526.

[Wood 1970] G. R. Wood and A. G. Walton, "Homogeneous Nucleation Kinetics of Ice from Water." *J. App. Phys.* **41**, 3027.

[Wyslouzil 1991] B.E. Wyslouzil, J.H. Seinfeld, R.C. Flanagan, and K. Okuyama, "Binary nucleation in acid–water systems. I. Methanesulfonic acid–water." *J. Chem. Phys.* **94**, 6827.

[Zeldovich 1943] J.B. Zeldovich, "On the theory of new phase formation; cavitation." *Acta Physicochim USSR* **18**, 1-22.

[Zeng 1991] X. C. Zeng and D. W. Oxtoby, "Gas–liquid nucleation in LennardJones fluids." *J. Chem. Phys.* **94**, 4472.

[Zhang 2008] Y. Zhang, *Geochemical Kinetics* (Princeton University Press, Princeton).